

Annual Report 2018

Laboratory of Radiochemistry

Cover

Transmutation can potentially mitigate problems related to the disposal of spent nuclear fuel. In a prominent class of advanced fast nuclear reactors designed for this purpose, liquid metals are planned to be used as coolants. In the Isotope and Target Chemistry group of LRC, we study the release of radionuclides from liquid metals to support safety assessments for these liquid metal cooled reactors.

Photographs: Members of the Target and Isotope Chemistry group performing experiments with liquid metal samples

Graph: Results of experiments studying the evaporation iodine from liquid lead-bismuth eutectic.

PAUL SCHERRER INSTITUT



Annual Report 2018

Laboratory of Radiochemistry

Editors

R. Eichler, A. Blattmann

Paul Scherrer Institut

Labor für Radiochemie

5232 Villigen PSI

Switzerland

Durchwahl +41 56 310 24 04

Sekretariat +41 56 310 24 01

Fax +41 56 310 44 35

Reports are available from

Angela Blattmann

angela.blattmann@psi.ch

Paul Scherrer Institut

5232 Villigen PSI

Switzerland



See also our web-page

<https://www.psi.ch/lrc/>

TABLE OF CONTENTS

Editorial.....	1
SUPERHEAVY ELEMENT ^{112}Cn & ^{114}Fl - CHALCOGEN INTERACTIONS USING GAS CHROMATOGRAPHY . 3 P. Ionescu, R. Eichler, B. Kraus, Y. Wittwer, R. Dressler, H. Gäggeler, D. Herrmann, A. Vögele, A. Türler, N.V. Aksenov, Y.V. Albin, G.A. Bozhikov, V.I. Chepigin, I. Chupranov, S.N. Dmitriev, A.S. Madumarov, O.N. Malyshev, Y.A. Popov, A.V. Sabelnikov, P. Steinegger, A.I. Svirikhin, G.K. Vostokin, A.V. Yeremin, T.S. Sato, N.M. Chiera	
INSIGHTS INTO SURFACE REACTIONS OF ^{211}Pb WITH SiO_2 AND Al_2O_3 ON THE SINGLE-ATOM SCALE	5
B. Kraus, R. Eichler, A. Türler	
CHALLENGES OF VACUUM CHROMATOGRAPHY WITH FISSION PRODUCTS FROM ^{252}Cf	7
B. Kraus, R. Eichler, D. Herrmann, P. Steinegger, T. K. Sato, A. Türler	
TOWARDS HIGH-TEMPERATURE ALPHA-SPECTROSCOPY SETUPS FOR SUPERHEAVY ELEMENT CHEMISTRY EXPERIMENTS.....	9
B. Kraus, R. Eichler, R. Dressler, M. Camarda, D. Herrmann, P. Steinegger, A. Türler, E. Griesmayer, C. Weiss	
OPTIMIZING THE IN-SITU FORMATION OF METAL CARBONYL COMPLEXES	11
Y. Wittwer, R. Eichler, D. Herrmann, A. Türler	
MASS SPECTROMETRIC SPECIATION OF METAL-CARBONYLS IN THE GAS PHASE	13
Y. Wang, Y. Wittwer, J. Zhang, J. Yang, H. Haba, Y. Komori, T. Yokokita, S. Cao, F. Fan, R. Eichler, A. Türler, Z. Qin	
MEASUREMENT OF Mn-53 CAPTURE CROSS-SECTION AT N_TOF FACILITY (PART I – TARGET PREPARATION AND EXPERIMENT REALIZATION).....	15
J. Ulrich, R. Dressler, D. Schumann	
MEASUREMENT OF Mn-53 CAPTURE CROSS-SECTION AT N_TOF FACILITY (PART II – DATA EVALUATION).....	17
J. Ulrich, R. Dressler	
DESIGN AND CONSTRUCTION OF MULTICHANNEL HVPS FOR PHOTOMULTIPLIER TUBES AT LRC.....	19
J. Ulrich, R. Dressler, D. Herrmann	
PRODUCTION AND SEPARATION OF PROMETHIUM ISOTOPES 143-148.....	21
J. Ulrich, S. Braccini, T.S. Carzaniga, N.P. van der Meulen, R. Dressler	
RADIOCHEMICAL SEPARATION OF LANTHANIDES FROM p-IRRADIATED Ta TARGETS, TOWARDS HIGH-PRECISION HALF-LIFE MEASUREMENTS	23
Z. Talip, D. Schumann	
PRODUCTION CROSS SECTIONS OF LONG-LIVED RADIONUCLIDES IN PROTON-IRRADIATED TUNGSTEN.....	25
Z. Talip, R. Dressler, D. Schumann, J.C. David, C. Vockenhuber	
NEUTRON CAPTURE CROSS SECTION OF ^{171}Tm	27
T. Heftrich, M. Weigand, Ch.E. Düllmann, K. Eberhardt, S. Fiebiger, J. Glorius, K. Göbel, C. Guerrero, R. Haas, S. Heinitz, J. Lerendegui-Marco, F. Käppeler, J. D. Kaiser, U. Köster, C. Langer, S. Lohse, F. Ludwig, R. Reifarth, D. Renisch, K. Scheutwinkel, D. Schumann, N. Wiehl, C. Wolf	
Cs-REMOVAL FROM HIGHLY ACIDIC SPENT FUEL SOLUTIONS: BATCH TESTS.....	28
M. Lin, I. Kajan, D. Schumann, A. Türler	

TOWARDS THE DETERMINATION OF MOLYBDENUM-93 HALF-LIFE.....	30
I. Kajan, S. Heinitz, R. Dressler	
THE PURIFICATION OF ²⁶ Al AND ¹⁷⁹ Ta RECOVERED FROM IRRADIATED STEELS OF THE SINQ TARGET IRRADIATION PROGRAM.....	32
S. Heinitz, D. Schumann	
THE PRODUCTION AND BEHAVIOUR OF ³ H AND ⁷ Be IN THE COOLING CIRCUITS OF THE SPALLATION NEUTRON SOURCE SINQ.....	33
S. Heinitz, D. Kiselev, M. Rüthi, B. Blau, D. Schumann	
MEASUREMENT OF THE ⁷ Be(n,p) CROSS SECTION AT THERMAL ENERGY	35
I. Tomandl, J. Vacík, U. Köster, D. Schumann, E.A. Maugeri, M. Ayrarov, S. Heinitz, L. Viererbl, J. Ballof, R. Catherall, K. Chrysalidis, T.D. Goodacre, D. Fedorov, V. Fedosseev, K. Johnston, B. Marsh, S. Rothe, J. Schell, C. Seiffert	
MEASUREMENT OF THE ⁷ Be(n,p) ⁷ Li REACTION CROSS SECTION FOR THE COSMOLOGICAL LITHIUM PROBLEM AT THE n_TOF FACILITY AT CERN.....	36
L. Damone, M. Barbagallo, M. Ayrarov, E.A. Maugeri, S. Heinitz, R. Dressler, N. Kivel, J.G. Martins Correia, J. Schell, K. Johnston, M.J.G. Borge, J. Ballof, T. Stora, B. Marsh, T.D. Goodacre, C. Seiffert, S. Rothe, U. Köster	
IMPLEMENTING NEW ISOTOPES FOR ENVIRONMENTAL RESEARCH: REDETERMINATION OF THE ³² Si HALF-LIFE, PART I: COLUMN CHROMATOGRAPHY (CC).....	38
M. Veicht, I. Mihalcea, D. Schumann, A. Pautz	
IMPLEMENTING NEW ISOTOPES FOR ENVIRONMENTAL RESEARCH: REDETERMINATION OF THE ³² Si HALF-LIFE, PART II: DISTILLATION	40
I. Mihalcea, M. Veicht, D. Schumann, A. Pautz	
LASER SPECTROSCOPY OF PROMETHIUM ISOTOPES	42
D. Studer, R. Heinke, P. Naubereit, J. Ulrich, S. Braccini, T.S. Carzaniga, R. Dressler, S. Heinitz, U. Köster, S. Raeder, K. Wendt	
REVIEW OF EXPERIMENTS ON IODINE EVAPORATION FROM LIQUID LEAD-BISMUTH EUTECTICUM, PART I: METHODOLOGICAL DEVELOPMENTS.....	44
I.I. Danilov, A. Vögele, D. Hermann, R. Dressler, R. Eichler, A. Türler, J. Neuhausen	
REVIEW OF EXPERIMENTS ON IODINE EVAPORATION FROM LIQUID LEAD-BISMUTH EUTECTICUM, PART II: PRELIMINARY RESULTS.....	46
I.I. Danilov, A. Vögele, D. Hermann, R. Eichler, A. Türler, J. Neuhausen	
POLONIUM DEPOSITION BEHAVIOUR IN THE EVENT OF A BEAM GUIDE WINDOW PUNCTURE IN AN ACCELERATOR DRIVEN SYSTEM.....	48
E. Karlsson, A. Vögele, R. Eichler, A. Aerts, D. Hermann, A. Türler, J. Neuhausen	
Cu-64 CHLORIDE AND Cu-64 LABELLED Cd-80/Cd-86-TARGETING FUSION PROTEINS FOR PET-IMAGING OF INFLAMMATION.....	50
M. Taddio, C. Castro, Z. Talip, R. Hasler, A. Blanc, R. Schibli, M. Behe, S. Krämer, N.P. van der Meulen	
USING THE (p,2n) NUCLEAR REACTION TO PRODUCE ⁴³ Sc FROM ⁴⁴ Ca	52
R. Hasler, N.P. van der Meulen	
TARGETRY DEVELOPMENTS TOWARDS ⁴⁴ Sc PRODUCTION USING ENRICHED CaO	54
R. Hasler, T.S. Carzaniga, S. Braccini, N.P. van der Meulen	
Sc-44 FOR KINETIC MEASUREMENTS OF GASTRIN DERIVATIVES.....	56
S. Krämer, A. Blanc, C. Keller, Z. Talip, R. Hasler, R. Schibli, N. P. van der Meulen, M. Behe	
PRODUCTION AND PURIFICATION PROCESS OF THE MEDICALLY INTERESTING RADIOLANTHANIDE TERBIUM-161.....	57
N. Gracheva, J.R. Zeevaart, U. Köster, Z. Talip, R. Schibli, N.P. van der Meulen	

PRODUCTION AND PURIFICATION OF THE PURE AUGER ELECTON EMITTER ERBIUM-165.....	58
N. Gracheva, R. Schibli, N.P. van der Meulen	
DEVELOPMENT OF NOVEL RUTHENIUM-BASED RADIOPHARMACEUTICALS	59
B. Happl, M. Brandt, T. Balber, P. Heffeter, Z. Talip, A. Vögele, R. Hasler, M. Jakupsek, R. Schibli, M. Mitterhauser, B. Keppler, W. Kandioner, N.P. van der Meulen, T.L. Mindt	
List of publications	60
Internal reports.....	63
Contributions to conferences, workshops, and seminars.....	64
Members of scientific committees, external activities	69
Bachelor thesis.....	70
Awards.....	70
Organigram.....	72
Author index	73
Affiliation index	75

EDITORIAL

Dear reader,

This traditional Annual Report of the Laboratory of Radiochemistry of the Paul Scherrer Institute overviews and summarizes research going on in our laboratory throughout the year 2018.

One of the most important political issues in year 2018 was our contribution to the success of the *ETH Evaluation of the Nuclear Energy and Safety Division* (NES) held at Paul Scherrer Institute in the week of September 10-13, 2018. The very positive outcome of this evaluation for the entire NES Department recognized the Laboratory of Radiochemistry as a vital and productive research unit strongly valued within NES and PSI. Our expertise is important for PSI and Switzerland. This outstanding success is founded on the professional and motivated work of all members of the laboratory.

It is my great pleasure to present here our awarded contributions, which beside our other scientific publications nicely demonstrate the national and international recognition of our research:

- At the 18th International Radiochemical Conference held traditionally in Mariánské Lázně May 13-18, 2018 two of our PhD-students, Yves Wittwer and Ivan Danilov were awarded the Poster prize for their contributions.
- At the largest European nuclear medicine conference ENAM'18 held in Düsseldorf, October 13-17, 2018 the outstanding collaborative works of Nick van der Meulen's group of LRC and Christina Müller's group from the Center for Radiopharmaceutical Research (CRS) with the isotopes ^{44,47}Sc were awarded the "EJNMMI: Best Paper Award EANM Springer Prize 2018" in the categories *Radiopharmacy and Chemistry* and *Research*.
- At the same conference the innovative work of Christina and Nick on ¹⁶¹Tb has been awarded the renowned ENAM *Marie Curie Award 2018*.

- At the 10th NES PhD-Day on May 24, 2018 Mu Lin presented the winning contribution for the category *Best 2-nd Year PhD*.

Sincere congratulations to these great successes!

In September 7-8, 2018 our yearly laboratory excursion, organized by Rugard Dressler and Dorothea Schumann, lead us to the Lausanne side of Lac Lemman. There, we had an impressive visit of the CROCUS reactor that is part of the research installations our department head Prof. Andreas Pautz operates at EPFL. We were hosted by a very professional team around Dr. Vincent Lamirand who gave us an exciting and comprehensive tour through this research facility. After a relaxing hike in the sunny vineyards around Cully and Epesses, we had an exceptional wine tasting at the winery *Dubois fils*, where Monsieur Dubois introduced us to the secrets of winemaking in these rather northern European realms. Our Christmas party at the *Waldhütte Würenlingen* with all the exciting *Wichtel* presentations was a great success and fun.

A warm welcome and welcome-back goes to our new PhD student Mario Veicht and to the Postdocs Ionut Mihalcea and Nadine Chiera, who have started this year well into their respective research projects. Dear reader, you will see in this report that our broad research topics within LRC focus generally on the chemistry of many elements all over the periodic table. 2019 is proclaimed by the United Nations General Assembly and UNESCO the *International Year of the Periodic Table of Chemical Elements*. Thus, our success next year will be a perfect way to mark this occasion. We take this as a perpetual driver to proceed with radiochemistry and nuclear chemistry at their finest. Have a nice read!



Robert Eichler

SUPERHEAVY ELEMENT ^{112}Cn & ^{114}Fl - CHALCOGEN INTERACTIONS USING GAS CHROMATOGRAPHY

P. Ionescu, R. Eichler, B. Kraus, Y. Wittwer (Univ. Bern & PSI), R. Dressler, H. Gäggeler, D. Herrmann, A. Vögele (PSI), A. Türler (Univ. Bern), N.V. Aksenov, Y.V. Albin, G.A. Bozhikov, V.I. Chepigin, I. Chupranov, S.N. Dmitriev, A.S. Madumarov, O.N. Malyshev, Y.A. Popov, A.V. Sabelnikov, P. Steinegger, A.I. Svirikhin, G.K. Vostokin, A.V. Yeremin (JINR-FLNR), T.S. Sato, N.M. Chiera (ASRC-JAEA)

INTRODUCTION

Superheavy elements (SHE) represent the frontier in the discovery of new elements and expansion of the periodic table. Prepared synthetically in fusion reactions for chemistry experiments we are able to deepen our understanding of their chemical properties. These properties are of interest due to relativistic effects [1,2] on the electron shells caused by the heavy nucleus, such as in Fl, where the mass of a 7s electron is approx. 1.79 times its rest mass leading to distorted atomic orbital shapes. This work aims to further investigate the chemistry of Cn and Fl, as well as improve existing experimental methods. Based on previous observations Cn and Fl are elements of considerable chemical inertness and high volatility. To prepare for second generation chemical experiments, the volatile group 12 homologue Hg is used as a surrogate. As Hg forms a stable selenide found in nature in the form of Tiemannite, the Hg-Se interaction was chosen as a model for Cn-Se investigations. When moving down group 12 in the periodic table, the metal-selenide bond decreases in stability, to the point that Cn may be expected to not form a stable bond [4, 5]. Experiments involve gas chromatography (GC) with Se as stationary phase in a column and Hg tracer isotopes in the mobile gas phase. Previous work established values for the enthalpy of adsorption of Hg on various allotropes of Se with $\Delta H_{\text{ads}}^{\text{Hg}}(\text{a-Se}) < -85 \text{ kJ/mol}$, and $\Delta H_{\text{ads}}^{\text{Hg}}(\text{t-Se}) > -60 \text{ kJ/mol}$ [4].

EXPERIMENTAL

The experimental is divided into two stages, the ‘off-line’ model experiments and the ‘on-line’ stage conducted at FLNR U-400 accelerator facilities in Dubna, Russia. Off-line experiments performed at PSI, Switzerland use the lighter homologue Hg to model later experiments using SHE. Further tasks performed off-line include the preparation and testing of the experimental equipment for a seamless installation in Russia. Off-line Se-covered GC columns were prepared by melting finely ground Se powder in a quartz column at 280 °C. A PTFE tube of lesser outer diameter to the quartz’s inner diameter was inserted into the molten Se, displacing it. The system was then quenched quickly in cold water, resulting in a solid black-amorphous Se column. This column was then placed in an oven heated to 75 °C at 2.5 °C/min, then slowly cooled causing a visible conversion of the black-amorphous Se to grey metallic trigonal Se (t-Se). These columns were then used in isothermal RT GC experiments with inert He carrier gas at 25 ml/min and ^{203}Hg tracer as the mobile phase

to determine the allotropic nature, i.e. the conversion rate of the Se columns using previously established ΔH_{ads} . Similarly, α -particle detectors for use in on-line experiments were prepared by thermal vapour deposition (TVD) of a ground Se powder source onto the quartz detector surface resulting in a red amorphous Se layer. This Se was also converted to grey t-Se using the thermal method above. On-line GC was performed using the COLD (Cryo On-Line Detector) array at FLNR, Dubna, Russia (Fig. 1). Cn was produced indirectly over the alpha decay of short-lived Fl in the nuclear reaction $^{242}\text{Pu}(^{48}\text{Ca}, 3n)^{287}\text{Fl}(\alpha) \rightarrow ^{283}\text{Cn}$ using the U400 cyclotron. Typically, 1.5 mg/cm² ^{242}Pu (99.5%) targets doped with $^{\text{nat}}\text{Nd}$ and deposited by molecular plaiting on 2 μm thin Ti foil backings were irradiated. The Nd admixture ensured to simultaneously produce $^{182-185}\text{Hg}$ as a tracer. The U-400 delivered a ^{48}Ca beam between 0.2 and 0.5 μA at 273 MeV. The beam was passed through a 4 μm Mylar foil and a 5 mm slit of carrier gas (70 vol-% He, 30 vol-% Ar) before entering the target material. Reaction products were recoiled through the target backing and were thermalized and collected in a gas stopping chamber and subsequently flushed within about 2 s to the COLD array. There, the reaction products were exposed to an isothermal 25 °C column of 8 cm t-Se detectors followed by a temperature gradient to -160 °C over 21 cm of Au-covered detectors (see Fig.1).

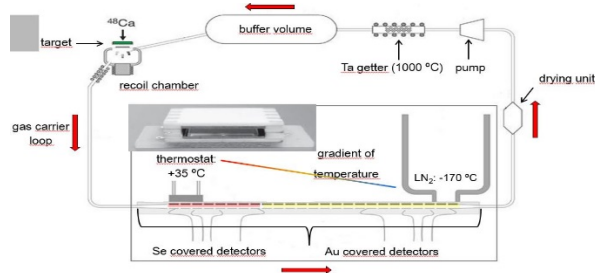


Fig. 1: Schematic of the COLD detector array connected to the gas loop. Evaporation residues are collected in the recoil chamber and transported to the COLD for GC. The remaining loop cleans and monitors the experiments using dew point meters (Michell EasiDew®) and an MKS CIRRUS2® mass spectrometer.

RESULTS

Off-line isothermal GC of thin TVD deposited Se films using ^{203}Hg , which was prepared by irradiating thallium metal with neutrons at the PSI-SINQ NIS facilities, showed that an almost complete conversion of red amorphous Se to t-Se had occurred during tempering. Using a Monte-Carlo (MC) simulation for

the gas chromatographic retention, it was established that the surface had converted approx. 95% to t-Se (Figure 2) which is a sufficiently good conversion rate. However, some Hg retention can be seen throughout the column, implying a not fully converted Se surface. Another explanation could be adsorption retention due to open-ended t-Se chains.

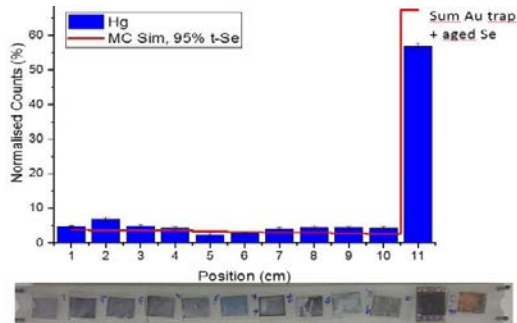


Fig. 2: Isothermal GC at 25 °C, 25 ml/min He flow showing deposition pattern of Hg on t-Se deposited on quartz slides (shown below). Monte-Carlo simulation showing the deposition pattern of 95% converted t-Se with 5% red Se component (red line).

On-line over a course of six weeks a total beam integral of approx. $3.3 \cdot 10^{18}$ ^{48}Ca particles was collected on the ^{242}Pu targets. Six events tentatively attributed to the decay of ^{283}Cn were identified (Table 1, in black letters). Taking into account all known efficiencies in an apparent formation cross section of ~ 2 pb was calculated.

Detected Event	$T_{\text{Se}}(^{\circ}\text{C})$	$T_{\text{obs}}(^{\circ}\text{C})$	Surface
α -SF	27	27	Au
SF	15	15	Se
SF	7	7	Se
SF	15	-75	Au
α -SF	13	-23	Au
α -SF	15	-80	Au
α -SF	15	15	Se
α -SF	15	15	Se

Tab. 1: Summary of recorded events 2018. Results from previous experiments 2015/16 [5] shown in green.

In the experiments from 2015/16, Cn was showing a surprisingly high affinity for a similar Se surface at room temperature, uncharacteristic of the trend for group 12 elements [5]. The current observation could be interpreted as a lesser interaction of Cn with t-Se. However, during the experiment it became apparent that the detected ^{185}Hg amounts were declining over time (Figure 3). From target monitoring it was ruled out that the Hg production fluctuated. Rather, it is suspected that due to impurities circulating in the gas, the detector surfaces become contaminated and the Hg can no longer interact with the original surface. Obviously the washing procedure of the detectors with methanol, tetrachloromethane, acetone, and diethyl ether before thorough drying reestablished the properties of the stationary gold surface. The primary

aim of this experiment was to test the affinity of Cn to t-Se however, which could not be washed. (Figure 4).

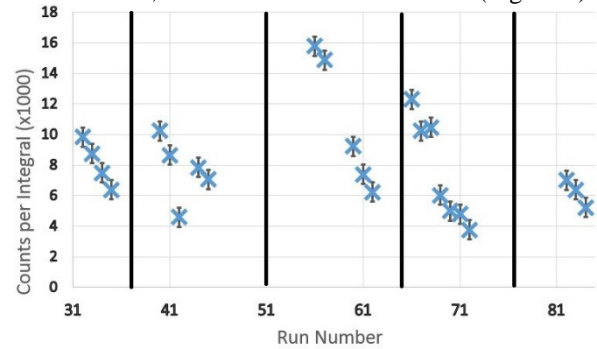


Fig. 3: Hg counts per collected integral beam for a series of runs showing the clear decline of detected Hg. Black bars indicate the washing of detectors.

It was found that the bulk of the contamination occurred on the Au-covered detectors (Figure 4). After successive runs, the Hg deposition did not change on Se or Quartz covered detectors, however the Hg could be observed to travel further into the COLD array between Det.#12-25 and the net sum of Hg decreasing suggested the Hg left the detector at the cold end, which can be expected only if no gold surface is available at all for adsorption (Det.#26-32).

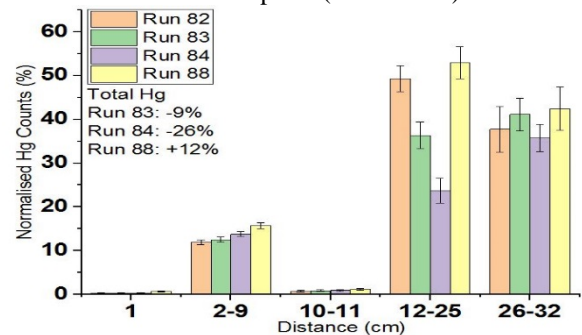


Fig. 4: Normalised Hg counts for COLD detector segments for successive runs. The Se and Quartz counts don't change significantly, while the counts on the first Au detectors drop dramatically, only restored for run 88 after exchanging the gas.

In conclusion, preparatory experiments led to a successful on-line experimental campaign with a number of Cn events recorded. It was found that gas contamination from an unknown source caused significant loss of detection rates on the Au covered detectors. The physisorption interaction of Hg with t-Se was not affected, but an influence on the chemical interaction of Cn with Se cannot be excluded. Further experiments at much cleaner conditions behind the newly established gas-filled separator at the SHE-Factory at FLNR Dubna are envisaged.

- [1] M. Schädel, D. Shaughnessy (Eds.), The Chemistry of Superheavy Elements, 2nd Ed. Springer (2014).
- [2] N. Chiera, PhD Thesis, University of Bern, (2016).
- [3] L.J. Norrby J. Chem., VV 110 (1991).
- [4] N. Chiera et al., J. Radioanal. Nucl. Chem. 310, 1233 (2016).
- [5] N. Chiera et al., Ann Rep. Lab. of Radio- & Environ. Chem., Univ. Bern & PSI, 1 (2016).

INSIGHTS INTO SURFACE REACTIONS OF ^{211}Pb WITH SiO_2 AND Al_2O_3 ON THE SINGLE-ATOM SCALE

B. Kraus, R. Eichler (PSI & Univ. Bern), A. Türler (Univ. Bern)

The scarce availability of superheavy elements (SHEs) is one of the reasons to prepare their investigations by model experiments with their lighter homologs in the corresponding groups of the periodic table [1]. Based on the observation in these homolog investigations one can deduce expected properties of the superheavy elements and design appropriate experimental setups. Here, we investigate the adsorption properties of Pb as homolog of Fl in a test-setup for isothermal vacuum chromatography (IVAC). The setup uses an alloyed source of Pt^{227}Ac to produce continuously ^{211}Pb , which releases the desired nuclide in high temperature. As chromatographic surface, we offer either fused silica (SiO_2) or aluminium oxide (Al_2O_3). We assumed that these surfaces are inert surfaces and do not show any other interaction but adsorption. The setup was already described in detail in [2, 3].

A thorough analysis of ^{211}Pb interaction with the fused silica surface showed unexpectedly the obvious formation of more than one species with different retention in the chromatography. We observed most likely ^{211}Pb , ^{211}PbO and other yet unidentified Pb-species. Pb and PbO were identified by their estimated $\Delta_{\text{ads}}H$ on SiO_2 . The third species remains unknown, but might be related to the intermediate formation of PbSiO_3 in a surface reaction. Currently, we have the best description by Monte-Carlo simulation of gas adsorption chromatography assuming the following ratio of the contribution of the species to the observed external chromatogram: 0.17 (Pb), 0.35 (PbO) and 0.48 (PbSiO_3). This might not yield the best fit for the experiment, as our simulation does not include reactive interactions with the surface besides adsorption and desorption processes.

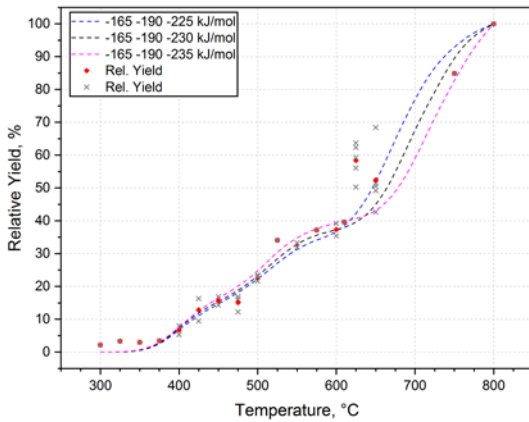
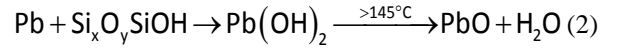
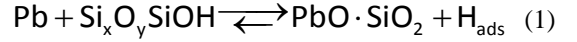


Fig. 1: Breakthrough curve of ^{211}Pb on SiO_2 (x and squares) with overlaying MCS for three different species with apparent ΔH_{ads} of -165 kJ/mol, -190 kJ/mol and the third ranging between -225 kJ/mol and -235 kJ/mol.

As we operate the setup in vacuum ($p \approx 1.7\text{E-}5$ mbar), and have several pieces of Ta in the start oven region, which serves as an oxygen getter at this temperature ($T_{\text{Start}} = 990$ °C), we can most likely exclude gaseous oxygen or water, which react with the ^{211}Pb isotopes. Therefore, the reactants have to be present on the surface of fused silica, even at temperatures above 900 °C. The most probable reactants are hydroxyl-groups on the surface, which are prevalent up to 1200 °C in vacuum conditions.[4] At 900 °C the major part of hydroxyl-groups are removed, but the remaining OH-groups are enough to cover ca. 1.5 % of the available adsorption sites. Upon adsorption of lead atoms, the following reactions might happen [5]:



The reactions 1 and 2 might explain the observations of the formation of ^{211}PbO . The high temperature retention of ^{211}Pb might be explained by reaction 3. Pb and PbO react readily with SiO_2 at higher temperatures and form lead metasilicate (PbSiO_3 ($\text{PbO} \cdot \text{SiO}_2$)). Nonetheless, at ca. 630 °C a back-reaction of $\text{PbSiO}_3(\text{s})$ to $\text{PbO}(\text{g})$ and $\text{SiO}_2(\text{s})$ is taking place. The thermodynamics of the reaction [6] reveals the following:

- $T = 900$ K, $\Delta_{\text{R}}G = 136.5$ kJ/mol
- $T = 1000$ K, $\Delta_{\text{R}}G = 121.1$ kJ/mol

Now, calculating the equilibrium constant K^\ominus with

$$K^\ominus = e^{-\frac{\Delta_{\text{R}}G}{RT}} \Leftrightarrow K^\ominus = \frac{p(\text{PbO})}{p^\ominus} \cdot \frac{p(\text{SiO}_2)}{p^\ominus} \quad (4)$$

As SiO_2 and PbSiO_3 are solids, their partial pressure is 1, resulting in:

$$K^\ominus = \frac{p(\text{PbO})}{p^\ominus} \quad (5)$$

Thus, the expected partial pressure of PbO is for our case at $T = 900$ K and 1000K equal to $p(\text{PbO}) = 1.20\text{E-}5$ mbar and $4.71\text{E-}4$ mbar, respectively (see Fig. 2). This pressure is very close to our operational pressure. This clearly indicates, that the back-reaction is expected to take place in our chromatographic setup at temperatures above 900 K (ca. 630 °C), which is in line with our observations (see Fig. 1).

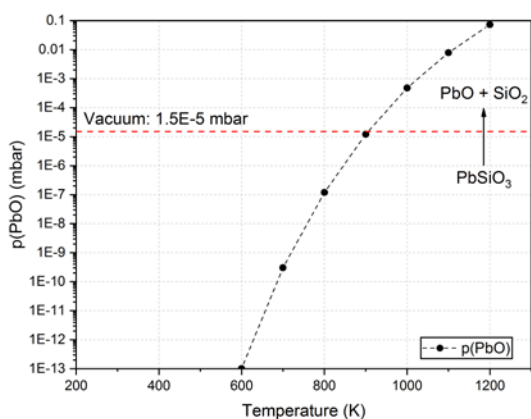


Fig. 2: Partial pressure of PbO(g) as function of temperature to determine the reaction of PbSiO₃ to PbO(g) and SiO₂. The intersection of experimental pressure in IVAC and the calculated partial pressure determines the start temperature of this reaction.

In order to investigate the influence of the surface material on the retention processes Al₂O₃ was used as stationary chromatography surface. Literature hints that we also have to deal with hydroxyl-groups on the surface (partially more stable than on fused silica) and above 500 °C with surface restructuring.[7, 8] The analysis of data is still ongoing, but the preliminary results can be seen in Fig. 3.

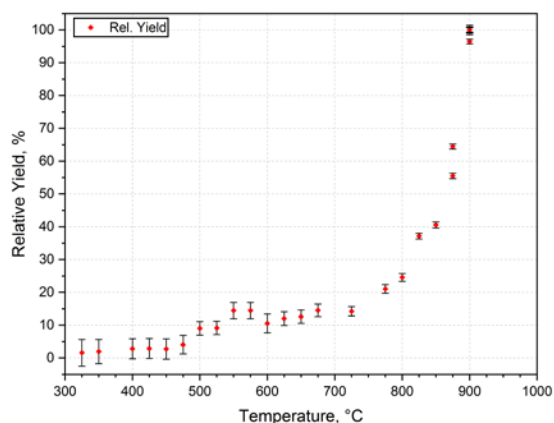


Fig. 3: Relative yield of ²¹¹Pb on Al₂O₃ as function of temperature. After 725 °C an exponential increase is clearly visible. It might be a similar reaction of PbO with SiO₂, but instead with Al₂O₃.

We conclude from our experiments that the use of untreated fused silica surfaces and other oxygen-based ceramics may infer undefined chemical states in chromatography experiments with group 14 elements and flerovium.

Based on these findings, tests with high-temperature non-oxide ceramics and metallic surfaces as alternative stationary surfaces for group 14 elements are envisaged. We suggest using materials such as nitride-based ceramics, e.g. TiN, BN and Si₃N₄, stainless steel or pure metals like Fe, Ni, Au, and Ag, which can be kept metallic at vacuum conditions in the setup.

This work was funded by the Swiss National Science Foundation (Grant no.: 200021_162769).

- [1] M. Schädel, D. Shaughnessy (Eds.), *The Chemistry of Superheavy Elements*, 2nd Ed. Springer (2014).
- [2] B. Kraus et al., *Ann Rep. Lab. of Radio-& Environ. Chem., Univ. Bern & PSI*, 7 (2016).
- [3] B. Kraus et al., *Ann Rep. LRC*, 5 (2017).
- [4] L. T. Zhuravlev, *Colloid Surface A*, **173**, 1 (2000).
- [5] D. E. Starr et al., *Surf. Sci.* **515**, 13 (2002).
- [6] I. Barin, O. Knacke, O. Kubsczewski, *Thermochemical Properties of inorganic substances*, 2nd Ed. Springer (1977).
- [7] Q. Fu et al., *Surf. Sci.* **600**, 4870 (2006).
- [8] M. Digne et al., *J. Catal.* **211**, 1 (2002).

CHALLENGES OF VACUUM CHROMATOGRAPHY WITH FISSION PRODUCTS FROM ^{252}Cf

B. Kraus, R. Eichler (PSI & Univ. Bern), D. Herrmann (PSI), P. Steinegger (JINR), T.K. Sato (JAEA),
A. Türlér (Univ. Bern)

Current gas chromatographic investigations work well with superheavy elements (SHEs) down to a half-life of 1 second. Therefore, vacuum chromatography is investigated to access even the shortest-lived elements and their compounds, e.g. Mc, Lv, and Ts. According to Monte Carlo simulations (MCS) based on Zvara's microscopic kinetic model [1] a subsecond transport of SHEs is possible dependent on the geometric design.

After setting up the isothermal vacuum chromatography (IVAC) (described in [2]) at the Hotlab of University Bern, a ^{252}Cf fission source (ca. $A = 227 \text{ kBq}$, $A_{\text{SF}} = 6.9 \text{ kBq}$) was mounted inside the vacuum chamber of the hot catcher (HC) to maximize the yield of fission product implants into the HC foil. Taking the geometric condition into account a yield of about 2 % was estimated to reach the HC. To validate this estimation we performed catcher foil measurements with aluminum foils in place of the HC mount within the hot catcher volume (HCV). The HCV consists of cylindrical fused silica cylinder with two openings, one to allow fission products (FPs) to enter the HCV, and the other leads to a fused silica chromatographic column. Top and bottom of the cylinder are closed with fused silica caps, and these three parts are held together by a tantalum-made heatshield, leaving the necessary holes open. To close the HCV we put a thin metal window in front of the FP entrance hole. First, we used $4 \mu\text{m}$ Ti and switched later to $3 \mu\text{m}$ Ta in order to assure the integrity of window after being exposed to temperatures above $1300 \text{ }^\circ\text{C}$. Nevertheless, due to the higher density of Ta, this resulted in smaller yield, as more particles are stopped within the window.

Catcher Foil Experiments

The asymmetric fission process of ^{252}Cf produces isotopes mainly in the region of ca. $Z = 95$ to 120 and $Z = 130$ to 155 . [3] The most volatile elements are in the heavier region, e.g. Sb, Te, I, Xe, or Cs. Table 1 shows the most prominent volatile elements and isotopes, which are likely to be investigated together with their sublimation enthalpies being a measure for volatility.

The before mentioned cold catcher foil experiments were carried out using Ti and Ta as window. Both windows yielded a reasonable activity to ensure the detection with γ -spectroscopy (see Fig. 1).

Thermodynamics vs. Kinetics

The most crucial steps determining the yield are related to the diffusion in and desorption from the HC and to the chromatographic retention of the species on the surfaces inside the setup.

Tab. 1: Table of expected volatile elements resulting from ^{252}Cf -fission and their most suitable isotopes for investigation.

Sr ($\Delta_{\text{subl}}H = 164.4 \text{ kJ/mol}$)	Sr-93
Sb ($\Delta_{\text{subl}}H = 262.3 \text{ kJ/mol}$)	Sb-129, Sb-130, Sb-131, Sb-132, Sb-133, Sb-134
Te ($\Delta_{\text{subl}}H = 196.7 \text{ kJ/mol}$)	Te-131, Te-132, Te-133, Te-134, Te-135, Te-136
I ($\Delta_{\text{subl}}H = 106.8 \text{ kJ/mol}$)	I-131, I-132, I-133, I-134, I-135, I-136, I-137, I-138
Cs ($\Delta_{\text{subl}}H = 76.5 \text{ kJ/mol}$)	Cs-137, Cs-138, Cs-139. Cs-140, Cs-141, Cs-142, Cs-143
Ba ($\Delta_{\text{subl}}H = 180 \text{ kJ/mol}$)	Ba-139, Ba-140, Ba-141, Ba-142, Ba-143, Ba-144, Ba-145, Ba-146

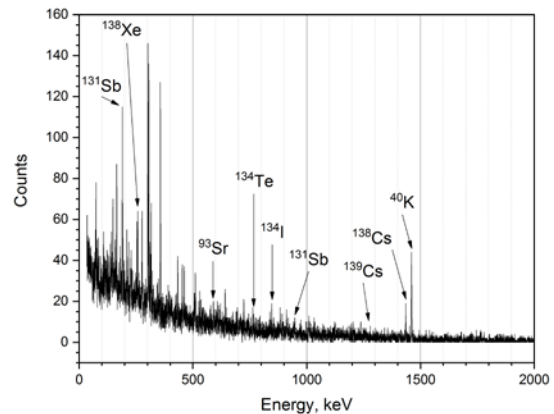


Fig. 1: γ -spectrum of a catcher foil with a $4 \mu\text{m}$ Ti window, $t_{\text{irr}} = 60 \text{ min}$ and $t_{\text{meas}} = 15 \text{ min}$.

Available diffusion data for a few homologs of the FPs [4] require the temperature of the HC to be sufficiently high to ensure the fast diffusion within lifetime of the nuclide (cf. Fig. 2).

When comparing Te to S, the available data shows about one or two orders of magnitude lower diffusion coefficients for Te. Therefore, Fig. 1 clearly shows that Nb and Ta are the only choices for HC material to ensure a fast diffusion in the subsecond region at a sufficiently high temperature (ca. $T/T_m \geq 0.7$).

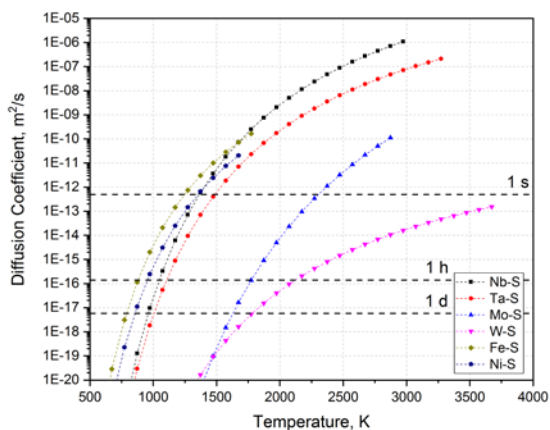


Fig. 2: Diffusion coefficients of S (as homolog of Te) in several metal matrices in dependence of temperature. The indicated times are related to the diffusion coefficients necessary to release sulfur from about 1 μm thick host material.

Based on the Miedema-Eichler model to estimate the adsorption enthalpies of elements on metals [5-10], we established that only some long-lived FPs might have the chance to desorb during their lifetime from the HC.

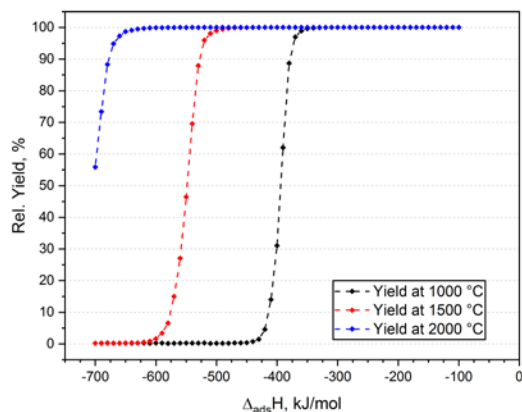


Fig. 3: Monte-Carlo simulation to estimate sufficient desorption at 1000 °C, 1500 °C and 2000 °C at different $\Delta_{\text{ads}}H$ with the nuclide ^{132}Te ($t_{1/2} = 76.3$ h).

Tab. 2: Adsorption enthalpies of FP-elements on Hf and Ta based on the Miedema-Eichler model.

Element	$\Delta_{\text{ads}}H$ on Hf, kJ/mol	$\Delta_{\text{ads}}H$ on Ta, kJ/mol
Sr	-224	-175
Sb	-534	-394
Te	-608	-481
Cs	-99	-37
Ba	-291	-250

Now combining the data from Fig. 3 and Tab. 2, we obtain a rough estimation for desorption of a long-lived species for other elements than Te (cf. Tab. 3).

The results shown in Tab. 3 indicate Ta to be also the

more favorable material for fast desorption of FPs. Nevertheless, a high temperature must be established to achieve high desorption rates.

Tab. 3: Desorption rates of FPs adsorbed on Hf and Ta. The three sub-columns for Hf and Ta show the desorption at 1000 °C, 1500 °C and 2000 °C, respectively.

Element	Desorp. Hf, %			Desorp. Ta, %		
Sr	100	100	100	100	100	100
Sb	0.3	87.9	100	62.0	100	100
Te	0.2	0.9	99.8	0.2	99.7	100
Cs	100	100	100	100	100	100
Ba	100	100	100	100	100	100

Thus, in order to reach the required high temperatures, a thin catcher foil of 6 μm thickness was used. All the inner the chromatographic surfaces have been pre-cleaned before the experiment at high temperatures.

Long-term Measurements

A long-term experiment of 24 h revealed that the achieved temperatures are high enough to desorb all volatile species from the surface of the HC. Further measurements will be carried out in smaller time-scales of 30 min to 2h.

For the first time also a transport of FPs was observed through the chromatography part of IVAC. The preliminary analysis of the γ -spectroscopic results revealed the transport of iodine, cesium and tellurium isotopes and their accumulation on the Ag-foil placed at the outlet of the chromatography column, which was held at 900 °C. The data analysis is ongoing.

This work was funded by the Swiss National Science Foundation (Grant no.: 200021_162769) and we acknowledge the help of Yves Wittwer and Paul Ionescu during the long-term measurement.

- [1] I. Zvara, The Inorganic Chemistry of Heavy Elements 1st Ed. (2008).
- [2] B. Kraus et al., Ann Rep. LRC, 6 (2017).
- [3] Ch. E. Düllmann, et al., NIM A **512**, 595 (2003).
- [4] H. Mehrer, Diffusion in Solids (2007).
- [5] A. R. Miedema et al., J Less-Common Met. **41**, 283 (1975).
- [6] A. R. Miedema, J Less-Common Met. **46**, 67 (1976).
- [7] B. Eichler, ZfK Report 396 (1977).
- [8] B. Eichler et al., Radiochimica Acta **33**, 121 (1983).
- [9] F. R. de Boer et al., Cohesion in Metals: Transition Metal Alloys (1988).
- [10] J. Neuhausen et al., PSI Report 03-13 (2003).

TOWARDS HIGH-TEMPERATURE ALPHA-SPECTROSCOPY SETUPS FOR SUPERHEAVY ELEMENT CHEMISTRY EXPERIMENTS

B. Kraus, R. Eichler (PSI & Univ. Bern), R. Dressler, M. Camarda (PSI/LMN), D. Herrmann (PSI), P. Steinegger (JINR), A. Türler (Univ. Bern), E. Griesmayer, C. Weiss (CIVIDEC)

Superheavy Element Chemistry - The Need for Extraordinary Materials

For superheavy element (SHE) chemistry, gas phase adsorption chromatography is currently the state of the art method to investigate volatile SHEs. The freshly produced elements are typically transported via a flowing gas phase to the detection system.[1] as an example, the Cryo On-Line Detector (COLD) [2] system is an array of several single detectors in a face-to-face geometry (“sandwich”) and placed in way that they form a channel (see Fig. 1).

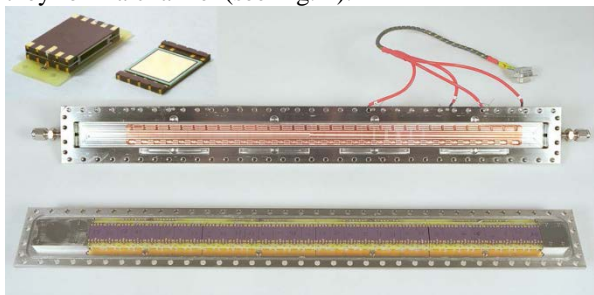


Fig. 1: Sandwich detector and the Cryo On-Line Detector (COLD) channel.

This channel serves as a chromatographic column with a stationary surface sensitive to radioactive decay. The most observed decay modes in the superheavy region are α -decay and spontaneous fission. For the chemical investigation of SHEs, a negative temperature gradient is applied to the detection channel, usually from room temperature to liquid nitrogen temperatures. However, the upper temperature can be set to maximum 40 °C via thermostat as the detectors are Si-based detectors. Silicon has a band gap of 1.1 eV.[3] This means an electron is promoted from conduction band to valence band by infrared radiation and visible light; therefore Si-based detectors have to be operated in darkness and at low temperatures. In order to overcome this hindrance several new materials have been tested in the recent years, e.g. diamond, silicon carbide, gallium nitride. The common property of these materials is that they are wide band gap semiconductors.[4-7]

The Laboratory for Radiochemistry investigated the alpha-particle spectroscopic detection with diamond materials in the past quite successfully [4]. However, the costs of electronic-grade single crystal diamonds were prohibitive so far to build a wide-area detection unit. Recently, silicon carbide is tested as an alternative to diamonds. The first measurements are promising as the offered spectroscopic resolution is nearly the same as of diamond (see Fig. 2), at a price tag being about two to three orders of magnitude less. The next step is the investigation of the high

temperature behavior of SiC, along with some of its electronic properties.

Electronic Grade Single Crystal Diamond

Electronic grade single crystal diamond's band gap is 5.5 eV, so it is wide enough not to be excited even by UV-light. Although these diamonds have superb properties for radiation detection sensors, the current standard production sizes of these electronic grade single crystal diamonds are 4.5 mm x 4.5 mm. It has been shown in previous studies that the temperature limit of diamond detectors is around 200 °C to 300 °C, which is far below the theoretical limit of around 1000 °C.[4, 8, 9]

Silicon Carbide

The 4H-polytype structure of silicon carbide is the material of choice for the production of the desired radiation detectors with a band gap of 3.3 eV.[5] The production of SiC is in the early state of mass production and it is therefore not an issue to supply even 6"-wafers in electronic quality. There have been also many studies [10-15], which tested 4H-SiC sensors, but only a few investigated the high temperature region, one study showed that the signal loss occurred at 375 °C.[16]

Alpha-Spectroscopy

In a first test, SiC was used as α -detector with an CIVIDEC Cx diamond shaping amplifier in front of a triple line source comprised of ^{239}Pu , ^{241}Am , and ^{244}Cm (cf. Fig. 2). The SiC single crystal of 5 x 5 mm² area is prepared by metallizing the surface by flash alloying with a thin layer of Si, Ti, Al and Ni. The structure is glued to a ceramic carrier by a conductive resin and wire-bonded. A bias voltage of 150 V was used.

The achieved resolution is only slightly lower if compared to escCVD diamond detectors (which are in the range of 1.6 to 1.8 % FWHM). In addition, several other bias voltages were investigated in the range from 100 V to 700 V. There was no strong dependence of the energy resolution of the SiC detector on the bias voltage observed. This means, silicon carbide sensors can be an alternative to diamond sensors with nearly equal spectroscopic resolution. A high-temperature experiment setup is now designed [17] and experiments will be performed to show if SiC can really outperform escCVD diamonds for α -spectroscopy at high-temperatures, i.e. UV-VIS-IR light emitting environments.

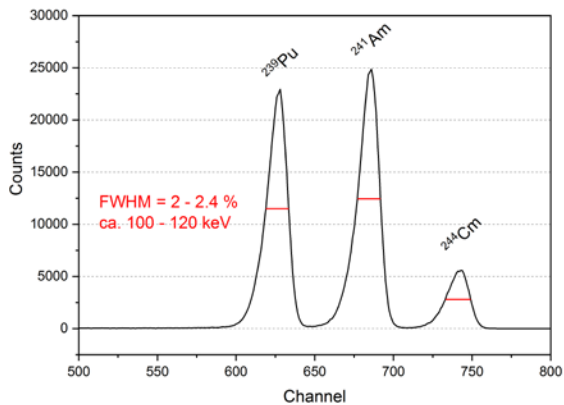


Fig. 2: α -spectrum of a ^{239}Pu , ^{241}Am and ^{244}Cm source, with determined resolution of ca. 100 to 120 keV.

Cleaning of SiC Sensors

In superheavy element chemistry, we investigate adsorption properties and therefore different chromatographic surfaces are needed. Therefore, possibilities were investigated to clean the surfaces of these metallized SiC sensors.

In a small test we submerged different sensors into various solutions, such as H_2SO_4 (conc.), HCl (conc./diluted), KOH , HNO_3 (conc.) and aqua regia.

After a day, only the KOH showed little corrosion, all other solutions were not able to dissolve the alloy. In order to speed up the reaction, we heated the KOH solution under reflux. The corrosion progressed further, but apparently only the Al was dissolved and the rest alloy remained on the surface of the SiC sensor. The acidic solution did not show significant corrosion within a week. Probably the surface passivation of all involved elements offer a strong protection against any chemical attack. The alloy made of Si , Ti , Al and Ni seems to be a very resistant inert compound, which might be a new candidate for stable adsorption chromatographic surfaces, or which might be important for their future use in electrochemistry or in other liquid phase experiments with alpha emitting nuclides including transactinides.

Intermediate Goals – Wide-area Detectors

In case silicon carbide proves to be the better choice the next step would be to envision a wide-area detector for isothermal chromatography (IC). In IC an end detector is needed to measure the external chromatogram. Currently, a plane diamond detector is employed in our vacuum chromatography system. As we want to scale up the dimensions of the column, a larger detection area is needed. Furthermore, we want to utilize other detector geometries to maximize the geometric detection efficiency also for correlated decay chains.

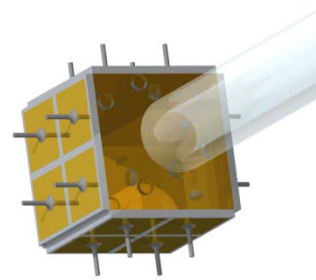


Fig. 3: Cube box detector with a detection efficiency of 92 %, as proposed by Steinegger.

A cube box detector with several pixels would be desirable for vacuum chromatography (cf. Fig. 3). Currently, a column outlet with a diameter of 30 mm needs to be covered by such a cube box detector. This means the dimensions of the detector have to be at least 35 mm x 35 mm x 35 mm. SiC might be an adequate cheaper alternative here to diamond.

This work was funded by the Swiss National Science Foundation (Grant no.: 200021_162769).

- [1] A. Türlér, V. Pershina, *Chem Rev*, **113**, 1237(2013).
- [2] R. Eichler et al., *Angew. Chemie Int. Ed.*, **47**, 3262 (2008).
- [3] W.M. Haynes (Ed.), *CRC Handbook of Chemistry and Physics 96th Ed.* (2015).
- [4] P. Steinegger et al., *NIM A* **850**, 61 (2017).
- [5] F. Nava et al., *Meas. Sci. Technol.*, **19 PP** (2008).
- [6] C. Weiss et al., *NIM A* **732**, 190 (2013).
- [7] J.H. Wang et al., *Appl Phys Rev* **2**, 0301102 (2015).
- [8] A. Kumar et al., *NIM A* **858**, 12 (2017).
- [9] A. Metcalfe et al., *J. Instr.* **12**, C01066 (2017).
- [10] M. Canino et al., *Mater Sci Forum* **483**, 649 (2005).
- [11] S.K. Chaudhuri et al., *NIM A* **701**, 214 (2013).
- [12] K.C. Mandal et al., *IEEE T. Nucl. Sci.* **58**, 1992 (2011).
- [13] F. Moscatelli et al., *Mater Sci Forum* **483**, 1021 (2005).
- [14] F. Nava et al., *NIM A* **510**, 273(2003).
- [15] A. Pullia et al., *Ieee T Nucl Sci* **55**, 3736 (2008).
- [16] E.V. Kalinina et al., *Tech. Phys. Lett.* **34**, 210 (2008).
- [17] B. Kraus et al., *Ann Rep. LRC*, 8 (2017).

OPTIMIZING THE IN-SITU FORMATION OF METAL CARBONYL COMPLEXES

Y. Wittwer (Univ. Bern & PSI), R. Eichler, D. Herrmann (PSI), A. Türler (Univ. Bern)

In 2018, an international research collaboration managed to synthesize the very first transactinide metal carbonyl complex in history, $\text{Sg}(\text{CO})_6$. [1] This outstanding achievement opened a lot of perspectives as $\text{Sg}(\text{CO})_6$ was not only the first chemical compound with a Superheavy Element (SHE) in an oxidation state of zero, but could allow the experimental determination of First-Bond-Dissociation Energies (FBDEs) not only for Sg, but also for Bh, Hs and Mt. Especially from a theoretical perspective [2,3] related to the impact of relativistic effects on chemistry in general, the experimental determination of FBDEs is very interesting. The possible synthesis of a volatile Mt-Carbonyl complex would be the very first chemical investigation of Mt. However the initial hopes were lowered quickly as a follow up campaign targeted at measuring the FBDE of $\text{Sg}(\text{CO})_6$ revealed very low reaction yields for this compound.

This work is dealing with prospects for increasing the yield for $\text{Sg}(\text{CO})_6$ in future experiments as well as opening the path for the successful synthesis of Bh, Hs and Mt-carbonyls. As SHEs have to be produced by nuclear fusion reactions, we successfully constructed a model-system, called FORA, as it was already described in [4] and [5]. In short, a ^{252}Cf -source produces a constant stream of short lived Mo, Tc, Ru and Rh isotopes that are recoiling into a reaction chamber, which is flushed with carbon monoxide. The Mo, Tc, Ru and Rh isotopes serve as models for their corresponding SHE-isotopes. If a recoiling model isotope manages to react with CO, the resulting, volatile carbonyl-complex will be transported out of the reaction chamber by the continuous CO-gas stream until it reaches a charcoal trap, where it will adsorb. The following decay of the radioactive central metal atom can then be measured using γ -spectroscopy, where higher signal-intensities are corresponding to higher yields. The entire system is constructed as a loop, meaning that the used gas mixture is constantly reused during operation.

Using a series of fast measurements, the influence of multiple parameters on the carbonyl-formation reaction is investigated. So far, those include pressure, gas flow rate, gas temperature, various impurities and the usage of various professionally and self-made purification-columns to constantly purify the used gas mixtures in the loop. To our surprise, it appears that especially the last parameter has a very large impact on the metal carbonyl formation yield. Despite various purification columns having the same specifications, it was found that many of them are actively suppressing the formation of metal-carbonyl complexes. Attempts to investigate the cause and mechanism of this effect using mass spectrometry and a series of proposed identification experiments were unsuccessful so far.

The effect may be linked to the formation of carbon, since all affected purification columns showed elemental carbon formation under the applied reaction conditions. On the other hand, it was found that another, smaller set of columns is increasing the yield for the formation of metal carbonyls considerably. Despite the mechanism of this favorable effect also being unknown yet, it may be linked to the occurrence of metallic nickel.

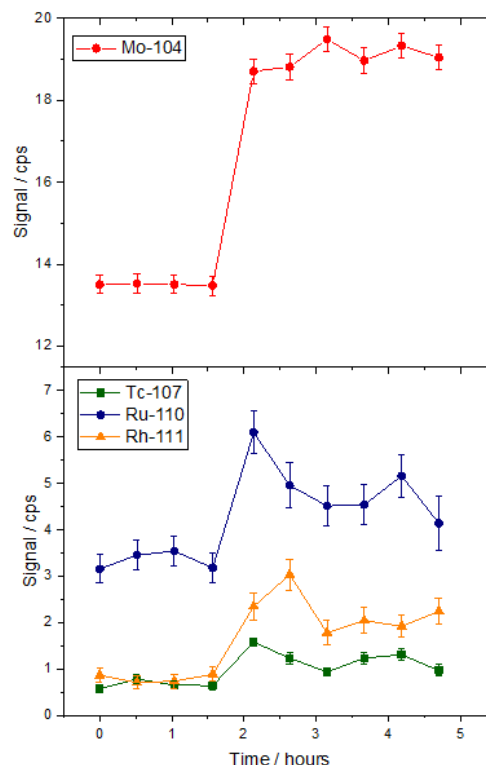


Fig. 1: Yield affected by addition of reduced nickel inserted into the FORA-Setup. Gas composition (100% CO), pressure and gas-flow were constant over the entire experiment. At the 2 hour mark, the nickel-sample was inserted. The lines are for guiding the eye.

Figure 1 illustrates the effect of nickel onto the reaction system. The gas was prepurified using a H_2O -Getter (Sicapent[®]), before a steel-pipe containing a sheet of nickel was introduced into the gas flow at room temperature. The nickel-sample was reduced with H_2 at 1000°C beforehand. For all monitored isotopes, a fast and strong increase of signal can be measured after the insertion of nickel. Unfortunately, FORA is not able to differentiate between different volatile species being produced in its current configuration. Only the amount of volatile Mo, Tc, Ru and Rh species arriving at the charcoal trap under certain conditions can be measured.

The current focus of this work is to increase the quality and reproducibility of our measurements and get a deeper understanding of the mechanisms involved. It appears that there are several practical problems in obtaining experimental data that is representative for the system behavior. In short, the main problems are related to difficulties in varying single reaction parameters independently from each other and a “drift-behavior”, which is basically a slow but constant change in carbonyl-yield despite the reaction system not being recognizably altered, as shown in figure 2.

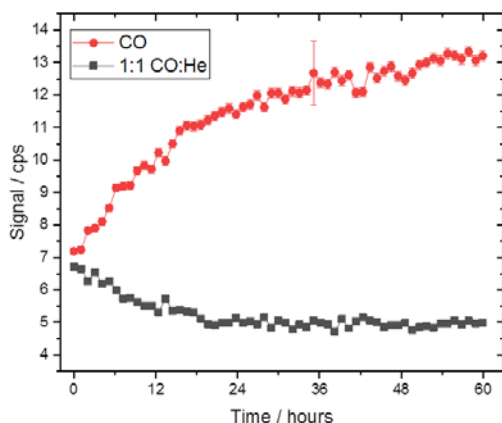


Fig. 2: Change of ^{104}Mo -signal during constant operation of FORA depicted for two different gas mixtures. Pressure and gas-flow were constant over all measurements.

The observed “drift-behavior” is difficult to deal with. Its effect on the yield can be stronger than the effect of actively changed parameters like pressure. Currently, there is no way to avoid these signal drifts. We are relying on long measurement times, pre-purification of the used gases and random repetitions of measurements in order to avoid misinterpretations.

Despite these problems, we think that finalized data should be available very soon. After that, our main focus will shift to experiments targeted at extending the obtained observation to actual accelerator-based systems as they are used in the formation of SHEs and mechanistic studies concerning the influence of impurities, adsorption-effects and the observed yield alterations associated with the occurrence of carbon and nickel. The goal is to obtain a deeper understanding of the processes associated with successfully synthesising metal-carbonyl complexes and provide a “catalogue” of methods to increase yields in further studies using accelerators.

By using a method based on directly measuring the number of recoiling isotopes produced by the ^{252}Cf -fission source, it was possible to deduce absolute yields from the counting rates measured by the γ -spectrometer. The calculated yields are a combination of the chemical yield for the carbonyl formation reaction and adsorption effects during transportation. Unfortunately, the quality of these calculations is strongly limited by the required literature values related to the ^{252}Cf fission yields. Nevertheless, according to our calculations, it is possible to

drastically increase the chemical yields for the synthesis of metal-carbonyl-complexes in general by optimizing the parameters investigated so far. For $\text{Mo}(\text{CO})_6$, the yield-values are currently as optimistic as >90% under well optimized conditions.

Acknowledgement

The work is supported by the Swiss National Science Foundation (200021_162769).

-
- [1] J. Even et al., *Science*, 1491, **345** (2014).
 - [2] M. Ilias et al., *Inorg. Chem.* **56**, 1638 (2017).
 - [3] C. Nash et al., *J. Am. Chem. Soc.* **121**, 10830 (1999).
 - [4] Y. Wittwer, *Ann Rep. Lab. of Radio-& Environ. Chem., Univ. Bern & PSI*, 5 (2016).
 - [5] Y. Wittwer, *Ann Rep. LRC*, 10 (2017).

MASS SPECTROMETRIC SPECIATION OF METAL-CARBONYLS IN THE GAS PHASE

Y. Wang (IMP), Y. Wittwer (Univ. Bern & PSI), J. Zhang, J. Yang (IMP), H. Haba, Y. Komori, T. Yokokita (RIKEN), S. Cao, F. Fan (IMP), R. Eichler (PSI), A. Türlér (Univ. Bern), Z. Qin (IMP)

The study of transactinide elements in the form of metal-carbonyl complexes is still a highly desirable project as it is expected to provide new insight into the chemical properties of these elements and the influence of relativistic effects. However, first investigations of $\text{Sg}(\text{CO})_6$ as well as mononuclear $\text{Re}(\text{CO})_n$, being a model system for $\text{Bh}(\text{CO})_n$, were both strongly hampered by low chemical yields. [1] This makes it necessary to further study the formation of metal-carbonyl complexes under single-atom-chemistry conditions. A modified laser-ablation time-of-flight mass spectrometer (LA-TOF-MS) was used to study the formation of Mo, W and Re carbonyl complexes in a gas mixture of CO and He. By adding varying amounts of O_2 , H_2 as well as O_2/H_2 -mixtures, the impact of impurities on the carbonyl formation was investigated.

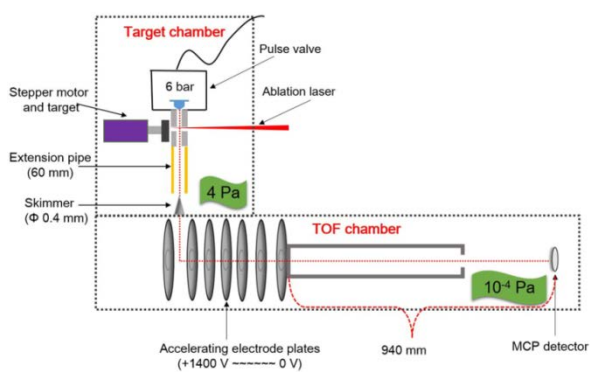


Fig. 1: Schematic diagram of the LA-TOF-MS setup used in this study.

Figure 1 shows the schematic of the LA-TOF-MS setup. Each measurement starts with the pulse valve opening (120 μs), thereby releasing a supersonic gas jet. The gas is directed over the target surface, where an ablation laser (Nd: YAG laser, 532 nm, 10 Hz, 15 mJ/pulse) is inducing a plasma to generate free metal atoms and ions. Some of the plasma is rapidly cooled down by the gas and then transported through a skimmer to a positive electric field, where a short pulsed high voltage is applied (20 μs , 10 Hz, +1400 V). After free drifting, the cations reach a MCP detector and the flight time is measured. From this, the mass of each ion is deduced. An extension pipe (i.d. = 4 mm; length = 60 mm) is added downstream of the metal target in order to increase the reaction time and strengthen the interaction between the generated ions and CO gas, making it possible to identify the most stable products formed.

As expected, $\text{Mo}(\text{CO})_6^+$, $\text{W}(\text{CO})_6^+$, and $\text{Re}(\text{CO})_6^+$ were identified to be the most stable products in He and CO gas mixtures. No intermediates or other significant products could be observed due to the added extension pipe. As shown in figure 2, small amounts of $[\text{MoH}(\text{CO})_6]^+$, $[\text{WH}(\text{CO})_6]^+$, and $[\text{Re}(\text{CO})_5(\text{H}_2)]^+$ were observed when adding 14% of H_2 to the He and CO gas mixtures. However, the hydride ions can be ignored when the H_2 concentration is lower than 0.9%, which suggests that trace amounts of H_2 gas will not strongly influence the formation of these carbonyl ions.

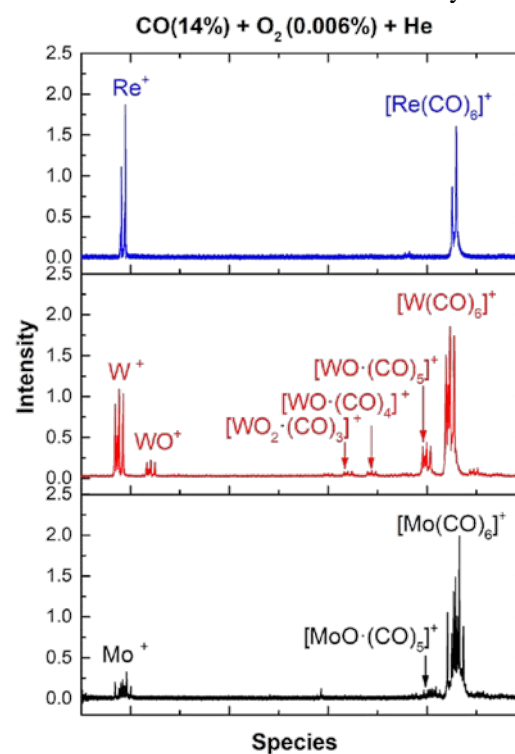


Fig. 2: Mass spectra obtained for the free metals using gas mixtures of 14% CO and 14% H_2 in He.

The mass spectra of Mo, W, and Re carbonyl ions with the addition of O_2 impurities are very similar to the spectra obtained with He and CO gas mixtures including H_2/O_2 impurities, because of the negligible impact of H_2 . As shown in figure 3, by varying the concentration of H_2/O_2 , formation of various oxides is observed, from which an estimate of their affinity towards oxide formation can be given.

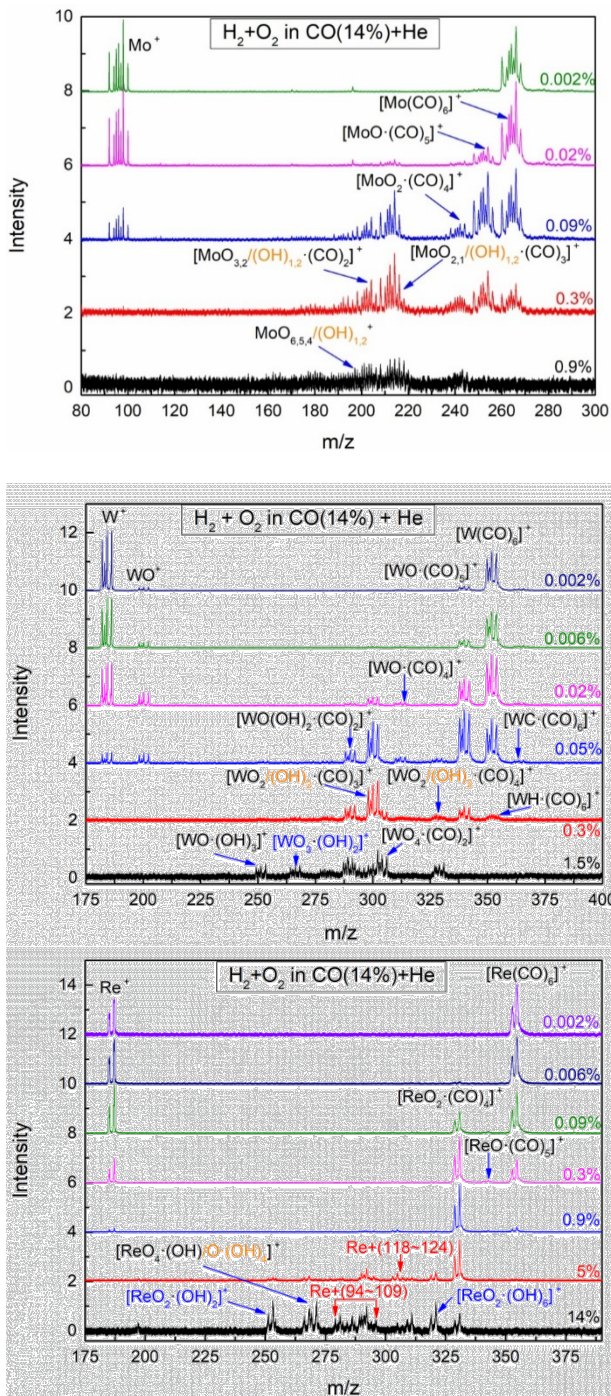


Fig. 3: Mass spectra obtained for Mo, W, and Re using gas mixtures of 14% CO in He. Different amounts of H_2 and O_2 were added to the gas mixture in equal concentrations.

As illustrated in figure 3, the affinity towards oxygen increases in the order $Re < Mo < W$. If the O_2 concentration exceeds 0.9%, basically no pure carbonyls ions can be formed. Significant amounts of $[ReO_2(CO)_4]^+$, $[MoO(CO)_5]^+$, and $[WO(CO)_5]^+$ could be observed when O_2 was more than 0.09%, 0.02%, and 0.006%, respectively. Preliminary studies using the FORA-setup described in [2] imply that also Tc is not very sensitive towards O_2 traces, hinting that Bh may not be strongly affected by O_2 as well, which would be an advantage over Sg, which is potentially

more sensitive towards O_2 than W [3]. Thus, group 6 elements appear to be more prone to form side-products upon addition of H_2/O_2 than group 7 elements.

We conclude that O_2 could indeed seriously impact the formation of metal carbonyl complexes in general, while H_2 should not be a concern. For Mo and W, the formation of side products could be observed at O_2 -concentrations as low as 0.006%, while Re shows significant formation of side products at O_2 -concentrations of 0.09%. The observation of $[Re(CO)_6]^+$ being the most stable species under the experimental conditions applied here is interesting, especially upon addition of H_2 , which was expected to feature $[Re(CO)_5H]^+$ at least partially.

Acknowledgement

This work was performed at the Institute of Modern Physics, Chinese Academy of Sciences (IMP, CAS). This work is supported by the National Natural Science Foundation of China, Grant No. 11675227 and 11079006, and by the Swiss National Science Foundation under contract 200021_162769.

- [1] Y. Wang et al., RIKEN Accel. Prog. Rep. **50**, 25 (2017).
- [2] Y. Wittwer, Ann Rep. Lab. of Radio-& Environ. Chem., Univ. Bern & PSI, 5 (2016).
- [3] B. Eichler et al., J. Phys. Chem. A **103**, 9296 (1999).

MEASUREMENT OF Mn-53 CAPTURE CROSS-SECTION AT n_TOF FACILITY (PART I – TARGET PREPARATION AND EXPERIMENT REALIZATION)

*J. Ulrich, R. Dressler, D. Schumann (PSI)
& the n_TOF Collaboration*

Mn-53 belongs to the group of short-lived ($t_{1/2} < 100$ Ma) cosmogenic radionuclides which are produced in explosive stages of stellar life and is according to calculations one of the major radionuclides produced in core-collapse (type II) supernovae. For better understanding of stellar evolution and cosmological nucleosynthesis, high quality nuclear data on involved isotopes are needed. Unfortunately, very little is known about the half-life and especially the neutron cross-section of Mn-53 at present time; only two values of the capture cross-section at thermal energies are available in the literature, which differ by a factor of more than two [1,2].

The goal of the project is the measurement of neutron capture cross-section of Mn-53 in different neutron energy regions spanning over the whole incident neutron energy range from cold neutron energies (< 9 meV) up to few hundreds keV (s. Fig. 1). These measurements were performed or are ongoing at different beamlines and facilities both at Paul Scherrer Institut (PSI) as well as at other high-grade research institutions (LVR-15 research reactor of ÚJV Řež, n_TOF facility at CERN, LiLit at SARAF). Sufficient amounts of starting Mn-53 material were extracted during the ERAWAST-project [3] and further purified by various radiochemical methods. Unlike to cross-section measurements by the activation method, which give an integrated cross-section value for a particular neutron spectrum, a neutron time-of-flight (TOF) measurement delivers the energy-dependence of the cross-section in a broad energy range, typically from thermal energies to the 100-keV-region at the n_TOF facility.

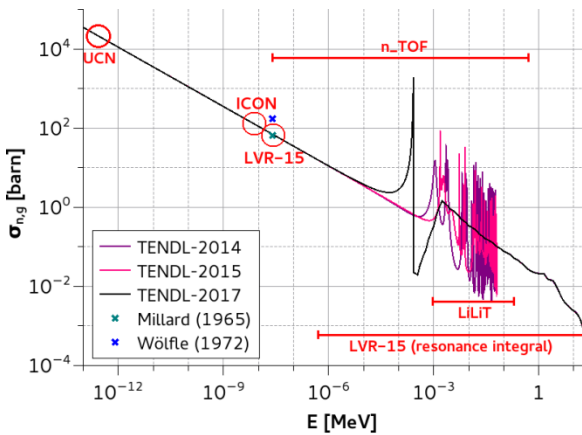


Fig. 1: Mn-53 cross-section: theoretical predictions (lines) [4], and measured thermal values (points) [1,2]. In addition, the energy regions of measurements in frame of our project are marked.

The original proposal for the experiment at CERN assumed that $5 \cdot 10^{17}$ atoms of Mn-53 are mass-separated and implanted into a suitable substrate in the ISOLDE facility and used subsequently as a target for the n_TOF measurement. Unfortunately, this attempt failed; the mass separation at ISOLDE yielded only a sample of about $3.7 \cdot 10^{17}$ atoms Mn-53 due to insufficient efficiency of the used FEBIAD ion source and the cut-down implantation time of only 27 h.

A last-minute-solution was the reprocessing of large amount of waste fractions generated during other Mn-53 related experiments. Finally, this approach made a similar amount of Mn-53 available for the experiment. Due to the missing mass-separation, the Mn-53 to (stable) Mn-55 ratio was around 1:2 for the final sample material, thus requiring production of a second target from stable manganese, which could be used as a reference for the Mn-55 contribution to the signal in the Mn-53 target. Furthermore, there were other contaminants identified on similar concentration levels as Mn, especially alkali and alkali-earth metals coming from the impurities of the used chemicals, which couldn't be removed entirely by chemical treatment during the very short available timeframe.

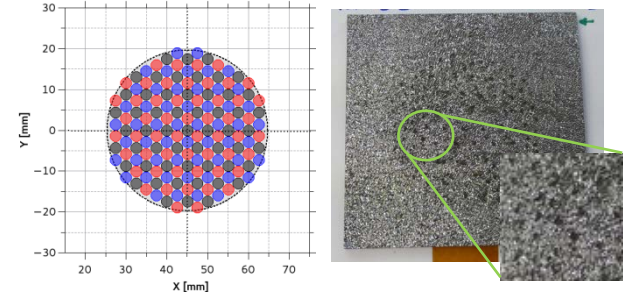


Fig. 2: The droplet pattern, marking the three printing steps by different colors (left) and the black calcinated droplets on the finished target (right).

Two droplet targets were prepared by putting individual $3 \mu\text{L}$ droplets of the respective Mn-53/Mn-55 (sample) or Mn-55 (reference) solutions on $60 \text{ mm} \times 60 \text{ mm} \times 2 \mu\text{m}$ graphene foil (KANEKA), creating a circular pattern with an overall diameter of 40 mm (s. Fig. 2). A hexagonal grid was selected for the droplets to maximize the surface coverage. The “printing” was divided into three steps to minimize the risk of droplets touching each other and merging. The manganese solution was converted to MnO_2 by calcinating the foil for 15 min at 300°C on air in a muffle oven after each step. The calcination step leads to an essential shrinking of the droplets to the final deposit as can be seen on the inset of Fig. 2. A “TOSCA DOSY” dispensing device (Dostal GmbH) mounted on a XYZ-positionable CNC machine was

used to produce the droplet targets in a semi-automated and reproducible way. The assumed material content was $5 \cdot 10^{17}$ atoms Mn-53 for the sample target and $5 \cdot 10^{19}$ atoms Mn-55 for stable manganese target.

The “printed” graphene foils were mounted on a 2 mm thick graphite frame to ensure mechanical stability during preparation and measurement and were additionally covered with a second 2 μm graphene foil. A 5 μm thick double-sided adhesive tape was used to attach the graphene foiles to each other and to the graphite frame. Using pure carbon materials reduces significantly the neutron induced background.

Three additional targets were prepared: a “blank” consisting of just two graphene foils stucked onto the graphite support; and two gold samples (10 μm and 50 μm) by sticking 60 mm x 60 mm Au foils with corresponding thickness onto the graphite support. The purpose of the latter is quality assurance and normalization during the TOF-measurement.

The TOF measurement was performed between 06.08. and 05.09.2018 in Experimental Area 2 (EAR2) of the n_TOF facility. With its flight-path of only 20 m and thus by a factor 40 times higher neutron flux than in EAR1; it is claimed to be the more suitable beamline for thin samples [5]. The targets were mounted on top of the vertical beam-tube with three Bicron C₆D₆ detectors symmetrically arranged around the target (see Fig. 3).

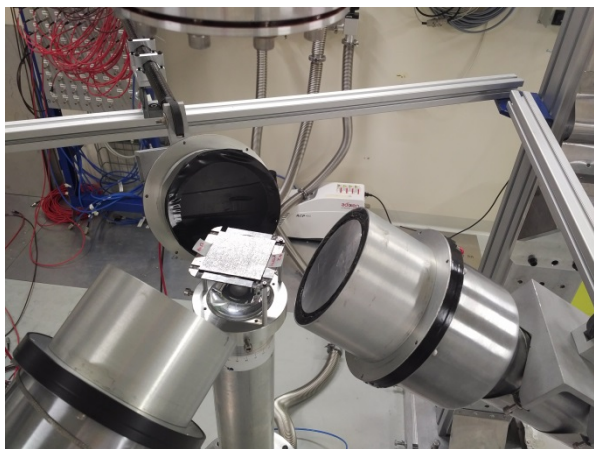


Fig. 3: The end of the vertical beam-line with mounted Mn-53 target and three C₆D₆ detectors.

Approx. $2.9 \cdot 10^{18}$ protons out of the approved budget of $3.5 \cdot 10^{18}$ protons were delivered during the entire experiment campaign; this number was divided between the individual targets in the following approximate manner: 60 % Mn-53 target, 10 % Mn-55 target and 20 % blank measurement; the missing 10 % were used for set-up, calibration and tests of the system. The stability of the detector system during the experiment was periodically checked by measurements with radioactive γ -sources (Y-88, Cs-137, Am-241/Be-9 and Cm-244/C-13) and the the gold foil targets. The system remained perfectly stable over the whole experimental period of 3 weeks; no drifts in gain or resolution were observed and most of the data could be

used for the subsequent analysis (see [6] for more details).

The authors would like to thank Dr. Peter Sprung (AHL/PSI) for the ICP-MS analysis of the materials.

- [1] H. T. Millard Jr., *Science* **147**, 503 (1965).
- [2] R. Wölfle et al., *Radiochim. Acta* **18**, 207 (1972).
- [3] D. Schumann, J. Neuhausen, *J. Phys. G.* **35**, 014046 (2008).
- [4] A. J. Koning, D. Rochman, *Nucl. Data Sheets* **113**, 2841 (2012).
- [5] C. Weiss et al., *Nucl. Instr. and Methods A* **799**, 90 (2015).
- [6] J. Ulrich et al., this report, p. 17.

MEASUREMENT OF Mn-53 CAPTURE CROSS-SECTION AT N_TOF FACILITY (PART II – DATA EVALUATION)

*J. Ulrich, R. Dressler (PSI)
& the n_TOF Collaboration*

This article summarizes the analysis of the data obtained during the measurement of the neutron capture cross-section of Mn-53 in Experimental Area 2 (EAR2) of the n_TOF facility at CERN (details of the sample preparation and the experimental setup are given in [1]). The individual steps of the analysis are summarized on Fig. 1.

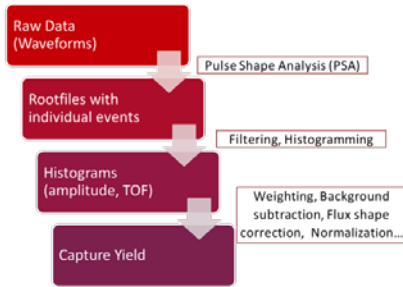


Fig. 1: Essential steps during the n_TOF experimental data evaluation.

The detector signals obtained during the measurements were digitized and the entire waveforms were saved using the SPDevices ADQ412 digitizer. For the extraction of the relevant data (i.e. signal arrival time and amplitude), a large number of individual parameters (20+), required for the pulse shape analysis, was carefully adjusted and optimized for the particular experiment and detector setup. This was done manually on a small number of samples of the measured data; once suitable values were found, the peak data from the whole experiment campaign were extracted in an automated process on the CERN HPC cluster and histogrammed, e.g. creating amplitude or TOF spectra.

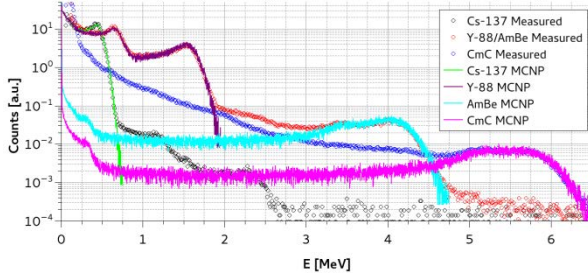


Fig. 2: Comparison between simulated and measured response functions of one detector for calibration sources.

The energy and peak shape calibration of the detectors was extracted by adjusting detector response functions simulated by MCNP v6.2 [2] to the spectra measured with the calibration sources. A model of the experimental setup was built with MCNP consisting of the target and the sample holder as well as the

detectors with their individual positions, angles and filling levels. It was realized during the experiment that the detectors are not tightly sealed and might have lost considerable amounts of the liquid C₆D₆ scintillator by evaporation during the past years. Comparing the absolute efficiencies measured with a Cs-137 calibration source with simulations, the effective scintillator volume of each detector was found to be between 15-20 % of the cavity volume. Finally, very good agreement between the simulated and measured detector responses was achieved, once the proper energy and peak-shape calibration as well as the actual filling level of the detectors were found (see Fig 2).

The total energy technique approach was utilized to overcome the unknown energies and intensities of the prompt capture gammas. The required weighting function for each detector was constructed from MCNP-simulated detector responses to monoenergetic gamma rays of various energies between 0.25 MeV and 10 MeV. The weighting was applied to the measured TOF-spectra and a background subtraction considering both the beam-on background (measured with the dummy sample) as well the ambient background was performed for the Mn-53 and Mn-55 targets as well as the 10 μm Au-foil measurement. A neutron flight path length of 19.48 m was used for the conversion between TOF and incident neutron energy. This value was obtained from the Au measurements fitting the well-known energies of first three Au-197 resonances to the observed peaks in the TOF-spectra.

The outcome of the data evaluation is the capture yield Y , which usually serves as input for further analysis steps, e.g. the cross-section extraction or resonance parameter analysis. Y is given as:

$$Y(E_n) = \frac{C_{W,Netto}(E_n)}{NE_x(E_n)\phi(E_n)}$$

where $C_{W,Netto}$ is the background-corrected, weighted TOF-spectrum (normalized to proton count), E_x the compound nucleus excitation energy (sum of the neutron separation energy of the product and the captured neutron kinetic energy), ϕ the neutron fluence spectrum (normalized to proton count) and N a normalization constant. The normalization N is typically found by the saturated resonance technique, i.e. measuring a thick absorber in similar geometry as the sample to reach saturation of one or more resonances and choosing N so that $Y = 1$ in the saturated region. Unfortunately, neither with the 10 μm nor with the 50 μm Au foils saturation could be reached, so this final normalization step was not possible. Fig. 4 shows the capture yields for the 10 μm Au foil, the Mn-55

target and the Mn-53 target. Whereas the expected cross-section shape is clearly visible for Au, the Mn-55 capture yield exhibits only the first resonance of Mn-55 at ~ 300 eV. Unfortunately, only the noise band is observed for Mn-53 making any further analysis of the data meaningless due to the unexpected high background. The availability of a rudimental background estimate prior to the experiment, e.g. from previous experimental campaigns or dedicated background measurements, could prevent such issues and guarantee sound data.

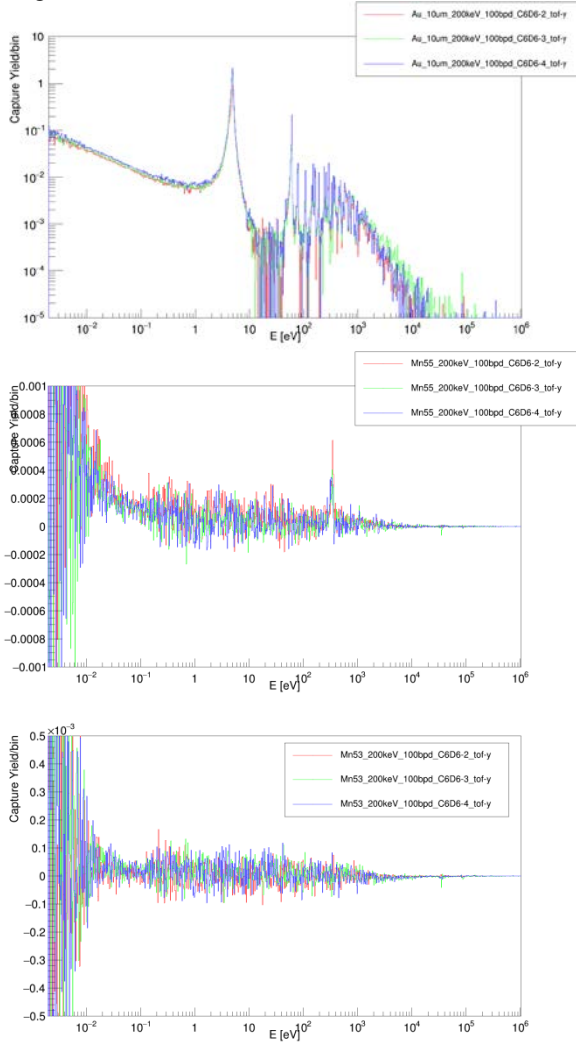


Fig. 3: The capture yields for 10 μm Au foil (top) as well as Mn-55 (middle) and Mn-53 (bottom) plotted independently for the three C_6D_6 detectors.

Using the neutron flux spectrum at EAR2 [3], the estimated atom counts of the targets and the cross-sections of Mn-55 and Mn-53 (utilizing TALYS-2015 predictions [4]), the actual Mn-53 signal strength during the experiment was estimated by anchoring the top of the first Mn-55 resonance to the respective peak on the weighted TOF-spectrum (see Fig. 4). It is clearly seen that the Mn-53 sample should contain at least about two orders of magnitude more Mn-53 (i.e. about the same level as the stable Mn-55 sample) to deliver usable output under these experimental conditions.

For fast assessment of feasibility of a future capture measurement with similar setup at EAR2, the product

of the usually well-known thermal cross-section and the number of atoms of the target build a “figure-of-merit” (FOM) which can be used. Based on the data from this experiment, a FOM $\sim 10^{21}$ atoms·barns (corresponding to the Mn-55 target) can be seen as an absolute minimum for a successful experiment. FOM $\sim 10^{21}$ (corresponding to 10 μm Au-foil, equivalent to $8.3 \cdot 10^{18}$ atoms) delivers a very clear signal even with reduced measurement time, but such material amounts might not be available in case of rare radioactive isotopes, such as Mn-53 in the near future.

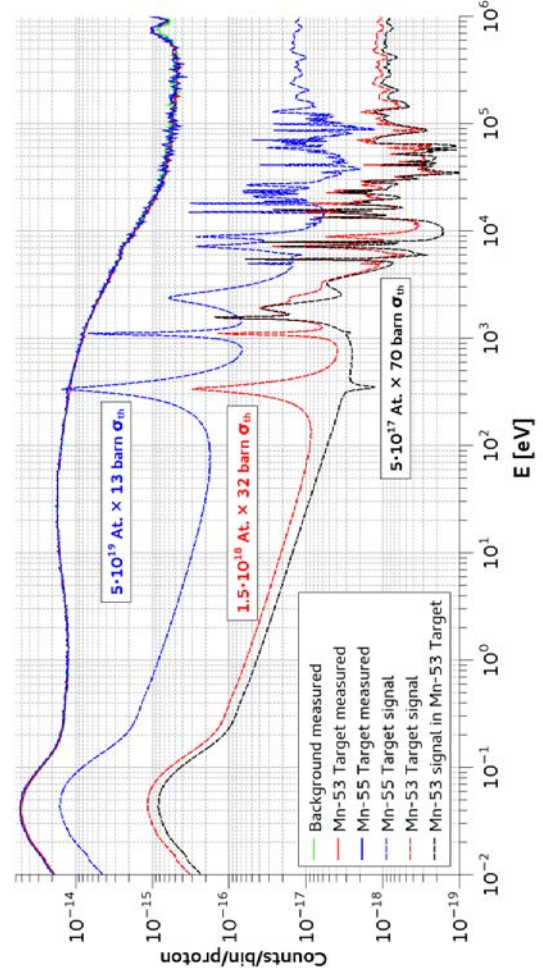


Fig. 4: *A posteriori* signal strength estimation for the Mn-53 target. The Mn-55-target signal (blue dashed line) is scaled to overlap with the visible “bump” of its measured TOF spectrum (solid blue line). The signal estimates for Mn-53 (black dashed) and the Mn-53/Mn-55 mixture (red dashed) are related to the Mn-55 signal taking into account the ratios between cross-sections and atom counts in the different targets.

- [1] J. Ulrich et al., this report, p. 15.
- [2] C. J. Werner et al., MCNP6.2 Release Notes, LANL, LA-UR-20808 (2018).
- [3] M. Sabaté-Gilarte et al., Eur. Phys. J. A **53**, 210 (2017).
- [4] A. J. Koning, D. Rochman, Nucl. Data Sheets **113**, 2841 (2012).

DESIGN AND CONSTRUCTION OF MULTICHANNEL HVPS FOR PHOTOMULTIPLIER TUBES AT LRC

J. Ulrich, R. Dressler, D. Herrmann (PSI)

In the present time a consecutive phaseout from generally usable, modular, analog standard NIM-electronics to compact single purpose devices utilizing digital signal processing hardware takes place. As example one of the main suppliers of nuclear measurement electronics, Mirion Technologies (Canberra) GmbH stopped completely the production and selling of NIM-electronic modules in April 2018. Therefore, the replacement of such modules with alternative devices must be performed at LRC in the near future as the currently used NIM modules reach their end of life.

In the course of the setup of different measurement systems at LRC utilizing photomultiplier tubes (PMT), design and realization of a standalone high voltage power supply (HVPS) was started. PMTs represent well-established and versatile tool to amplify the light output of solid or liquid scintillation radiation detectors.

The main focus was given to the following requirements:

- ≥ 2000 V output voltage with positive polarity
- High currents (few mA) for supplying PMTs
- Low electrical noise of the output voltage
- 3-4 independent HV channels per device

Although there are appropriate devices available on the market, development of own design was pursued due to their high price point.

Fig. 1 shows the schematics of the circuit for single HV channel. The needed 12 V DC power is generated by Daitron LFS series low-ripple noise switching power source from the 230 V AC mains. The HV voltage is generated by the Hamamatsu C9619 series module, with maximum rating of +2000 V and 2 mA. Following the manufacturers recommendation, the 12 V power input is HF-decoupled by a large electrolytic capacitor and small ceramic capacitors (C1 and C2). The ripple noise of the output is additionally reduced with a foil capacitor (C3) on the load side of the HV module. A schottky-type diode D1 is used as rectifier on the 12 V input and an NTC-thermistor TH1 protects the circuit against high inrush currents.

A LED (D2) signals the power status of the HV module. The output voltage of C9619 is regulated by adjusting the control voltage on pin 3 of the module using a precision 10-turn potentiometer (RV1) connected to the module's 5.2 V reference voltage source. The control voltage is monitored by a programmable volt-meter and converted to the output voltage by the stored calibration. Alternatively, the control voltage can be read by a multimeter on

corresponding test points. A thermofuse F1 protects the voltmeter.

The PCB design was developed with emphasis on simple assembly and maintenance as well as modularity. The control and display elements (switch, LED, potentiometer, voltmeter and the control voltage testpoints) are connected to the PCB using moxex-type connectors. The board was designed using the KiCAD EDA software, produced in small series by a professional PCB manufacturer and assembled at LRC.

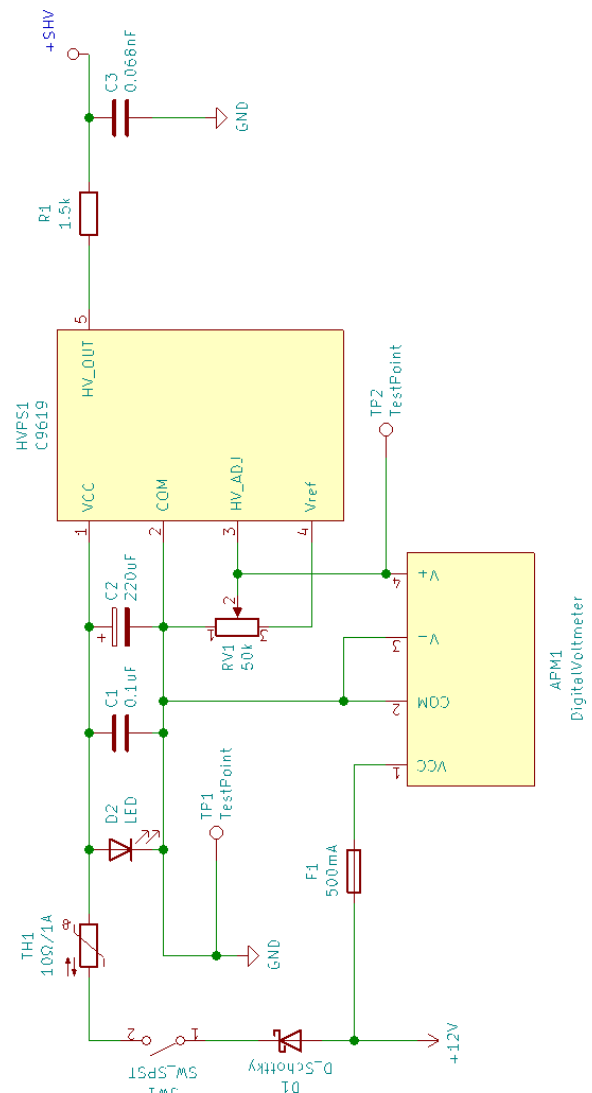


Fig. 1: Schematics of the circuit integrating the Hamamatsu C9619 HV module.



Fig. 2: Front panel (top) and rear panel (bottom) of the HVPS unit integrating 3 HV channels in 19" chassis.

A chassis was designed and manufactured using CNC machining at PSI. With the current design, 3 HV modules with all necessary controls and one 12 V power supply fit in a single 2U 19" rack mountable enclosure (s. Fig. 2). The controls of the power modules are on the front panel. The back panel contains SHV-type plugs for the high voltage output and 4 mm banana jacks to easily monitor the control voltage with external voltmeter. Low-RPM 60 mm fan on the rear prevents overheating.

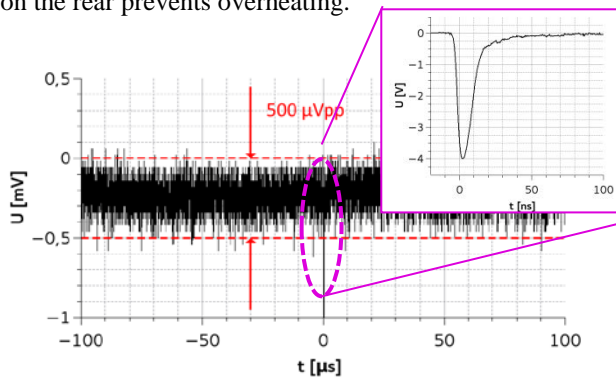


Fig. 3: Baseline of a PMT signal using the designed HVPS with a Hamamatsu R331 PMT and E5859 base. Only very low random noise in the order of $500 \mu\text{Vpp}$ is observed. In comparison, the magnitude of real signals is few volts (see inset).

Initial tests verified the correct electrical functionality of individual boards and of the assembled multi-board setup. The ripple noise of HV output cannot be measured directly with equipment available at LRC. Nevertheless, investigating signals from a PMT connected to the designed HVPS-board with an oscilloscope shows random baseline oscillations on the very low level of $500 \mu\text{Vpp}$ (see Fig. 3) and no visible harmonic frequencies over the whole frequency range.

PRODUCTION AND SEPARATION OF PROMETHIUM ISOTOPES 143-148

*J. Ulrich (PSI), S. Braccini, T.S. Carzaniga (AEC-LHEP & Univ. Bern),
N.P. van der Meulen (PSI/LRC & ZRW), R. Dressler (PSI)*

For purposes of high-resolution optical spectroscopy studies at University Mainz [1] a sample was desired containing a mixture of multiple promethium ($Z = 61$) isotopes with atom masses lower than the most common Pm-147. Especially interesting for the studies was the isotope Pm-143 with a closed neutron shell ($N = 82$).

From a practical point of view, the isotopes Pm-143 to Pm-147 and Pm-148m exhibit half-lives long enough to enable production, separation and measurement as well as transporting between the institutes within a realistic time schedule. As a rule of thumb, around 10^{12} atoms of particular promethium isotope are needed for a successful spectroscopical measurement at the RISIKO mass separator at University Mainz. Furthermore, the maximum impurity of the sample material with other lanthanides is not allowed to exceed 1000 times the amount of promethium. This demands both efficient production pathway and selective subsequent chemical separation method from the starting material.

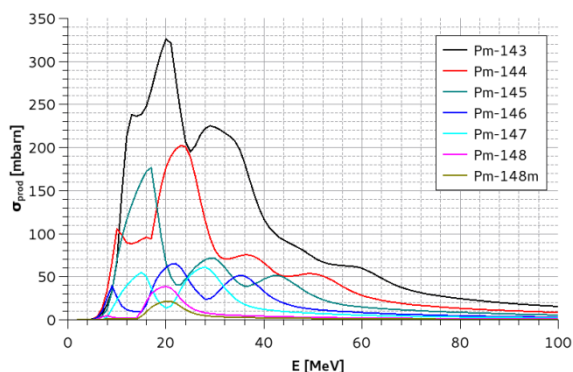


Fig. 1: Predicted cross-sections for production Pm-143 to Pm-148 with protons in natural neodymium. The peak shapes result from convolution of individual reaction channels of different Nd-isotopes yielding the same Pm-product.

Unlike Pm-147, lighter promethium isotopes cannot be produced by reactor neutron activation due to lack of corresponding β -active neodymium precursors. However, the large number of stable neodymium isotopes can be exploited by proton activation. The production cross-sections of Pm-143 to Pm-148 from natural neodymium were calculated using the TALYS v1.9 code [2] for proton energies up to 100 MeV (see Fig. 1). The predictions suggest a mixture of all longer-lived promethium isotopes in comparable amounts can be obtained.

Since the utilization of the PSI proton cyclotron facility (HIPA) was not possible in the requested

timeframe, collaboration was established with University of Bern and irradiation was scheduled using the 18 MeV proton cyclotron at Inselspital Bern. As shown in Fig. 1, energies <20 MeV are well suited for production of Pm-143 to Pm-148, since all production cross-sections, dominated mostly by (p,n) and (p,2n) channels from respective Nd-target nuclei, have their maxima around 20 MeV.

The irradiation target consisted of natural Nd_2O_3 powder (Aldrich, 99.99%) mixed with graphite powder in 3:1 mass ratio and pressed to a pellet with 10 mm diameter and 0.65 mm thickness. The mass of the pellet was 113 mg. The addition of graphite was necessary for mechanical reasons since pellets pressed from pure Nd_2O_3 couldn't be extracted undamaged from the punch-and-die tool due to their high brittleness. For the irradiation, the pressed pellet was put into an aluminum sample holder ("coin") with front window thickness of 0.3 mm. The target pellet and the "coin" are shown in Fig. 2. The target assembly was irradiated with $\sim 4 \mu\text{A}$ of 18 MeV protons for 3 hours, yielding an accumulated dose of approx. $12 \mu\text{Ah}$. The induced activity of promethium isotopes was roughly assessed by gamma spectroscopy after sample delivery at PSI and is summarized in Table 1. It shows that the material quantity requirement is fulfilled for the isotopes Pm-143 to Pm-146, whereas for mass number 148 (sum of Pm-148 and Pm-148m), the produced amounts lie slightly below the envisaged 10^{12} atoms. Pm-145 and Pm-147 were not visible in the gamma spectrum, due to their low gamma ray emission probabilities, but are assumed to be present in the sample in amounts in the order of 10^{12} atoms as well.



Fig. 2: Pressed Nd_2O_3 /Graphite pellet with clearly visible heterogenous structure (left). The opened "coin" irradiation target holder (right, courtesy of AEC-LHEP, Univ. Bern).

The target was carefully removed from the "coin" and leached with 2 mL 7 M HNO_3 . The lanthanide-containing solution was separated from the undissolved graphite remains by centrifugation and filtration, evaporated to dryness under nitrogen gas stream and redissolved in 2 mL MilliQ H_2O . To enable

tracing of the neodymium fraction during the radiochemical separations, 220 kBq of Nd-147 ($t_{1/2} = 11$ d) were produced by activating 12 mg of natural Nd_2O_3 in the research reactor of Univ. Mainz and delivered to PSI shortly before the separation. The dissolution procedure of this material was identical to that of the Pm-containing sample.

Tab. 1: Activities and amounts of produced promethium isotopes measured via gamma spectroscopy.

Isotope	Activity [kBq]	Atoms [$\times 10^{12}$]
Pm-143	71	2.4
Pm-144	100	4.5
Pm-146	8.1	2.1
Pm-148	140	0.097
Pm-148m	22	0.74

The separation was performed by ion exchange chromatography using approx. 45 mL of SYKAM strong cation exchange resin (18% cross-linked) in a 1 cm diameter glass column according to the method described in [3]. Prior to separation, the resin was washed with 100 mL 7 M HNO_3 and 100 mL MilliQ H_2O , transformed into the ammonium-form with 100 mL 1M NH_4NO_3 solution and rinsed again with 100 mL MilliQ H_2O . The separation was performed in two independently, but identically treated batches, each processing roughly half of the starting material. 1 mL of sample solution and 1 mL of the tracer solution were combined, diluted with MilliQ H_2O and adjusted to pH to 3.5-4 with NH_4OH , giving a total volume of approx. 30 mL. This solution was applied onto the column where Nd was retained in the top 4 mm of the resin, clearly visible as a violet band. The elution was started with 0.2 M α -HIBA solution at a flow rate of 0.5 mL/min. The initial fraction volume of 20 mL was reduced to 10 mL as soon as the purple neodymium band moved close to the bottom of the column. The neodymium and promethium content in each fraction was monitored by gamma spectroscopy. Fig. 3 shows the recorded chromatogram of the second separation; clear baseline separation of the Pm and Nd elution peaks was achieved. After the Pm-elution was completed, the α -HIBA concentration was increased to 0.25 M to speedup the Nd-elution. Subsequently, the column was washed with 7 M HNO_3 to remove all other possible impurities from the resin.

The Nd content was measured in each Pm-containing fraction individually, using MC-ICP-MS and was determined to be ≤ 1 ppb, giving a Nd:Pm ratio of ca. 50:1 for both batches, thus, surpassing the requirements of the spectroscopy measurements by a factor of 20. For this calculation, only the gamma spectroscopically quantified Pm isotopes (see Table 1) were taken into account, i.e. the actual Nd:Pm ratio was substantially lower. A decontamination factor of approx. 600 000 between the neighbouring lanthanides promethium and neodymium was achieved during the separation.

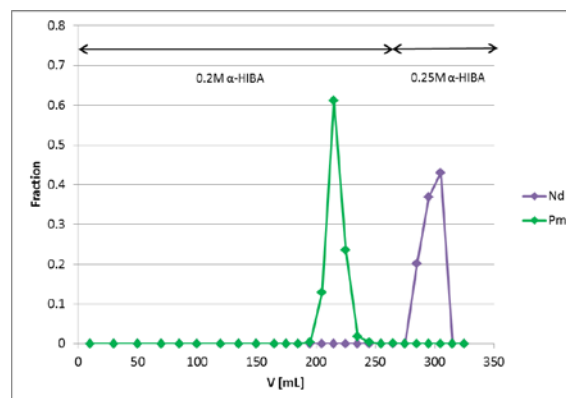


Fig. 3: Elution peaks of Pm and Nd during the separation of second batch. Gamma-ray spectroscopy was utilized for monitoring the Pm and Nd elution, using the gamma-ray lines of Pm-144 (697 keV) and Nd-147 (531 keV), respectively.

Subsequently, the selected product fractions were concentrated on LN chromatographic resin (TrisKem), reducing the volume of the product by factor of 12 and removing the α -HIBA complexing agent. Each fraction was acidified to pH ~ 2 with HNO_3 and applied onto a 2 mL LN-resin plastic column, preconditioned with 0.01 M HNO_3 . After washing the column with 15 mL 0.01 M HNO_3 and 20 mL MilliQ H_2O , the lanthanides were eluted from the column with 5 mL 7 M HNO_3 . The solution was evaporated to dryness and redissolved in 30 μL 1 M HNO_3 , corresponding to the chemical form and volume requested for the spectroscopy measurements.

The authors would like to thank Dr. Peter Sprung (AHL/PSI) for the ICP-MS analysis of the samples and Dominik Studer (Univ. Mainz) for the production and delivery of the Nd-147 radiotracer.

- [1] D. Studer et al., this report, p. 43.
- [2] A. J. Koning et al., Proceedings of the International Conference on Nuclear Data for Science and Technology, 22-27/04/2007, Nice, 211.
- [3] S. Heinitz et al., *Radiochim. Acta*, **105**, 801 (2017).

RADIOCHEMICAL SEPARATION OF LANTHANIDES FROM p-IRRADIATED Ta TARGETS, TOWARDS HIGH-PRECISION HALF-LIFE MEASUREMENTS

Z. Talip, D. Schumann (PSI)

INTRODUCTION

Long-lived lanthanide isotopes are unique material for astrophysical studies with a high impact to understanding the nuclear processes of the element synthesis in the lanthanide region. However, the half-lives of these radionuclides are not known precisely (Tab. 1).

In this study, radiochemical separation of sufficient amount of these radionuclides from highly activated metallic tantalum pieces (Fig. 1) from the second PSI SINQ Target Irradiation Program (STIP II) [1], was developed/optimized to perform a high precision half-life measurements.

Tab. 1: Lanthanides of interest with their half-life and uncertainty.

Radionuclide	Half-life
^{137}La	60 ± 20 ky
^{146}Sm	103 ± 5 My
^{148}Gd	74.6 ± 3 y
^{150}Gd	1.78 ± 0.8 My
^{154}Dy	3 ± 1.5 My
^{157}Tb	71 ± 7 y
^{158}Tb	180 ± 11 y

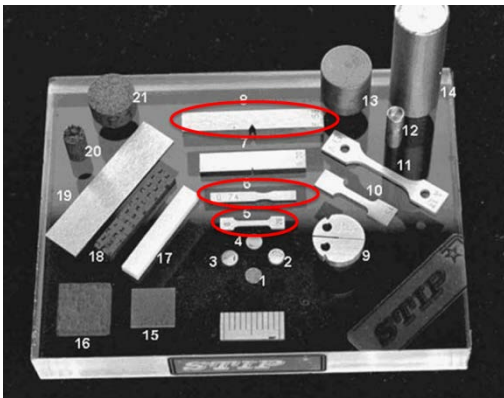


Fig. 1: Picture of the irradiated target materials in STIP II program (bend, charpy and tensile samples are shown in red circles).

EXPERIMENTAL

Table 2 lists the Ta targets. In this study, 3 bend and 1 tensile samples were treated. IB55 tensile sample was dissolved in 4 mL 10 M HNO_3 and 4 mL conc. HF. Then, 1 mg of Lu carrier (Sigma-Aldrich Lu standard for ICP) was added. The solution was centrifuged and

the LnF_3 precipitate separated from the supernatant. It was washed three times with 5 mL of water. A solution of 4 mL 10 M HNO_3 and 4 mL conc. HF only partially dissolved the bend samples. However, without adding additional Lu carrier, precipitation of LnF_3 was observed. The supernatant was removed and transferred to another centrifuge tube. The remaining part of the target was dissolved in additional HNO_3 and HF. The schema of LnF_3 precipitation from the bend samples is presented in Fig. 2.

Tab. 2: The list of the Ta targets (dissolved targets were shown in bold).

Sample ID	Type	Sample ID	Type
IB1	charpy	IB11	bend
IB2	charpy	IB16	bend
IB3	charpy	IB17	bend
IB4	charpy	IB18	bend
IB5	charpy	IB19	bend
IB6	charpy	IB20	bend
IB7	charpy	IB22	bend
IB8	charpy	IB24	bend
IB55	tensile		

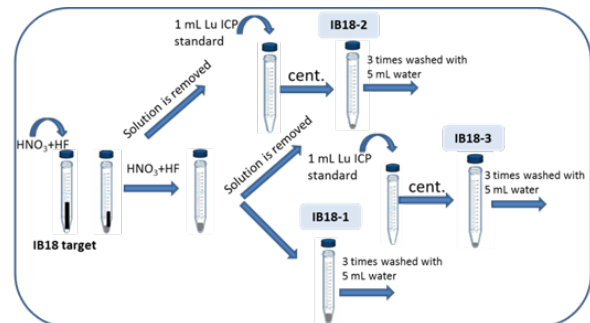


Fig. 2: Lanthanides separation procedure (IB18-2 and IB18-3 samples contain 1 mg Lu carrier).

Fractional lanthanides separation test experiments were performed with Aminex and Sykam cation exchange resins. Chemical separations were monitored by short-lived γ -emitter lanthanides. Then, Sykam resin was chosen to be used for the lanthanides separation of IB18-3 sample (Fig. 3).

PRODUCTION CROSS SECTIONS OF LONG-LIVED RADIONUCLIDES IN PROTON-IRRADIATED TUNGSTEN

Z. Talip, R. Dressler, D. Schumann (PSI),
J.C. David (Irfu CEA & Univ. Paris-Saclay), C. Vockenhuber (ETHZ)

INTRODUCTION

In this study, proton-irradiated W targets up to 2.6 GeV were investigated for the purpose of the cross-sections determination. Tungsten is the foreseen target material of the European Spallation Source (ESS, Sweden), which is going to be the world's most powerful neutron source [1, 2].

Reliable cross section data of the radionuclides produced in target materials are essential for the safety assessment of such facilities. Especially long-lived and volatile radionuclides are of special interest for the decommissioning and accidental conditions. In addition, these data are important to evaluate and improve the existing computer simulation codes.

Radiochemical separation methods for the separation of the long-lived β -emitters ^{129}I , ^{36}Cl , and α -emitters ^{154}Dy , ^{148}Gd from proton irradiated W targets were reported in the previous report [3]. The $^{129}\text{I}/^{127}\text{I}$ and $^{36}\text{Cl}/^{35}\text{Cl}$ ratio measurements were performed at ETH Zurich (Laboratory of Ion Beam Physics) with the 0.6 MV TANDY and the 6 MV EN TANDEM Accelerator Mass Spectrometry (AMS) facilities, respectively [4]. Molecular plating technique was used to prepare thin lanthanides samples to obtain a good quality α -spectrum with high resolution and small low energy tail contribution [5].

The experimental results were compared with theoretical studies and calculations obtained with the combination of Liège intra-nuclear cascade (INCL++) [6, 7] and de-excitation phase (ABLA07) codes [8].

Production Cross Sections

^{129}I and ^{36}Cl

Cumulative cross sections of ^{129}I and ^{36}Cl were calculated with the following equation ($^{36}\text{Cl}/^{35}\text{Cl}$ ratios were converted to $^{36}\text{Cl}/\text{Cl}$ ratios by applying the conversion factor 0.7577);

$$\sigma = \frac{R_c R_s N}{R_r N_t \phi t_i} \quad (1)$$

where R_c is the nominal isotopic ratio in reference standard (the nominal $^{36}\text{Cl}/\text{Cl}$ ratio of the internal standard is $17.36 \pm 0.35 \times 10^{-12}$ (K382/4N) [4], R_r is the measured isotopic ratio in reference standard, R_s is the measured isotopic ratio in the sample, t_i is the irradiation time, N_t is the number of target atoms, ϕ is the proton flux density.

^{148}Gd and ^{154}Dy

Cumulative cross sections of $^{\text{nat}}\text{W}(p,x)^{148}\text{Gd}$ and $^{\text{nat}}\text{W}(p,x)^{154}\text{Dy}$ were deduced by using α -spectrometry results with equation 2;

$$\sigma = \frac{\lambda C e^{\lambda t_w}}{N_t \phi (1 - e^{-\lambda t_i}) (1 - e^{-\lambda t_c}) \epsilon I Y} \quad (2)$$

where λ is the radionuclide decay constant, C is the number of observed counts, t_w is the time between irradiation and counting, t_i is the irradiation time, t_c is the counting time, N_t is the number of target atoms, ϕ is the proton flux density, ϵ is the detector efficiency, I is the branching ratio and Y is the total chemical yield.

Main uncertainty components considered for the cross section calculations are due to the flux density (6%).

AMS measurement results showed that cross contaminations during sample preparation should be taken into consideration. Therefore, blank corrections were performed for all the samples. Only the data, which have values significantly higher than blanks were used for the cross-section calculations (Fig 1).

The comparisons of the experimental and theoretical cross section results showed a satisfactory agreement for the ^{36}Cl and ^{148}Gd (Fig 2 and 3). It was clearly shown that radiochemical separation has a high impact on improving the accuracy of the results. Similar to the previous studies with Pb and Ta targets [5, 9], theoretical ^{154}Dy cross sections data were underestimated (Fig 4), which could be due to the high uncertainty of the accepted half-life of ^{154}Dy (3 ± 1.5 My). However, it is difficult to explain the observed high cross section results of ^{129}I compared to the theoretical calculations.

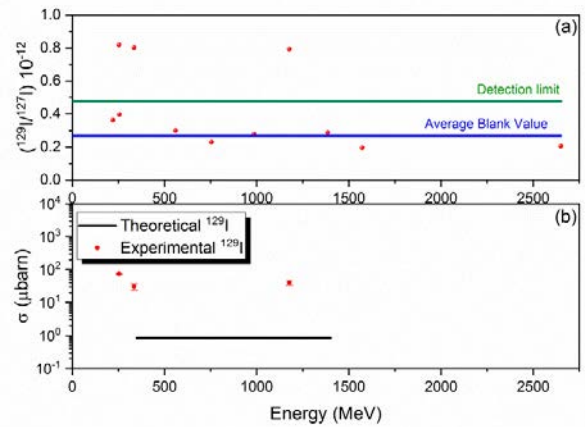


Fig. 1: Results of the AMS measurements without blank correction (a), experimental and calculated excitation function of ^{129}I production in W (b.)

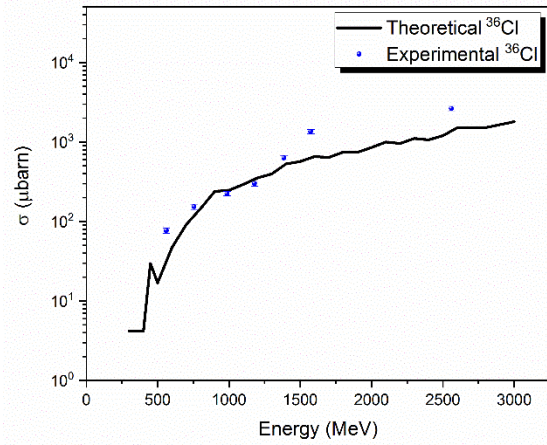


Fig. 2: Experimental and calculated excitation function of ^{36}Cl production of in W.

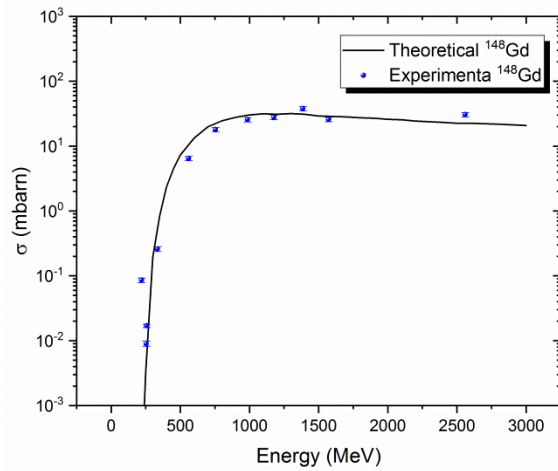


Fig. 3: Experimental and calculated excitation function of ^{148}Gd production in W.

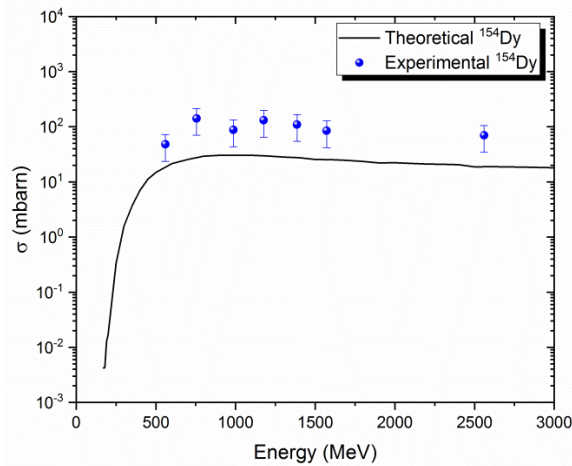


Fig. 4: Experimental and calculated excitation function of ^{154}Dy production in W.

To increase the accuracy of the experimental cross-section data more precise half-life measurements are required. In the follow up project (ERAWAST II), high precision half-life measurements of ^{154}Dy and ^{148}Gd are going to be performed, which will also help to improve the accuracy of these cross-section data.

Then, cross section results (σ) of ^{148}Gd and ^{154}Dy will be re-calculated with new measured half-life values ($T_{1/2}^*$) according to the following equation.

$$\sigma^* = \sigma \frac{T_{1/2}^*}{T_{1/2}} \quad (3)$$

ACKNOWLEDGEMENT

This project is funded by the Swiss National Science Foundation (SNF grant no 200021-159738).

- [1] <https://europeanspallationsource.se/spallation>.
- [2] T. Jorgensen et al., Nucl. Eng. Des. **282**, 28 (2015).
- [3] Z. Talip, Ann Rep. Lab. of Radio-& Environ. Chem., Univ. Bern & PSI, (2015).
- [4] M. Christl et al., A. Nucl. Instrum. Methods Phys. Res., Sect. B **294**, 294(2013).
- [5] Z. Talip et al., Anal. Chem. **89**, 13541 (2017).
- [6] D. Mancusi et al., Phys. Rev. C **90**, 054602 (2014).
- [7] A. Boudard et al., Phys. Rev. C **87**, 014606 (2013).
- [8] A. Kelic et al., Trieste, Italy, 2008.
- [9] Z. Talip et al., Anal. Chem **89**, 6861 (2017).

NEUTRON CAPTURE CROSS SECTION OF ^{171}Tm

T. Heftrich¹, M. Weigand¹, Ch. E. Düllmann^{2,3,4}, K. Eberhardt², S. Fiebiger¹, J. Glorius^{1,3}, K. Göbel¹, C. Guerrero⁵, R. Haas^{2,4}, S. Heinitz⁶, J. Lerendegui-Marco⁵, F. Käppeler⁷, J. D. Kaiser¹, U. Köster⁸, C. Langer¹, S. Lohse^{2,4}, F. Ludwig¹, R. Reifarth¹, D. Renisch^{2,4}, K. Scheutwinkel¹, D. Schumann⁶, N. Wiehl^{2,4}, C. Wolf¹

1) GU, 2) JGU, 3) GSI, 4) HIM, 5) US, 6) PSI, 7) KIT, 8) ILL

Motivation

One main goal of experimental astrophysics is to understand the elemental abundances in the universe. Most of the heavy elements are produced by a sequence of neutron captures and beta decays on stable isotopes (s-process). To constrain the interior conditions of a star during the s-process, so called branching points can be studied. Branching points are nuclei which have comparable neutron capture rate and beta decay rate. Therefore the s-process path depends on temperatures and neutron densities inside the involved layers in stars. The beta-unstable ^{171}Tm acts as such a branching point [1]. It is produced by neutron captures on the stable ^{169}Tm isotope (Fig.1). The produced isotope ^{170}Tm either decays to ^{170}Yb or captures another neutron leading to ^{171}Tm .

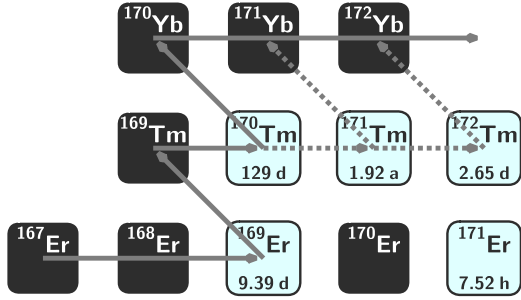


Fig. 1: The production of ^{171}Tm during the s-process by a sequence of neutron captures on the stable isotope ^{169}Tm .

The radioactive sample

The ^{171}Tm nuclei for this experiment were produced by irradiating a ^{170}Er sample for 55 days in the V4 beam tube of the high flux reactor of Institut Laue-Langevin, Grenoble. The resulting ^{171}Er nuclei decayed with a half-life of 7.52 h to the desired ^{171}Tm .

At Paul-Scherrer-Institut, Villigen, Switzerland, a radiochemical Tm/Er separation was performed. Afterwards, gamma-spectrometry measurements of the sample yielded the number of ^{171}Tm nuclei. Observing the only γ -emission line of ^{171}Tm at 67 keV resulted in an activity of about 50 MBq.

Experiment

For the determination of the neutron capture cross section an activation experiment was performed at the TRIGA reactor in Mainz, Germany [2,3]. The neutron fluence during the irradiation was determined using so-called monitors with well known neutron capture cross sections. Monitors of Au, Sc, and Ta surrounded the ^{171}Tm sample during the irradiation.

The neutron spectrum of reactors consists of thermal and epithermal neutrons. To discriminate both parts of the spectrum, a second activation using 1 mm thick cadmium shielding surrounding the sample, absorbing thermal neutrons.

The produced nuclei of ^{172}Tm in the sample and the monitor activities were determined by gamma spectrometry.

Results

The thermal neutron capture cross section of ^{171}Tm was determined to (preliminary)

$$\sigma_{\text{th}} = (9.9 \pm 0.8_{\text{stat}} \pm 0.3_{\text{sys}}) \text{ b},$$

and the resonance integral to

$$\sigma_{\text{RI}} = (193 \pm 12_{\text{stat}} \pm 8_{\text{sys}}) \text{ b}.$$

Summary

The study of properties of moderately neutron-rich radioactive nuclei is very important for the understanding of the s-process path. To constrain the conditions during the s-process, branching points are particularly useful to study. This was the first direct measurement of the neutron capture cross section on ^{171}Tm beyond thermal energy. The thermal neutron capture cross section was determined to $(9.9 \pm 0.8_{\text{stat}} \pm 0.3_{\text{sys}}) \text{ b}$ and the resonance integral to $\sigma_{\text{RI}} = (193 \pm 12_{\text{stat}} \pm 8_{\text{sys}}) \text{ b}$. This shows that the direct component of the cross section can be neglected for the keV-regime of the s-process.

-
- [1] R. Reifarth, C. Lederer, F. Käppeler, J. Phys. G: Nucl. Part. Phys. **41**, 053101 (2014).
 - [2] K. Eberhardt and A. Kronenberg, Kerntechnik **65**, 5 (2000).
 - [3] G. Hampel, K. Eberhardt, and N. Trautmann, Atomwirtschaft **5**, 326 (2006).

Cs-REMOVAL FROM HIGHLY ACIDIC SPENT FUEL SOLUTIONS: BATCH TESTS

M. Lin (Univ. Bern & PSI), I. Kajan, D. Schumann (PSI), A. Türler (Univ. Bern)

Previous studies on distribution coefficients have shown that AMP (ammonium molybdophosphate) is a better option than CLEVASOL[®] for selective Cs-removal from highly acidic spent nuclear fuel solutions (8 M HNO₃) [1]. The optimum acid concentration for Cs-removal was found to be 4 M HNO₃ with respect to the desired high distribution coefficient and minimum volume for dilution [1]. Since the particle size of AMP is too small to be applied in column operations, two engineered products based on AMP were tested for column applications: AMP_PAN, where the AMP is bound to polyacrylonitrile (TRISKEM), and AMP/SiO₂, where the AMP is immobilized on silica gel, which was manufactured in-house [2].

This report described the results of kinetics and static exchange capacity studies of Cs adsorption on AMP, AMP_PAN and AMP/SiO₂.

Experimental

Preparation of AMP/SiO₂

AMP is very soluble in basic solutions [3], thus ammonia solution was used to dissolve it before addition of silica gel supports. Firstly, 6.9 g of AMP were dissolved in 175 ml of 25% of ammonia solution, then 6.3 g of silica gel were added. This mixture was stirred overnight by a magnetic stirrer at 300 rpm. After that, the excessive ammonia was evaporated by heating the mixture for several hours at 70°C on a heating plate (Heidolph MR Hei-Standard). Afterwards, 15 ml of 6 M HNO₃ were added to re-precipitate ammonium molybdophosphate (AMP). The re-precipitated AMP was successfully immobilized on the silica gel. The product was filtered with paper filter (Whatman[™] and air-dried in a ventilation fume hood for 2 days.

Kinetics Studies

Tracer amounts of ¹³⁷Cs were added into 100 ml of 4 M HNO₃ to prepare the stock solution. The weighed sorbent (10 mg for AMP; 30 mg for AMP_PAN and AMP/SiO₂) and 2 ml of the stock solution were mixed in glass vials, then these vials were shaken for different time intervals (10s ~ 4h) by a shaking machine (IKA[®] VIBRAX VXR basic) at 1500 rpm. After that, the phases were separated using syringe filters (0.1 μm pore size for AMP and AMP/SiO₂, Whatman[™]; 2 μm pore size for AMP_PAN, Miller[®]). Finally, 1 ml of the separated aqueous phase and 1 ml of stock solution were measured by gamma detector (Canberra EFPC 25, S/N: 7747) to quantify the count rate of Cs-137. The experimental temperature was kept at 22°C.

Static Exchange Capacity Studies

Tracer amounts of ¹³⁷Cs were added into several plastic vials containing 100 ml of 4 M HNO₃ with different concentrations of CsNO₃ (0.67 g / L ~ 13.4 g / L) to make the stock solutions. The weighed sorbent and 1.5 ml of the stock solutions were mixed in glass vials and shaken for 4 hours at 1500 rpm. Quantifications were performed similar to the kinetic studies.

Results

Kinetics Studies

The amount of adsorbed ¹³⁷Cs was calculated following equation (1) :

$$C/C_0 = \frac{C_{initial} - C_{liquid}}{C_{initial}} \quad (1)$$

Where: $C_{initial}$ is the count rate of Cs-137 in 1 ml of solution before contacting with sorbent (cps); C_{liquid} is the count rate of Cs-137 in 1 ml of solution after contacting with sorbent (cps).

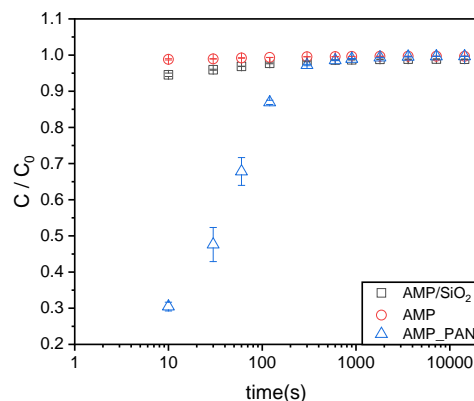


Fig. 1: Dependence of Cs exchange on AMP and AMP-based sorbents on the time in 4 M HNO₃.

The kinetic behaviour of the Cs adsorption on the sorbents is presented in figure 1. In the case of AMP and AMP/SiO₂, the value of C/C_0 reaches > 0.9 within 10 seconds, and it slightly changes from 30 minutes to 4 hours. Comparing AMP with AMP/SiO₂, Cs adsorption on AMP_PAN is slower. The value of C/C_0 reaches > 0.9 after 300 seconds and then it slightly changes from half an hour to 4 hours. The slower adsorption kinetics of AMP_PAN is probably caused by its larger particle size and its much more compact internal structure which could inhibit the mass transfer during the adsorption process [4]. The kinetics studies confirm that the 4 hours contacting time is sufficient although the equilibrium is not fully reached.

Static Exchange Capacity Studies

The Cs concentration in the sorbent was calculated according to equation (2).

$$[M_{solid}] = \frac{c_{initial} - c_{liquid}}{c_{initial}} \times \frac{[M_{Cs}] \times V}{m} \quad (2)$$

Where: $[M_{solid}]$ is the Cs concentration in the solid phase (g Cs / g sorbent); $[M_{Cs}]$ is the concentration of Cs in initial solution before contacting with sorbent (g / L); m is the mass of dry sorbent (g); V is the volume of stock solution in the solid-liquid system (L).

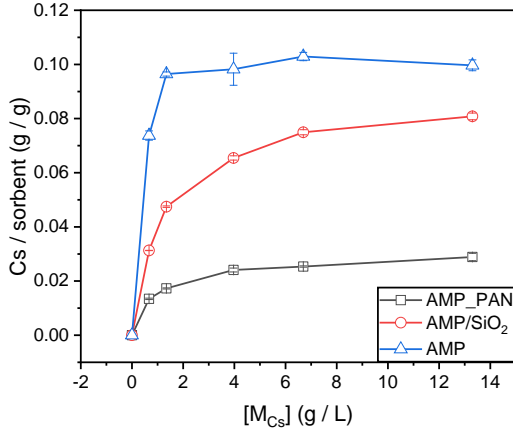


Fig. 2: Amount of adsorbed Cs on sorbent after 4 hours contacting time.

The results are presented in figure 2 by plotting the adsorbed Cs concentration in the sorbent against the Cs concentration in the initial solution. As shown in figure 2, the adsorbed Cs concentration in the sorbent increases with the Cs concentration till reaching the maximum value with indicates the exchange capacity of the sorbent to Cs. In order to accurately calculate the exchange capacity of these sorbents towards Cs in 4 M HNO₃, the experimental data are analyzed by the Langmuir isotherm model in linear form (equation (3)) [5]. The classical Langmuir model assumes the sorbent has a homogeneous flat surface and a monolayer adsorption on the surface [6].

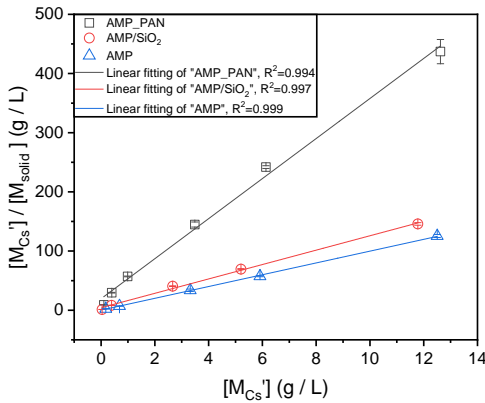


Fig. 3: Linearized Langmuir adsorption isotherm plot for AMP_PAN, AMP/SiO₂ and AMP.

The maximum Cs adsorption and the Langmuir coefficient can then be graphically determined from the slope and intercept according to equation (3).

$$\frac{[M_{Cs}']}{[M_{solid}]} = \frac{[M_{Cs}']}{Q} + \frac{1}{K \times Q} \quad (3)$$

Where: $[M_{Cs}']$ is the Cs concentration in solution after contacting with sorbent (g / L); Q is the exchange capacity towards Cs (g Cs / g sorbent); K is the Langmuir coefficient related to the energy of adsorption (L / g).

As shown in figure 3, the experimental data fit the Langmuir model very well with $R^2 > 0.99$. The maximum Cs adsorption in AMP_PAN, AMP/SiO₂ and AMP are obtained by calculating the inverse of the slope. Their values as well as the value of Langmuir coefficient are presented in table 1.

Tab. 1: Langmuir parameters of Cs adsorption on sorbents.

Sorbent	Slope	Q (g/g)	Intercept	K (L/g)
AMP_PAN	33.84 ± 1.13	$(29.6 \pm 1.0)E-3$	19.41 ± 6.67	1.74 ± 0.60
AMP/SiO ₂	12.16 ± 0.36	$(82.2 \pm 1.1)E-3$	4.25 ± 2.10	2.86 ± 1.42
AMP	9.97 ± 0.11	$(100.3 \pm 2.4)E-3$	0.20 ± 0.07	51.06 ± 18.36

The obtained exchange capacity (Q) of AMP_PAN towards Cs is agreement with the value (~ 33 mg / g dry AMP_PAN) given in the product sheet provided by TRISKEM. The exchange capacity of AMP towards Cs indicates 48% of ammonium ion is exchanged, which confirms the the work done by C. J. Coetzee that approximately 50% of ammonium ion on AMP can be maximally exchanged with Cs [7].

Conclusion

AMP and AMP/SiO₂ show faster kinetics of Cs adsorption than AMP_PAN in 4 M HNO₃. In the case of these three sorbents, the value of C / C_0 reaches > 0.9 after 300 seconds contacting time. The capacity of AMP_PAN and AMP towards Cs is approximately 30 mg / g and 100 mg / g respectively, these values fit well with other studies. The capacity towards Cs of AMP_PAN is less than of AMP/SiO₂, probably because AMP_PAN has less weight% of AMP than AMP/SiO₂.

For an efficient selective removal of Cs from spent nuclear fuel solutions, AMP-PAN is the material of choice. Further studies will comprize the optimisation of application of AMP-PAN in column mode, considering the necessary remote-controlled operation under harsh radiation environment conditions

We acknowledge funding from SWISSNUCLEAR.

- [1] M. Lin et al., Ann Rep. LRC, (2017).
- [2] Y. Wu et al., Sep. Purif. Technol. **181**, (2017).
- [3] P. Cannon, Talanta, **3**, (1960).
- [4] D. Ding et al., J. Hazard. Mater. **324**, (2017).
- [5] T. J. Tranter et al., Adv. Environ. Res. **6**, (2002).
- [6] R. H. Perry et al., Perry's Chemical Engineer's Handbook, 7th ed, (1997).
- [7] C. J. Coetzee et al., J. Inorg. Nucl. Chem., **32**, (1970).

TOWARDS THE DETERMINATION OF MOLYBDENUM-93 HALF-LIFE

I. Kajan, S. Heinitz, R. Dressler (PSI)

The molybdenum isotope ^{93}Mo is a long-lived solely electron capture nuclide disintegrating to the ground and first excited state (^{93}Nb , $^{93\text{m}}\text{Nb}$) of the stable niobium daughter. In nuclear power plants it originates mainly through activation of structural materials of the facility (steel, concrete) although it is produced in research and medical cyclotrons from niobium used as targets, beam degraders, beam windows or beam dumps. The experimental determination of ^{93}Mo half-life was performed only once with obtained value 3000(600) years [1] without a direct determination of the number of atoms in the samples assuming an almost constant production rate of odd mass isotopes in deuteron induced compound reactions around mass 100. The currently adopted value of 4000 years with an uncertainty of 20% [2] is regarded as tentative by the data evaluators.

In this work we describe separations of radiochemically pure ^{93}Mo from the 72 MeV proton irradiated high purity niobium disc in order to prepare the sample for half-life determination. This will be performed through combination of high-resolution ICP-MS and activity measurements.

Molybdenum-93 was produced via the $^{93}\text{Nb}(p,n)^{93}\text{Mo}$ reaction during prolonged proton irradiations of a 2.1mm thick niobium disc utilized as beam energy degrader at PSI isotope production facility. After the usage as degrader, the disc was stored in a hotcell for at least 5 years, leading to the decay of shorter-lived radioisotopes such as $^{91\text{m}}\text{Nb}$, ^{88}Zr , ^{88}Y or ^{85}Sr . In Table 1 the most relevant nuclides formed after a 3 year long irradiation with a 5 μA proton beam and 5 years of cooling are shown as calculated with MCNPX 2.7.0.

Tab. 1: Calculated nuclide inventory of proton irradiated niobium disc after 5 years cooling period.

Nuclide	Specific activity (Bq/g)
$^{93\text{m}}\text{Nb}$	$1.50 \cdot 10^6$
^{91}Nb	$5.31 \cdot 10^5$
^3H	$6.43 \cdot 10^4$
^{93}Mo	$7.33 \cdot 10^3$
^{94}Nb	$3.11 \cdot 10^2$
^{88}Y	$2.52 \cdot 10^2$
^{88}Zr	1.86
^{92}Nb	1.34
^{93}Zr	0.508

For monitoring the niobium behaviour during chemical separations, carrier free ^{95}Nb radiotracer was prepared as follows: High purity (99.9%) zirconium foil was neutron irradiated at PSI SINQ facility for 14 days with flux of $3 \cdot 10^{13} \text{ cm}^{-2} \cdot \text{s}^{-1}$. The produced ^{95}Zr ($t_{1/2} = 64.0 \text{ d}$) decayed consecutive to ^{95}Nb

($t_{1/2} = 35.0 \text{ d}$). After irradiation the foil was dissolved in 0.5 ml of 6.5 M HCl / 1 M HF. Dissolution was complete after ca. 5 min. This solution was thereafter applied on TEVA resin (TRISKEM) filled column preconditioned with the same acids composition. The column was then washed with 3 ml of the same acid mixture. Under these conditions, niobium was quantitatively retained on the resin whereas zirconium passed through the column. Niobium was thereafter eluted from the column with 6.5 M HCl / 0.1 M HF acid mixture. Based on gamma spectroscopic measurements (Canberra EFPC-25) the separation factor of niobium from zirconium was at least $4 \cdot 10^4$.

Separation of molybdenum from niobium and other impurities (mainly Ta and Fe) was performed by two step ion exchange chromatography procedure. Parts with weight of 0.6 g each were cut from the degrader and dissolved in concentrated HF with a few added drops of HNO_3 . The solution was then transformed into composition of 6.5 M HCl / 0.1 M HF and carrier free ^{95}Nb tracer was added in order to determine the decontamination factor of molybdenum from niobium. This solution was passed through a TBP resin chromatographic column. That was afterwards washed with 40 column volumes of the same acid mixture. During this step niobium fraction passing through the column was purified from tantalum with decontamination factor Nb/Ta of $5 \cdot 10^4$ measured by emissions originating from the decay of ^{179}Ta utilizing X-ray spectroscopy (Canberra LEGe). With the used acids composition, niobium passed through the column whereas molybdenum together with impurities of iron and tantalum were retained. During this step the niobium fraction passing through the column was purified from tantalum with decontamination factor Nb/Ta of $5 \cdot 10^4$ measured by emissions originating from the decay of ^{179}Ta utilizing X-ray spectroscopy (Canberra LEGe). Molybdenum was consequently eluted from the column utilizing Milli-Q water (18 M Ω). Decontamination factor of molybdenum from niobium obtained in this separation step was no less than $1 \cdot 10^5$.

In the next step the molybdenum eluate was spiked with additional ^{95}Nb tracer and the resulting mixture was evaporated to near dryness and converted into a 0.1 M HF solution. It was then applied on chromatographic column containing Al_2O_3 (Sigma-Aldrich). In this procedure both molybdenum and niobium, together with traces of tantalum and iron were retained on alumina substrate. The column was washed with Milli-Q water and molybdenum was then eluted with 25% ammonia solution. In this procedure, niobium remained retained on the column during the molybdenum elution process together with iron and tantalum. Decontamination factor of molybdenum

from niobium and as well iron and tantalum was no less than $5 \cdot 10^4$.

Both separation steps described above were repeated twice leading to achieve an overall decontamination factor of Mo/Nb of about 10^{15} .

Three independent stock solutions were purified using the described methods. From these samples three different ^{93}Mo point-like sources were prepared by evaporating one droplet (20 μL) on circular Teflon supports for X-ray spectroscopic measurements. A Mettler-Toledo AT261 DeltaRange ($d = 0.01 \text{ mg}$) balance was used to gravimetrically trace the source preparation step. All sources were sealed using a 50 μm thick Kapton tape.

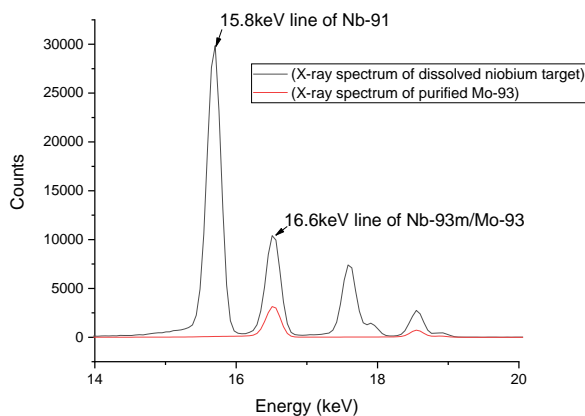


Fig. 1: X-ray spectra of dissolved niobium target and purified Mo-93 fraction.

The prepared point sources from individual stock solutions were measured at the endcap of a low-energy germanium detector (Canberra LEGe HPGe) with about 10% efficiency for the used geometry at 16.6 keV. As a calibration reference a certified $^{93\text{m}}\text{Nb}$ source with an activity of 1830(6) Bq (certified on 01.09.2007 by Physikalisch-Technische-Bundesanstalt (PTB), Braunschweig, Germany) was used. Measurements of the ^{93}Mo samples were performed for at least 24 h to achieve not less than 10000 counts in the regions of interest giving counting uncertainties in the range of 1%. Based on the X-ray emission probabilities for 16.6 keV line from ^{93}Mo decay [2]. Superimposed X-ray spectra obtained before and after molybdenum separation are shown in Figure 1. The activities of the purified stock solutions were deduced to be 4500 Bq, 3000 Bq and 4200 Bq, respectively, each of them with no radioactive contamination measurable by gamma- or X-ray spectroscopic means.

-
- [1] P.P. Dmitriev, I.O. Konstantinov, N.N. Krasnov, *Sov. J. Nucl. Phys.* **6**, 153 (1968).
 [2] C.M. Baglin, *Nuclear data sheets* **112**, 1268 (2011).

THE PURIFICATION OF ^{26}Al AND ^{179}Ta RECOVERED FROM IRRADIATED STEELS OF THE SINQ TARGET IRRADIATION PROGRAM

S. Heinitz, D. Schumann (PSI)

In the frame of the ERAWAST project aiming towards the extraction of exotic long-lived radionuclides from irradiated materials of the PSI accelerator complex, the extraction of ^{44}Ti , ^{53}Mn , and ^{26}Al from steel samples of the STIP program has commenced in 2009. Since then, more than 200 MBq of ^{44}Ti and up to 10^{19} atoms of ^{53}Mn have been successfully extracted from dozens of grams of Fe, Cr, and Ni by M. Ayranov, M. Bunka, and at a later stage by T. Stowasser. A detailed description of the project as well as the involved scheme for the applied chemical separation process has been reported in [1].

While the separation of ^{44}Ti and ^{53}Mn has been completed – the latter has recently been used for an activation measurement at the CERN n_TOF facility [2] – the fractions containing ^{26}Al still required further purification from activities of ^{44}Ti , ^{60}Co , ^{54}Mn , and other radiocontaminants. All ^{26}Al recovered from the STIP samples was distributed between three 25 mL flasks containing big amounts of Fe carrier in 8 M HCl. Each flask still contained 500 kBq of ^{44}Ti as major contaminant. In order to purify the Al fraction to the best possible extend, the following chemical procedure was applied:

At first, each solution was basified with 5 M NaOH in order to initiate the precipitation of $\text{Fe}(\text{OH})_3$ while leaving $\text{Al}(\text{OH})_4^-$ in solution. In this way, most of ^{44}Ti is carried with Fe which made an efficient counting of ^{26}Al via γ -spectrometry possible. After centrifuging and separating the supernatant, additional washing of the precipitate with 1 M NaOH assured a complete transfer of Al into the hydroxide solution. The Fe precipitate was kept for the separation of ^{44}Ti and ^{179}Ta at a later stage.

The basic solution containing ^{26}Al still showed the presence of a few kBq of ^{44}Ti , ^{172}Hf , ^{60}Co , ^{54}Mn , and ^{133}Ba . The solution was carefully acidified with 5 M HNO_3 and the pH adjusted to $\text{pH} = 2$. The resulting solution, having a final volume of approx. 150 mL, was pumped on a column containing the 2 mL of LN resin provided by Triskem International. While specifically designed for the extraction of lanthanides, this resin material does not sorb elements in the +1 or +2 oxidation state, while increasingly strongly retaining elements with oxidation states +3 to +6. Thus at $\text{pH} = 2$, the main matrix element Na^+ as well as Co^{2+} , Mn^{2+} and Ba^{2+} do not sorb and are eluted while the elements of Al^{3+} , Fe^{3+} , Ti^{4+} , and Hf^{4+} are adsorbed. After washing the column with 20 mL 0.01 M HNO_3 , Al is specifically eluted from the column using 1 M HNO_3 , leaving behind Fe, Ti and Hf. In this way, ^{26}Al is practically free from any ^{44}Ti yielding separation factors from this radionuclide in the order of 10^5 .

The final spectrum of ^{26}Al separated from all STIP samples is given in Figure 1. Small quantities of ^{101}Rh , $^{102\text{m}}\text{Rh}$, and ^{60}Co are still visible as contaminants. The

total activity of ^{26}Al was estimated to be 350 Bq with an overall separation yield of 95%. This material might be used in relevant experiments for astrophysical research.

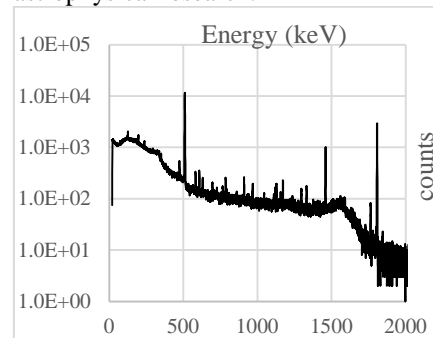


Fig. 1: Spectrum of purified ^{26}Al originating from all processed STIP samples.

For the final recovery of ^{44}Ti that was present in the ^{26}Al fractions, a similar procedure as already applied in [1] was chosen. The $\text{Fe}(\text{OH})_3$ residue was dissolved in 5 M HF and loaded on a 10 mL column containing a preconditioned anion exchange resin Dowex 1x8, provided by BioRad. While Ti is retained on the column as TiF_6^{2-} complex, Fe and traces of ^{60}Co and ^{54}Mn do not sorb and are eluted during the washing with 20 mL 5 M HF. The absence of Fe can be visually checked by the discoloration of the eluent. ^{44}Ti can then be eluted from the column using 1 or 0.1 M HNO_3 . It should be noted that since both, ^{44}Ti and its daughter ^{44}Sc are retained on the column in HF media, the elution of ^{44}Sc using HNO_3 precedes first and a Ti/Sc separation is practically possible on Dowex 1x8 column.

At the end of the ^{44}Ti purification a measureable activity originating from an unknown nuclide still retained at the very top of the anion exchange column. Tries to elute the activity using different concentrations of HNO_3 or HCl failed. In order to identify the unknown activity, the first 2 cm of the column material have been extracted using a syringe and by applying γ -spectrometry the nuclide was identified as ^{179}Ta from the pronounced presence of x-rays as well as from very weak γ -lines originating from ^{182}Ta . Only 75% of the activity could be separated from the column material immersing it in 10 M HNO_3 overnight. A rough estimation of the total ^{179}Ta activity resulted in approx. 100 kBq of this isotope, while the content of ^{182}Ta was estimated to be only 50 Bq. This material might be used for the development of liquid scintillation counting techniques for pure electron capture nuclides.

[1] R. Dressler et al., J. Phys. G: Nucl. Part. Phys., **39** 29 (2012).

[2] J. Ulrich, this report, p. 15.

THE PRODUCTION AND BEHAVIOUR OF ^3H AND ^7Be IN THE COOLING CIRCUITS OF THE SPALLATION NEUTRON SOURCE SINQ

S. Heinitz (PSI), D. Kiselev (PSI/GFA), M. Rütthi (PSI/LOG), B. Blau (PSI/NUM), D. Schumann (PSI)

The Paul Scherrer Institute operates the world's most powerful continuous spallation neutron source SINQ producing thermal and cold neutrons. A beam of 590 MeV protons with a current of 1.5 mA is guided to a solid target consisting of lead in zircalloy cladding. During this process, a continuous heat load of ~ 1 MW is generated and an efficient cooling of the target is mandatory. For this purpose, SINQ is equipped with a set of cooling circuits of which the main ones are operating with heavy water, see Fig. 2:

- the target cooling circuit „JEC“ in direct contact with the zircalloy tubes filled with Pb
- the target enclosure circuit „JER“ cooling the beam entrance window
- the moderator circuit „RNM“ surrounding the spallation target in order to thermalize generated spallation neutrons.

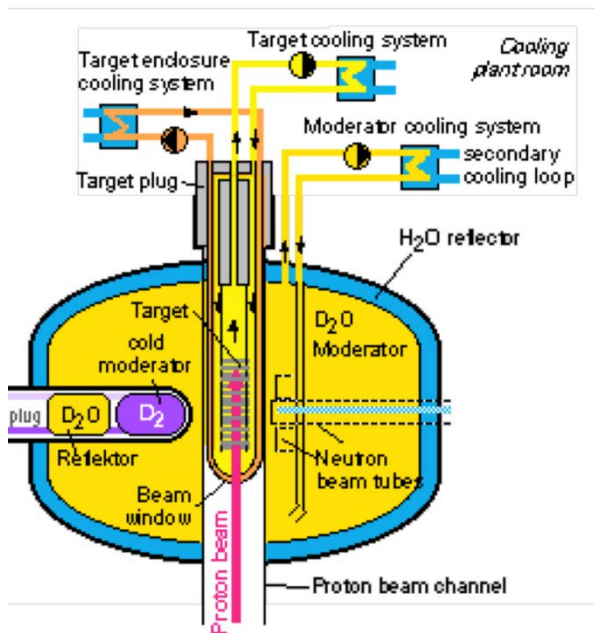


Fig. 2: Vertical cut of the SINQ target station and its cooling circuits, taken from [1].

During operation of the SINQ facility, the D_2O in each circuit is under constant irradiation with fast neutrons and protons producing substantial activities of spallation and activation products. Short-lived isotopes such as ^{15}O , ^{13}N and ^{11}C are constituting the major radioactive burden during SINQ operation. However, also longer-lived isotopes such as ^3H , ^7Be , and activation products such as ^{22}Na , ^{59}Fe , or ^{95}Zr are formed upon irradiation of D_2O and its impurities. In order to keep the heavy water in each loop as clean as possible as well as to reduce the dose rate in the cooling plant room during maintenance breaks, each cooling circuit is equipped with a set of redundant

mixed-bed ion exchangers that constantly filter the heavy water. In Table 1 the major parameters of each of the three heavy water cooling circuits are given. A picture of the cooling plant room is given in Figure 2.

Tab. 1: Technical parameters of the three D_2O cooling loops of SINQ [2].

circuit	JEC	JER	RNM
total volume [L]	3740	500	6280
flow rate [kg/s]	10	2	3
flow rate into ion filter [kg/s]	0.4	0.08	0.4
filter volume [L]	48	12	114



Fig. 3: The cooling plant room with shielded ion exchange vessels (front).

In order to monitor the point of saturation of the ion exchangers and to check D_2O purity, online conductivity measurements are performed in all heavy water circuits during operation. Additionally, a radiochemical analysis of the nuclide inventory is usually performed on water samples of each cooling loop taken at the beginning of the annual shutdown period approximately 2 weeks after the regular beam stop. Data gathered since 2002 on the inventory of ^3H ($T_{1/2} = 12.32$ a) in the loops of JEC, JER and RNM are given in Figure 4 [3].

As can be seen from Figure 4, the largest inventory of ^3H is produced in the moderating tank of the SINQ facility, since the thermalization and capture of neutrons by deuterium is mainly occurring there. There is a steady increase in ^3H activity in the moderation circuit, while the activity in the other D_2O circuits remains constant. A gradual increase of ^3H activity is not apparently visible since an intentional mixing of D_2O from each loop was performed in 2007 and 2016.



Fig. 4: Activity concentration of ^3H (in GBq/kg) in the SINQ D_2O cooling loops as function of operational year. The „jumps“ in ^3H concentration for year 2007 and 2016 are due to intentional mixing of heavy water between the circuits [3].

Another important nuclide formed during SINQ operation is ^7Be ($T_{1/2} = 53.23$ d). This isotope is formed by spallation reactions with neutron or protons on oxygen and it represents the most dominant γ -active radionuclide several hours after shutdown of the beam. It has been observed that ^7Be tends to plate out on tubes and pipes in all D_2O circuits thus being the major dose contributor in the cooling plant room after ^{11}C decay [4]. Unlike ^3H , ^7Be can be constantly stripped from the heavy water using ion exchangers. This technique has already been successfully implemented into a small scale filter system that is used to collect ^7Be from the RNM circuit for research experiments, see [1].

In order to be able to predict the increase of ^3H and to compare it to the measured inventory given in Fig. 4, MCNP6.1 calculations have been performed using the INCL-ABLA code to simulate the production rate of ^3H and ^7Be for a 1 mA proton beam interacting with D_2O of the JEC and RNM cooling loops [5]. The result of this calculation is given in Tab. 2.

Tab. 2: Calculated production rate of ^3H and ^7Be in the target and moderator cooling loops [5].

	atoms / mA / s	Bq / mA / s
RNM		
^3H	1.65E+15	2.94E+06
^7Be	1.89E+13	2.84E+06
JEC		
^3H	1.46E+14	2.60E+05
^7Be	2.62E+13	3.95E+06

Assuming a constant proton current of 1.5 mA on the SINQ target and using the numbers given in Tables 1 and 2, it is possible to calculate the concentration of ^3H and ^7Be in equilibrium with its decay. For the target cooling circuit JEC, the equilibrium ^3H concentration would be roughly 50 GBq/kg D_2O , while for the moderating circuit this activity would be up to 360 GBq/kg ($\rho(\text{D}_2\text{O}) = 1.1$ g/cm 3). While SINQ is operational about 50 % throughout the year, the above values should be reduced by a factor of two. This is in fair agreement with the current measured ^3H activity concentration in the JEC loop, see Fig. 4, whereas the

calculated saturation activity for the RNM loop will not be reached within the next 20 years of operation assuming similar neutron fluxes as hitherto.

The calculation of the ^7Be activity can hardly be compared to any measurement, since experimental data scatter significantly between the years [3] and do not allow any solid predictions about ^7Be behaviour in the cooling circuits. While its activity concentration is measured to be in the kBq/kg D_2O range, it is strongly dependent on the performance of the ion exchangers, the mass flow over the filter and the exact timing between the beam stop on SINQ and sample taking.

From data in Table 2, however, it is possible to calculate the equilibrium concentration of ^7Be in the target and moderator loop in analogy to that of ^3H . Assuming no filtering or plating out effects, the ^7Be concentration in the JEC and RNM loop would be 11 GBq/kg and 5 GBq/kg D_2O , respectively. This is exceeding any experimentally determined activity concentration by at least three orders of magnitude, indicating that an efficient ^7Be filtering is indeed occurring via the mixed bed ion exchangers.

The filtering kinetics and the resulting decrease in ^7Be activity concentration has been already studied for a water beam dump system at the Stanford Linear Accelerator Center [6]. Within this study it was found that using filtration, the saturation activity of ^7Be is reached within several days of operation and is not, as one might expect in analogy to the case of ^3H , a matter of several ^7Be half-lives. The concentration of ^7Be in the cooling circuit during operation using filters was found to be at least 280 times lower than calculations would predict for a system without filtration.

In order to tackle the lack of experimental data, experiments similar to those reported in [6] should be undertaken in order to understand the behaviour of beryllium and other elements in the SINQ cooling system. This knowledge is required to be able to safely predict the amount of collected ^7Be in future collection campaigns.

- [1] D. Schumann, M. Ayranov, T. Stowasser, Radiochemical separation of ^7Be from the cooling water of the neutron spallation source SINQ at PSI. *Radiochim Acta* 101, 509–514 (2013).
- [2] F. Heinrich, private communication.
- [3] ASI Analyserapporte für SINQ Wasserproben, Analysen 2002 - 2019.
- [4] H. Heyck, B. Amrein, G.S. Bauer, K. Geissmann, Lessons learned from the first 500mAh of beam on SINQ, *Proc. ICANS XIV*, 374–381 (1998).
- [5] R. Bergmann, private communication.
- [6] D. D. Busick: ^7Be build-up in a large water beam dump system at the Stanford Linear Accelerator Center, SLAC-PUB-521 (1968).

MEASUREMENT OF THE ${}^7\text{Be}(n,p)$ CROSS SECTION AT THERMAL ENERGY

I. Tomandl, J. Vacík (NPI Řež), U. Köster (ILL), D. Schumann, E.A. Maugeri, M. Ayrarov, S. Heinitz (PSI), L. Viererbl (RC Řež), J. Ballof, R. Catherall (CERN), K. Chrysalidis (CERN/Univ. Mainz),

T.D. Goodacre (CERN/Univ. Manchester), D. Fedorov (NPI Petersburg/CERN), V. Fedosseev, K. Johnston, B. Marsh (CERN), S. Rothe (CERN/Univ. Manchester), J. Schell (CERN/Univ. Duisburg-Essen), C. Seiffert (CERN)

The standard theory of Big Bang Nucleosynthesis (BBN) can provide a relatively precise prediction of primordial abundances of the light isotopes [1]. While the BBN predictions for abundances of primordial deuterium, ${}^3\text{He}$ and ${}^4\text{He}$ relative to hydrogen, are in a good agreement with experimentally observed values, the prediction of ${}^7\text{Li}$ abundance data exceeds the telescope observations of very old metal-poor halo stars, which are considered a good surrogate for the primordial abundance, by more than a factor of three [2]. One of the possible causes of this discrepancy, which became known as the "Cosmological ${}^7\text{Li}$ Problem", might be not precisely known nuclear reaction rates. Because the primordial ${}^7\text{Li}$ is predominantly produced by electron capture decay of the primordial ${}^7\text{Be}$, the production and destruction reaction rates of ${}^7\text{Be}$ play crucial role in the evaluation of the ${}^7\text{Li}$ abundance. The reaction rate of the indirect ${}^7\text{Be}$ destruction chain ${}^7\text{Be}(n,p){}^7\text{Li}(p,\alpha)$ is one of the very important parameters that are still not well known. The cross section of the ${}^7\text{Be}(n_{th},p){}^7\text{Li}$ reaction at thermal neutron energy, 25 meV, is essential for precise normalization of neutron capture data that correspond to primordial temperatures, i.e. in the neutron energy range of tens to hundreds of keV.

The complexity of the measurement of this cross section is mainly caused by a relatively short half-life of the ${}^7\text{Be}$ target ($T_{1/2} \sim 53.2$ d). Especially, the preparation of a high-quality ${}^7\text{Be}$ target with well-defined size, homogeneity and long-time mechanical stability is a very challenging task. The ${}^7\text{Be}$ target for our ${}^7\text{Be}(n_{th},p){}^7\text{Li}$ cross section measurement was the result of the effort of many scientists and several institutions. Primary ${}^7\text{Be}$ material was produced in the cooling water (D_2O) of the spallation neutron source SINQ at PSI [3]. This material undergoes several separation steps and purification in a shielded hotcell. The purified ${}^7\text{Be}$ sample was introduced into an ISOLDE target and ion source unit and shipped to CERN. While heating this ${}^7\text{Be}$ sample, released ${}^7\text{Be}$ atoms were resonantly laser ionised, accelerated to 35 keV. The mass-separated ${}^7\text{Be}$ beam was implanted into a 1.5 μm thin Al foil mounted in a larger, thick aluminium frame, see Fig. 1.

This target was transported to NPI Řež for the measurements at the thermal neutron beam of the LVR-15 research reactor [4]. Before the measurement, the accurate position of the ${}^7\text{Be}$ spot with respect to the Al frame was examined by an autoradiographic measurement using a flat panel detector imaging plate. The number of the ${}^7\text{Be}$ atoms in the implanted spot was determined via their activity.

The comparative method with a high-quality ${}^6\text{LiF}$ standard, a ${}^6\text{LiF}$ homogeneous layer with a thickness of 30.2(2) $\mu\text{m}/\text{cm}^2$ deposited on a 1.5 μm Al foil, was used for determination of the ${}^7\text{Be}(n,p)$ cross section. This standard was mounted on a plastic frame with the same external size as the Al frame of the ${}^7\text{Be}$ target. To keep the measurement geometry for both ${}^6\text{LiF}$ and ${}^7\text{Be}$ samples similar and to fit the height of the thermal neutron beam, 4 mm, the measured area of the standard was shrunk from an original diameter of 30 mm to 11 mm by means of a paper diaphragm. The ${}^7\text{Be}$ sample and the ${}^6\text{LiF}$ standard were irradiated with the collimated thermal neutron beam in a large vacuum chamber. In order to avoid self-shielding, both targets were tilted by 15° with respect to the neutron beam plane. The charged particle spectra for both samples were taken with a fully depleted surface barrier detector at a distance of 36 mm. Using spectra from these measurements, taking into account a perfect $1/v$ dependence of the neutron cross-sections for both ${}^6\text{Li}$ and ${}^7\text{Be}$ and employing the cross section for ${}^6\text{Li}(n_{th},t){}^4\text{He}$, 940(4) b, we arrived at the thermal neutron cross section of the ${}^7\text{Be}(n,p){}^7\text{Li}$ reaction to be 44300 ± 1400 b [5].

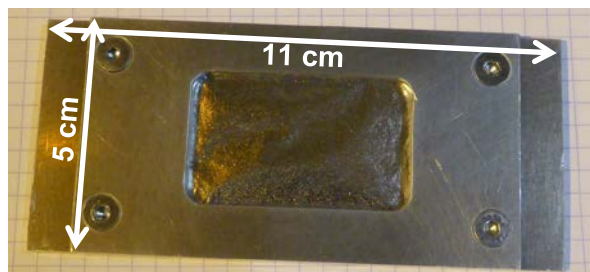


Fig. 1: Photo of the ${}^7\text{Be}$ target.

We acknowledge funding from the Ministry of Education, Youth and Sports of the Czech Republic (LM2015056 and LM2015074).

- [1] R.H. Cyburt, B.D. Fields, K.A. Olive, T.H. Yeh, *Rev. Mod. Phys.* **88**, 015004 (2016).
- [2] F. Spite, M. Spite, *Astron. Astrophys.* **115**, 357 (1982).
- [3] E.A. Maugeri et al., *Nucl. Instr. Meth. A* **889**, 138 (2018).
- [4] J. Honzátko et al., *Nucl. Instr. Meth. A* **376**, 434 (1996).
- [5] I. Tomandl et al., *Phys. Rev. C* **99**, 014612 (2019), DOI: 10.1103/PhysRevC.99.014612.

MEASUREMENT OF THE ${}^7\text{Be}(n,p){}^7\text{Li}$ REACTION CROSS SECTION FOR THE COSMOLOGICAL LITHIUM PROBLEM AT THE n_TOF FACILITY AT CERN

L. Damone, M. Barbagallo (INFN), M. Ayranov (European Commission, DG-Energy), E.A. Maugeri, S. Heinitz, R. Dressler (PSI), N. Kivel (PSI/GFA), J.G. Martins Correia, J. Schell, K. Johnston, M.J.G. Borge, J. Ballof, T. Stora, B. Marsh, T.D. Goodacre, C. Seiffert, S. Rothe (CERN-ISOLDE), U. Köster (ILL) and the n_TOF Collaboration

Theoretical models of the Big Bang Nucleosynthesis (BBN) correctly predict the abundance of the stable isotopes of hydrogen and helium, but not for ${}^7\text{Li}$ which is overestimated by factors of 3-5. This significant discrepancy between observation and predictions is known as the Cosmological Lithium Problem (CLiP) [1]. Since 95% of the primordial ${}^7\text{Li}$ is the product of the electron capture decay of ${}^7\text{Be}$, a higher destruction rate of ${}^7\text{Be}$ could potentially solve or at least partially explain the CLiP. In this scenario, reactions induced by neutrons on ${}^7\text{Be}$, in particular the ${}^7\text{Be}(n,\alpha){}^4\text{He}$ and the ${}^7\text{Be}(n,p){}^7\text{Li}$ reactions, could play an important role. However, data on these reactions have been so far scarce or completely missing. The recent construction of the second experimental area (EAR2) of the n_TOF (Neutron Time of Flight) facility at CERN [2], in combination with high purity samples produced at Paul Scherrer Institute (PSI), offered the unique opportunity to perform high accuracy time-of-flight measurements of ${}^7\text{Be}(n,p){}^7\text{Li}$ and ${}^7\text{Be}(n,\alpha){}^4\text{He}$ cross sections over a wide energy range, covering the one of interest for the Big Bang Nucleosynthesis. Results on the ${}^7\text{Be}(n,\alpha){}^4\text{He}$ reaction have been published in 2016 [3], while results on the ${}^7\text{Be}(n,p){}^7\text{Li}$ reaction cross-section have been recently published [4]. The measurement of the ${}^7\text{Be}(n,p){}^7\text{Li}$ reaction cross-section was performed using a telescope made out of two silicon strip detectors mounted at an angle of 90 degrees relative to the beam direction [5]. To minimize the energy straggling of emitted protons inside the ${}^7\text{Be}$ deposit, the sample was tilted relative to the neutron beam direction by 45 degrees.

A high-purity ${}^7\text{Be}$ sample of 1.1 GBq was prepared starting from 200 GBq ${}^7\text{Be}$ solution collected at PSI. The samples were produced at ISOLDE CERN by implantation of a ${}^7\text{Be}$ -beam at 35 keV into an aluminum backing and later installed in the vertical neutron beam of EAR2 [6].

In order to calibrate the detector and to be used as a reference, the ${}^6\text{Li}(n,t){}^4\text{He}$ reaction, whose cross section serves as standard from thermal energy up to 1 MeV, was measured first. The results compared with the evaluation from ENDF/B-VII.1 [7], show a good agreement, within 5 %, from thermal neutron energy up to 1 MeV. The protons emitted from the ${}^7\text{Be}(n,p){}^7\text{Li}$ reaction were identified in the telescope. The ${}^7\text{Be}(n,p){}^7\text{Li}$ cross section was extracted relative to that of the ${}^6\text{Li}(n,t){}^4\text{He}$ reaction (σ_{LiF}), from the ratio of the number of counts (C_{Be} and C_{LiF}), normalized to the respective total neutron fluence and taking into account the ratios of the efficiencies (ϵ_{Be} and ϵ_{LiF}), beam-sample convolution factors ($f_{C_{\text{Be}}}$ and $f_{C_{\text{LiF}}}$) and

the total number of atoms in the ${}^7\text{Be}$ and in the ${}^7\text{Li}$ sample (N_{Be} and N_{Li}).

$$\sigma_{n,p}(E_n) = \frac{C_{\text{Be}}(E_n)}{C_{\text{LiF}}(E_n)} \cdot \frac{\epsilon_{\text{LiF}}}{\epsilon_{\text{Be}}} \cdot \frac{f_{C_{\text{LiF}}}}{f_{C_{\text{Be}}}} \cdot \sigma_{\text{LiF}}(E_n) \cdot \frac{N_{\text{Li}}}{N_{\text{Be}}} \quad (1)$$

f_C represents the convolution of the normalized neutron beam spatial profile and target nuclei distribution and has a dimension of b^{-1} [4]. Fig. 1 shows the background-subtracted reduced cross section of the ${}^7\text{Be}(n,p){}^7\text{Li}$ reaction as a function of neutron energy, compared with the two previous direct measurements and with the ENDF/B-VII.1 evaluation. The high purity of the sample, the use of a telescope for particle identification, and the very high instantaneous neutron flux of EAR2 resulted in a practically negligible background, in particular the one associated with the natural γ -ray activity of ${}^7\text{Be}$. The only source of background affecting the measurement is related to ${}^{14}\text{N}(n,p){}^{14}\text{C}$ reactions in the sample backing. Its contribution was found important only for neutron energies above ~ 500 keV.

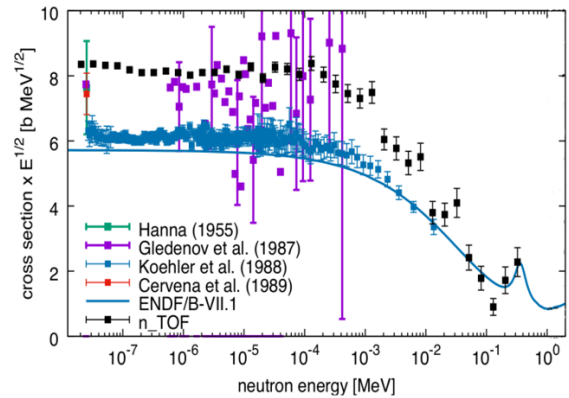


Fig. 1: The ${}^7\text{Be}(n,p){}^7\text{Li}$ reduced cross section measured at n_TOF compared to the results of previous measurements and with the ENDF/B-VII.1 library.

In conclusion, the ${}^7\text{Be}(n,p){}^7\text{Li}$ cross section has been measured at the second experimental area of the n_TOF facility at CERN, using a 1.1 GBq pure ${}^7\text{Be}$ sample implanted at the ISOLDE facility, starting from a 200 GBq ${}^7\text{Be}$ solution collected at PSI. For the first time, the energy range of interest for the Cosmological Lithium Problem (20-200 keV) was covered.

At thermal neutron energy the cross section measured at n_TOF is 52.3 ± 5.2 kb, higher than previous results. Above 50 keV, it is consistent with current evaluations. As shown in Tab. 1, the new results from this work essentially lead to a 10% decrease in the lithium production with respect to the previous calculation made using the "standard" rate (the rate from Ref. [8])

for the ${}^7\text{Be}(n,p){}^7\text{Li}$ reaction, and this is insufficient to provide a viable solution to the Cosmological Lithium Problem.

Tab. 1: BBN ${}^7\text{Li}$ abundance (relative to H) in units of 10^{-10} from recent calculations, compared with the observation of the Spite-plateau in low-metallicity stars.

Mishra and Basu (2012) [24]	5.02
Coc <i>et al.</i> (2014) [25]	$4.94^{+0.40}_{-0.38}$
Coc <i>et al.</i> (2015) [26]	5.61 ± 0.26
Singh <i>et al.</i> (2017) [27]	4.45 ± 0.07
This work with standard rates	4.35
This work with present rate ($\eta_{10} = 6.09 \pm 0.06$)	4.09 ± 0.09
This work with present rate ($5.8 \leq \eta_{10} \leq 6.6$)	3.68 – 4.85
Observations [1]	1.6 ± 0.3

-
- [1] M. Asplund *et al.*, *Astrophys. J.* **644**, 229 (2006).
 [2] C. Weiss *et al.*, *Nucl. Instr. Meth. A* **799**, 90 (2015).
 [3] M. Barbagallo *et al.*, *Phys. Rev. Lett.* **117**, 152701 (2016).
 [4] L. Damone *et al.*, *Phys. Rev. Lett.* **121**, 042701 (2018).
 [5] M. Barbagallo *et al.*, *Nucl. Instr. Meth. A* **887**, 27 (2018).
 [6] E.A. Maugeri *et al.*, *Nucl. Instr. Meth. A* **889**, 138 (2018).
 [7] M.B. Chadwick *et al.*, *Nucl. Data Sheets* **112**, 2887 (2011).
 [8] R. H. Cyburt *et al.*, *Phys. Rev. D* **70** (2004) 023505.

IMPLEMENTING NEW ISOTOPES FOR ENVIRONMENTAL RESEARCH: REDETERMINATION OF THE ^{32}Si HALF-LIFE PART I: COLUMN CHROMATOGRAPHY (CC)

M. Veicht (EPFL & PSI), I. Mihalcea, D. Schumann (PSI), A. Pautz (EPFL & PSI)

INTRODUCTION

Cosmic-ray-induced spallation of ^{40}Ar in the atmosphere leads to a continuous production of ^{32}Si , which is rapidly transferred to Earth's surface by precipitation, and subsequently deposited in terrestrial sediments, snow and ice. Since the annual atmospheric input of ^{32}Si on Earth is very poor (around 3×10^3 atoms $\text{cm}^{-2} \text{a}^{-1}$ [1]), following the overall abundance of this radionuclide is extremely low. In the past, several attempts to determine the half-life of ^{32}Si with different samples lead to large deviations including high uncertainties in its determination (Fig. 1). Clearly, a more precise and more accurate determination of the ^{32}Si half-life remains compelling.

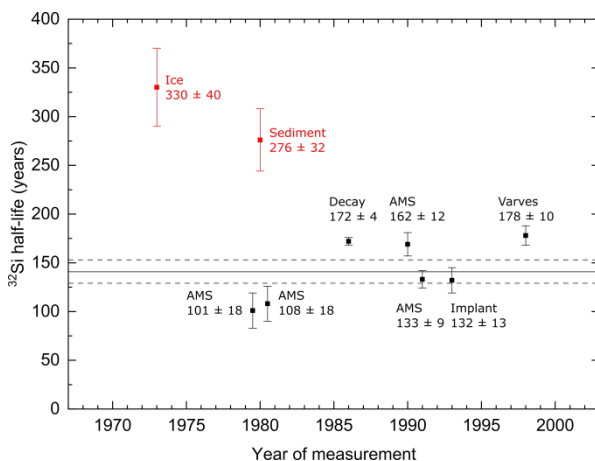


Fig. 1: Illustration of the ^{32}Si half-life determinations, that vary widely and show high uncertainties (modified after [1]).

The redetermination of ^{32}Si half-life with a small uncertainty is of crucial importance, because its application as geochronometer is ideally suited to fill the current time gap between 100 and 1000 years (Fig. 2). Hence, ^{32}Si dating has the potential to help identify human impacts on local and global environmental processes – such as the impact of European colonisation and industrialisation during the last 300 years, the Little Ice Age between AD 1650 and 1850, and the last part of the Medieval Climatic Optimum (AD 950 to 1250) [1]. Moreover, there are other interesting aspects e.g. the use as a potential generator for the daughter nuclide ^{32}P ($t_{1/2} = 14.27$ d) and as a target for nuclear reaction studies.

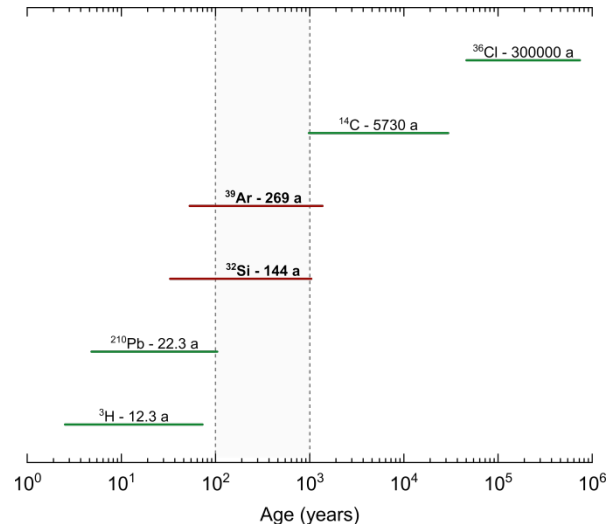


Fig. 2: Potential of ^{32}Si to fill the dating gap that lies between those chronologies based on the shorter-lived isotopes of ^3H and ^{210}Pb , and those based on the longer lived ^{14}C and ^{36}Cl , respectively (modified after [1]).

Although separation schemes for the extraction of ^{32}Si from different samples are published and even from proton-irradiated vanadium discs [2], by far there is only little information available how production and purification of suitable ^{32}Si samples can be achieved in general. So, the SINCHRON project will encounter the problem to make this silicon isotope available in high quantity from 40 vanadium discs that have been irradiated for two years with 590 MeV protons at the SINQ facility of the Paul Scherrer Institute (PSI). As a result, a world-wide unique amount of approximately 20 MBq can be extracted from these discs using different chemical separation methods, that are currently being investigated. Therefore, efforts in silicon separation with the use of stable and unstable silicon isotopes in an expected sample matrix (vanadium) are presented.

Furthermore, the high activity of ^{32}Si will allow fundamental scientific investigations that will also encompass the development and improvement of the measurement techniques enabling both half-life measurements and age determinations. Subsequently, a reliable and accurate recommended half-life value for ^{32}Si with the lowest possible uncertainty shall be provided, whereby PSI will work in close cooperation with well-known partners (ETH Zurich (CH), IRA Lausanne (CH), PTB Braunschweig (DE), ANU Canberra (AU)).

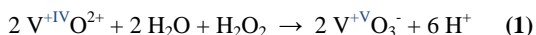
EXPERIMENTAL

These experiments were performed to review the behaviour of other radionuclides besides silicon in solution and also to simplify the solution's matrix, along with a reduction of the expected dose rate, of which one is e.g. ^{44}Sc ($t_{1/2} = 3.9$ h) – the daughter of ^{44}Ti ($t_{1/2} = 58.9$ a).

Therefore, a vanadium disc (m(V-disc) ~ 400 mg) was irradiated for 12 minutes with 41 MeV protons at PSI to obtain ^{48}V , a β^+ -emitting radionuclide ($t_{1/2} = 15.98$ d) that was used as tracer, as it can be easily identified γ -spectroscopically. After dissolution of the disc in 5 mL HNO_3 , each time a 50 μL aliquot was taken and several hundred μL of different tracers (^{22}Na , ^{60}Co , ^{95}Nb , ^{44}Ti , ^{65}Zn , ^{54}Mn) plus ultrapure water were added to end up with a final volume of 5 mL. Further, the addition of H_2O_2 , as an oxidizing agent was also examined. Subsequently, different cationic- (DOWEX[®] 50WX8-200 H^+ , DGA, TEVA[®]) and anionic-exchange (AG[®] 1-X8 Cl^-) resins were used. To follow the separation process, each fraction was γ -spectroscopically checked. The short-lived ^{31}Si ($t_{1/2} = 2.62$ h, 1266 keV) was used for evaluating the chemical behaviour of silicon during the experiments – as it is the only suitable tracer. For its production, around 10 mg of dried TraceCERT[®] solution was used and subsequently irradiated at the SINQ-NIS facility using the neutron induced reaction $^{30}\text{Si}(n,\gamma)^{31}\text{Si}$.

RESULTS AND DISCUSSION

Generally, column chromatography (CC) was used not only to separate silicon, but also to study the behaviour of other nuclides in the matrix. First of all, the addition of H_2O_2 allowed a quantitative separation of vanadium, using DOWEX[®] 50WX8-200 H^+ cationic exchange resin. The addition of H_2O_2 lead to an oxidation of vanadium (Eq. 1), so that the speciation of vanadium changed from a cationic into an anionic species, turning from the vanadyl to vanadate:



Subsequently, all other nuclides have been separated by step-wise increasing of the eluent's (HCl) molarity. Moreover, DGA (TrisKem International, France) was used to retain Sc(III) as described in [3], so that scandium could be completely separated from the matrix.

TEVA[®] (TrisKem International, France) was used to investigate its potential for retaining silicon, as its particular purpose is to be used to separate tetravalent lanthanides. Following the measurements γ -spectroscopically, it could be shown that silicon is completely retained on the resin and subsequently can be eluted with 1 M HF. However, the application of ^{31}Si as tracer faced difficulties due to its short half-life and the very low γ -branching ratio of 0.07 %.

Since it is very important to add HF, in order to turn silicon into H_2SiF_6 , other nuclides such as titanium and scandium are forming fluoro complexes ($[\text{TiF}_6]^{2-}$,

$[\text{ScF}_6]^{3-}$), which lead to a completely different separation behaviour, which was proven with the use of DOWEX[®] 50WX8-200 H^+ cationic exchange resin. Therefore, no suitable application was found so far, if HF is already added in the beginning.

Experiments with AG[®] 1-X8 Cl^- revealed problems, as it was not possible to achieve a quantitative separation of any added isotope under the chosen conditions.

CONCLUSION AND OUTLOOK

Studies of the behaviour of the nuclides in CC confirmed difficulties when adding HF from the beginning. For this reason, further processing of the solution using the CC would be possible after silicon distillation, if subsequently the dried residue is dissolved in HNO_3 to avoid any fluoro-complexes that will inhibit the separation of e.g. titanium and scandium. Although the TEVA[®]-resin has proven to be suitable for silicon separation, further studies are required, since V(IV) can be present in the solution and could interfere with Si(IV) [2]. Because of this, the separation scheme will likely include both distillation and CC.

ACKNOWLEDGEMENT

This project is funded by the Swiss National Science Foundation (SNSF) as part of SINERGIA (No.177229).

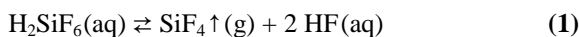
-
- [1] L. K. Fifield, U. Morgenstern, *Quaternary Geochronology*, 400-405 (2009).
 - [2] P. Polak, et al., *Radiochimica Acta*, 73-78 (1985).
 - [3] N. P. van der Meulen et al., *Nuclear medicine and biology*, 745-751 (2015).

IMPLEMENTING NEW ISOTOPES FOR ENVIRONMENTAL RESEARCH: REDETERMINATION OF THE ^{32}Si HALF-LIFE PART II: DISTILLATION

I. Mihalcea (PSI), M. Veicht (EPFL & PSI), D. Schumann (PSI), A. Pautz (EPFL & PSI)

EXPERIMENTAL

The separation of Si as the volatile silicon tetrafluoride (SiF_4) has already been applied and proved in the past being a very specific separation method [1]. In this regard, hexafluorosilic acid (H_2SiF_6) is prerequisite in the solution, because it can be thermally decomposed (at around $135\text{ }^\circ\text{C}$), which leads to the following reaction (Eq. 1):



Therefore, silicon can be transferred into a gaseous chemical state and subsequently trapped in a solution (trapping solution), so that H_2SiF_6 is formed again. Thereby, a low pH is important to prevent the acid from deprotonation and to keep the initial speciation as double proton acid.

To begin with, 10 mL of a « reference solution (RS) » were prepared: 5 mL were used for distillation and 5 mL were kept to determine the initial amount of silicon (blank sample). The RS was prepared from a 1000 ppm silicon standard solution for ICP in a HNO_3/HF -matrix (TraceCERT[®] Merck KGaA, Darmstadt, Germany). 100 ppm of silicon ($c(\text{Si}) = 3.6\text{ mM}$) and 180 ppm of vanadium ($c(\text{V}) = 3.53\text{ mM}$) were chosen for the RS. The amount of hydrofluoric acid (HF) was chosen to be stoichiometric with the formation of H_2SiF_6 , but with an 10 % excess to ensure the speciation in solution. Finally, the matrix of the RS contained about 2 % HNO_3 , to match the requirements for the measurements. In the course of further experiments, a decreased amount of Si(IV) in the RS was used (50 ppm and 25 ppm) to check, if the yield of the distillation depends on the concentration of the actual silicon in solution. As mentioned above, a « trapping solution (TS) » was used, of which 5 mL were placed in a 15 mL centrifuge tube. The matrix of the TS consisted of 2 % HNO_3 and 0.36 mM HF.

In order to test the system and apply it to the envisaged experimental conditions, a distillation setup was built up: Nitrogen (N_2) was being used as a carrier gas, a 100 mL round-bottom PTFE-flask (Bohlander GmbH, Grünsfeld, Germany) was placed in a bath of PEG-400 on top of a heating plate to boil the 5 mL aliquot of the RS. The heating plate was set to maximum ($300\text{ }^\circ\text{C}$) to achieve the desired temperature (around $135\text{ }^\circ\text{C}$). After the RS was boiled to dryness (after approx. 1-1.5 h), the TS was brought to a final volume of 10 mL using a plastic graduated cylinder.

Subsequently, the yield was determined with an OPTIMA 3000 (Perkin Elmer Inc., USA) inductively

coupled plasma optical emission spectrometry (ICP-OES) at PSI.

RESULTS AND DISCUSSION:

In total 15 distillations (5 each for 100 ppm, 50 ppm and 25 ppm) were performed. Figure 1 depicts the scattered results, that indicate general problems with the reproducibility of the silicon separation procedure and the final quantification, using ICP-OES.

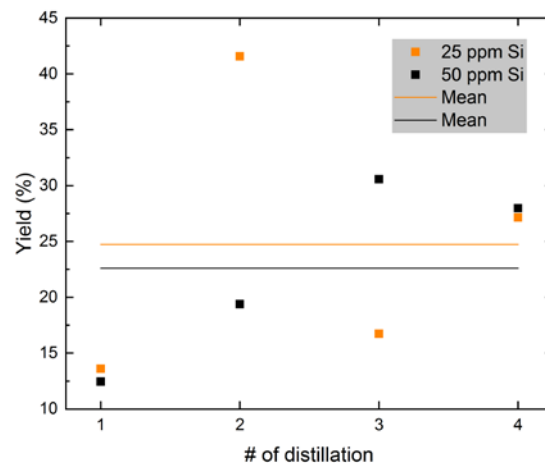
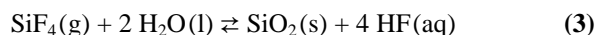


Fig. 1: Calculated yield (%) plotted against count (#) of distillations. Instead of five, only four distillations are displayed, because one value exceeded 100 % and therefore this series was considered as being an outlier. However, the mean of the yield for 25 ppm (24.8 %) and 50 ppm (22.6 %) was determined. The results for 100 ppm are not displayed since the first measurements were only for testing purposes, to establish the measurement method.

At first, a comparison of the pipes of the experimental setup (cleaned and uncleaned), strongly indicated a built up in the pipes, so that silicon is retained. Further, condensation within the flask was observed, which is a potential problem, since the SiF_4 undergoes a reaction with water, that leads to the formation of non-volatile species e.g. silicon dioxide (SiO_2) [2], so that a loss of silicon occurs, as this cannot be transferred anymore into the gaseous state (Eq. 2 and 3):



Moreover, minor Si-impurities in the HNO_3 were determined as well as in the ultra pure water. In conjunction with the tubing (sample introduction) of the ICP-OES, repeated measurements could not accurately determine the actual silicon content.

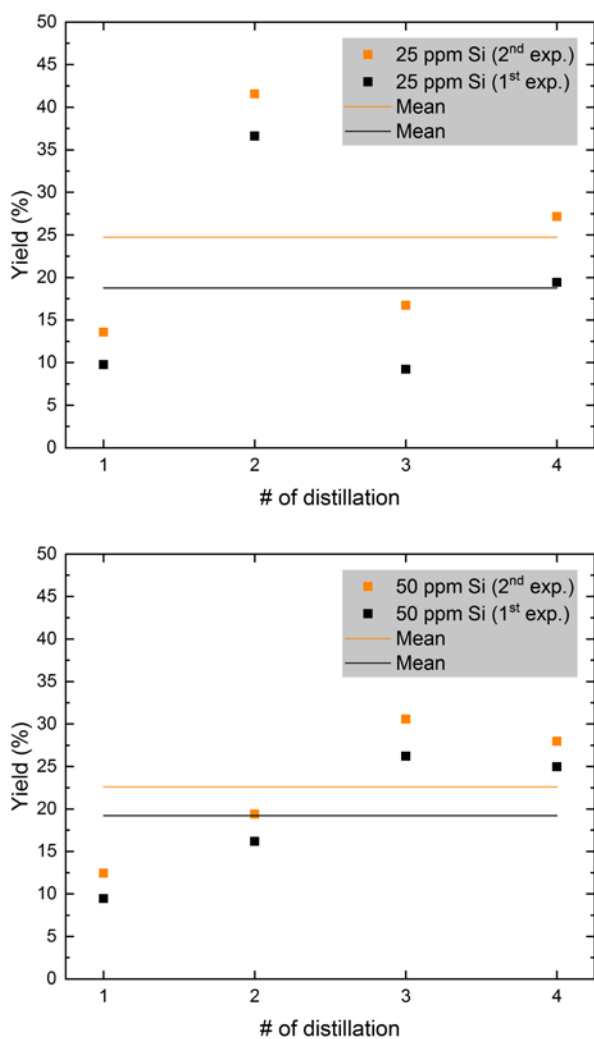


Fig. 2: Data points revealing the problems of measuring the actual silicon content (both for the 25 ppm and 50 ppm series), as repeated measurements show remarkable deviations but still following the same trend. Supposingly, the built-up of silicon lead to a higher Si-content and a higher yield, respectively.

CONCLUSION AND OUTLOOK

Until now, the promising potential of volatile SiF_4 to specifically separate silicon out of a matrix containing several different radionuclides has proven true. However, improvements of the distillation apparatus and the measurement method itself need to be urgently evaluated, because repeated measurements of each series showed remarkable deviations.

Therefore, only a rough determination of the yield was possible which refers to a mean of 25 %. Other problems such as a silicon built-up and Si impurities in general (e.g. HNO_3) are also of special interest. The improvement of the current set-up is ongoing and e.g. an airflow meter was installed and a custom-made PTFE-flask will be used for further distillations. The volume of the flask will be as small as possible to reduce the condensation at the inner surface.

Based on previous experiments with the dried initial solution, a new approach will be undertaken, whereby the vanadium disc will be dissolved with HF, subsequently evaporated to dryness and afterwards the solid residue will be heated up above 135 °C to distill the volatile species (SiF_4). Thus, the problem with water vapors can be avoided.

ACKNOWLEDGEMENT

This project is funded by the Swiss National Science Foundation (SNSF) as part of SINERGIA (No.177229).

-
- [1] G. Jander, E. Blasius, Einführung in das anorganisch-chemische Praktikum (1970).
 - [2] M. Mizuhata et al., Journal of the Ceramic Society of Japan, **335-339** (2009).

LASER SPECTROSCOPY OF PROMETHIUM ISOTOPES

D. Studer, R. Heinke, P. Naubereit (Univ. Mainz), J. Ulrich (PSI), S. Braccini (AEC-LHEP, Univ. Bern), T.S. Carzaniga (AEC-LHEP, Univ. Bern), R. Dressler, S. Heinitz (PSI), U. Köster (ILL), S. Raeder (HIM, GSI), K. Wendt (Univ. Mainz)

Promethium (Pm, $Z = 61$) is an exclusively radioactive lanthanide element with isotopes of only up to 17 years half-life. Optical spectroscopy studies are scarce and only atomic transitions from the lowest fine-structure multiplets are given in literature [1]. In fact Pm is, along with Pa, the last element below $Z = 100$ where the first ionization potential (IP) was never directly measured. A value of $44985(140) \text{ cm}^{-1}$ was determined from lanthanide IP systematics [2], but is rather unprecise. In order to extract atomic and nuclear properties using the accessible miniscule sample amounts, extensive spectroscopic studies were performed at Mainz University by laser resonance ionization spectroscopy. This sensitive technique relies on the stepwise ionization of the element under investigation by pulsed laser radiation. Using the unique atomic structure of each element, an inherent elemental selectivity is achieved, usually together with high ionization efficiencies.

Broadband spectroscopy studies

For the development of laser ionization schemes for Pm, a sample containing Pm-147 was produced in the high-flux reactor at ILL Grenoble by neutron irradiation of enriched Nd-146. The produced Nd-147 decays with a half-life of 11 days to Pm-147 ($t_{1/2} = 2.7 \text{ y}$). The sample was chemically purified at PSI and 10 MBq were delivered to Mainz University. The laser mass spectrometric apparatus is shown in Fig. 1.

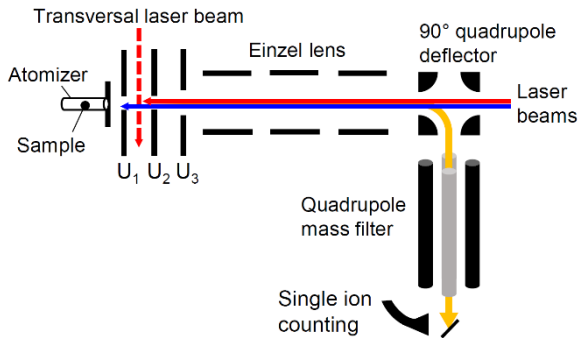


Fig. 1: Scheme of the compact atomic beam mass spectrometer MABU (Mainz Atomic Beam Unit). Ionization may either take place directly in the atomizer by anticollinear laser-ion beam geometry or alternatively within the effusing atomic beam in front of the oven by transversal laser beams.

The sample is atomized in a resistively heated graphite oven and irradiated by tunable laser light. Laser-ionized species are guided through a quadrupole mass filter and are finally detected with a channel electron multiplier in single ion counting mode. The laser system consists of three pulsed Ti:sapphire lasers, which are operated at a repetition rate of 10 kHz and have pulse lengths of typically 40 ns. The tuning range is 680 nm to 960 nm and can be extended by

frequency doubling, tripling or quadrupling. Spectroscopy is performed by tuning one laser in the excitation scheme while monitoring the ion count rate. By doing this successively for first, second and third excitation steps, over 1000 new transitions were discovered in the atomic spectrum of promethium.

Determination of the first ionization potential

As no Rydberg convergences could be identified due to the high level density at high excitation energies, an approach of electric field ionization was used for the determination of the ionization potential. According to the saddle point model, the photoionization energy threshold is proportional to the square root of an external electric field. A measurement of photoionization thresholds for different electric field strengths allows an extrapolation to a zero-field and thus a determination of the ionization potential [3]. In our experiment this approach was implemented with a crossed laser beam geometry between the electrodes U_1 and U_2 , as shown in Fig. 1. The lasers excite atoms into weakly bound states, which only ionize at sufficient field strengths. By tuning either the frequency of the final excitation step or the electric field strength, the photoionization threshold is determined. The former case is shown in Fig. 2. The spectra in perpendicular ionization geometry (lower trace) are subsequently cut off towards lower

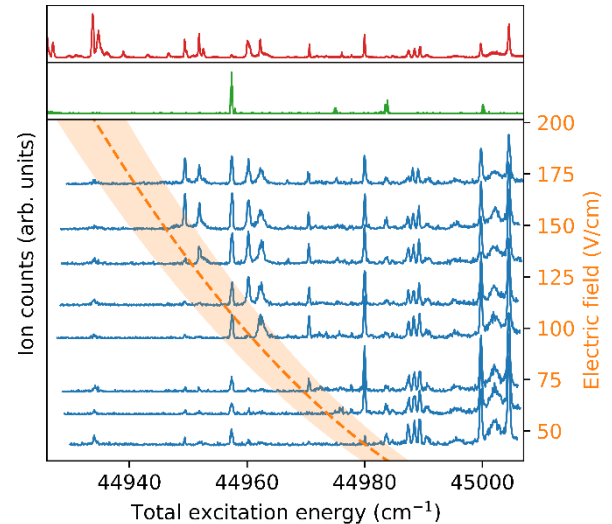


Fig. 2: Determination of ionization thresholds from scans of the final laser excitation step. Upper trace: Fully resonant in-source laser scan; middle trace: In-source laser scan with detuned second excitation step, revealing parasitic resonances; lower trace: Laser ionization scans with external electric field. The dashed line and range illustrate the ionization threshold.

excitation energies, in contrast to the full spectrum obtained from ionization inside the atomizer (upper

REVIEW OF EXPERIMENTS ON IODINE EVAPORATION FROM LIQUID LEAD-BISMUTH EUTECTICUM, PART I: METHODOLOGICAL DEVELOPMENTS

I.I. Danilov (Univ. Bern & PSI), A. Vögele, D. Hermann, R. Dressler (PSI), R. Eichler (Univ. Bern & PSI), A. Türler (Univ. Bern), J. Neuhausen (PSI)

Introduction

Last year we reported the first results on iodine evaporation from liquid lead-bismuth eutectic (LBE) samples studied by the transpiration method, performed within the H2020 project MYRTE in support of licensing the LBE cooled MYRRHA transmutation reactor [1]. Meanwhile, experimental techniques and evaluation methods were improved and a large number of additional experiments on the topic have been performed to obtain results of higher accuracy and to study the influence of LBE purity and interaction with different cover gases on iodine evaporation. The results of these experiments will be evaluated in detail during next year. In this report we will give an overview of the methodological developments that were performed in support of these studies. In a second report, we will present the most important preliminary results and discuss the steps remaining for a final evaluation of the data.

Methodological developments

In our very first series of transpiration experiments performed on the evaporation of iodine from liquid LBE we encountered problems caused by inhomogeneities of the iodine distribution in the LBE samples that hampered precise evaluation of the data. To mitigate these problems, we strived for achieving better homogeneity, to better understand the limitations of our experimental approach and to develop a reasonable strategy to obtain data of the highest possible quality.

In a transpiration experiment, we measure the amount of radiotracer present in the original sample before the experiment, the amount remaining in the sample after the experiment and the amount of radiotracer evaporated and deposited in a cold zone downstream of the evaporation zone. The Henry constant can then be determined from the measured activities using the following equations [2]:

$$K_H = -\ln\left(\frac{A_{\text{remaining}}}{A_{\text{before}}}\right) \cdot m_{\text{LBE}} \cdot RT / (M_{\text{LBE}} \dot{V} t) \quad (1)$$

$$K_H = -\ln\left(1 - \frac{A_{\text{evap}}}{A_{\text{before}}}\right) \cdot m_{\text{LBE}} \cdot RT / (M_{\text{LBE}} \dot{V} t) \quad (2)$$

(K_H : Henry constant, $A_{\text{before/remaining/evap}}$: Activity of the sample before and after experiment and activity of evaporated material, respectively, m_{LBE} : mass of LBE, R : universal gas constant, T : temperature at which the volumetric flow is measured, M_{LBE} : molar mass of LBE, \dot{V} : volumetric flow, t : experiment duration). Thus, a prerequisite for a precise determination of K_H is a reliable assessment of A_{before} and either $A_{\text{remaining/evap}}$. We preliminarily examined the effects of counting statistics and uncertainties of the parameters in eqs. (1 and 2) on the uncertainty of the derived K_H values in [3]. Meanwhile, an evaluation routine based on a full implementation of error propagation rules has been

developed. This routine has been used to determine the results presented in the following report.

A_{before} can be determined by γ -spectrometry, either by measuring the full LBE sample as is, or by measuring several aliquots cut from the sample before the experiments dissolved in 7M HNO_3 and determining their mean activity concentration. The latter method avoids problems of γ -ray attenuation in the LBE-matrix, but nevertheless requires the iodine to be homogeneously distributed in the LBE. The first method requires the correction of absorption effects of the LBE-matrix that affect the relative intensities of γ -quants of different energies. This can be achieved in an approximate manner by assuming that the iodine is homogeneously distributed in the LBE and comparing the detection efficiencies of γ -quants calculated for a geometry approximating the real dimensions of the LBE sample to that of a point source. Thus, finally both methods require that the iodine distribution in the sample before the experiment is reasonably homogeneous to obtain reliable results.

Fig. 1 shows a comparison of the efficiency as a function of γ -ray energy of a point source with the efficiency for a spherical LBE source with homogeneous distribution of the dissolved radionuclide, both calculated using the ISOCS-program in GENIE 2000. Strong absorption effects can be seen especially for the low energy γ -rays.

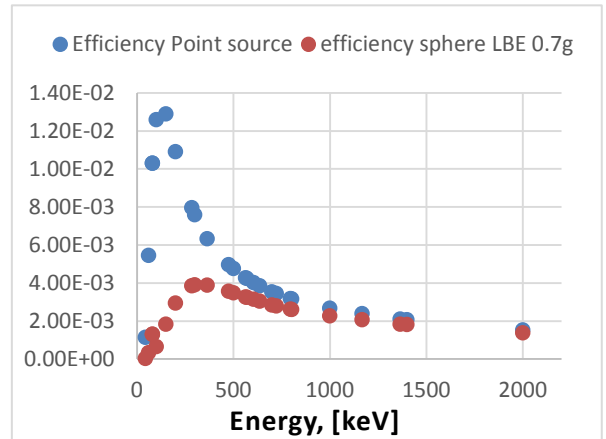


Fig. 1: Comparison of the efficiency vs energy of a point source with that of a spherical LBE sample of 0.7 g, both calculated using the ISOCS-program in Genie 2000.

Meanwhile, we investigated both methods for the determination of A_{before} in more detail. For the first series of experiments, two measurements of the LBE samples were performed before the experiments, with opposite orientations, and 3 aliquots were cut, dissolved in 7M HNO_3 and analysed individually. The results from the LBE sample were corrected for absorption effects using calculated efficiency ratios of a point source and a

spherical LBE specimen whose radius was determined by the mass of the actually used sample. For samples produced by mixing of LBE with 2 mass-% Te at 850°C, rapidly quenched in a water bath and subsequently n-irradiated to produce ^{131}I , both good consistency of the activity concentrations of the 3 liquid aliquots was achieved. Also, good agreement between data from the analysis of liquid aliquots and data from measuring the full LBE samples was achieved by applying the absorption correction (Fig. 2).

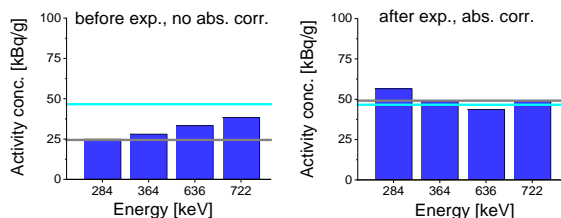


Fig. 2: Comparison of apparent activity concentrations determined from γ -lines of different energy of a ca. 0.7 g LBE sample, without (left) and with (right) absorption correction. The activity concentration obtained as average, weighted according to the emission probability of the 4 γ -rays before and after absorption correction is indicated as grey horizontal line, whereas the average obtained from measurements of 3 dissolved aliquots of the same LBE sample is indicated as a blue line.

In conclusion, we have proven that the iodine distribution in the samples used for transpiration experiments is reasonably homogeneous and we can determine the iodine content with sufficient accuracy by two methods.

For use of eq. (1) $A_{\text{remaining}}$ needs to be determined. This could in principle be done in a similar manner as outlined above for A_{before} . However, our measurements show that iodine tends to enrich at the top surface of the LBE sample after the experiments. This is indicated by larger apparent activity measured when the top-side of the sample is facing the detector, compared to the bottom side, especially for the lower energy γ -rays. Because of these surface enrichment effects, the absorption correction useful for the homogeneous samples doesn't give meaningful results (Fig. 3). Also, aliquots taken from the samples give inconsistent results because they can contain different relative amounts of the surface enriched material and thus are not representative for the total sample. We have tried to minimize the enrichment effect by cooling the samples to solidification after the experiment relatively fast (within 1-2 min) using a blower, but this did not sufficiently suppress surface enrichment. As a consequence, to reliably determine the activity left in the sample after the experiment, either more rapid quenching would have to be applied, or the complete samples would have to be dissolved in e.g. HNO_3 to form a homogeneous specimen that can be measured in the desired geometry. In the present study, we have not yet developed a method that allows faster quenching in our apparatus. For some experiments at high temperature where it is useful to apply eq. (1) for evaluation, the full LBE sample was dissolved and analysed.

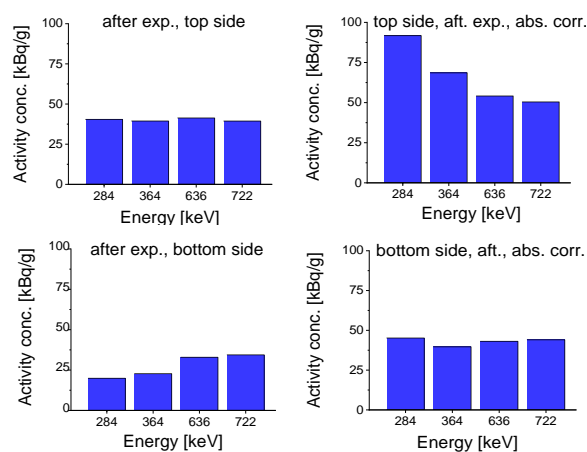


Fig. 3: Comparison of the apparent activity concentrations of the same ^{131}I -containing LBE sample measured with the bottom and top side of the sample facing the detector. The left side shows raw data, while on the right side a correction for absorption effects was applied that was derived assuming homogeneous distribution of the ^{131}I in a spherical sample. Comparing the raw data of the top and bottom side indicates enrichment on the top surface. The sample behaves approximately as if a point source would be stuck to the top surface. The right side indicates that the absorption correction using a spherical model – as expected – doesn't give useful results in this case.

For most of the experiments, eq. (2) has been used to determine Henry constants. For the determination of A_{evap} , the evaporation tubes were carefully rinsed several times, first with 4M NaOH, then with water and with 7M HNO_3 , to ensure >99% retrieval of the evaporated iodine. The washing solutions as well as a charcoal filter that was placed at the exhaust of the transpiration tube were carefully measured by γ -spectrometry to determine their ^{131}I -content. Quantitative evaluation was achieved by calibration of the detector using multinuclide calibration sources of the same geometry.

Several series of transpiration experiments have been performed in a temperature range between 150 and 845 °C, using different sources of LBE (technical and high purity), with and without pretreatment for reduction of its oxygen content, using various carrier gases (He , H_2 , N_2) and different iodine concentrations. The preliminary results of these studies will be summarized in the following report.

This work was funded by the project MYRTE under EURATOM HORIZON2020 Grant Agreement No. 662186.

- [1] I. I. Danilov et al., Ann Rep. LRC, 20 (2017).
- [2] B. Gonzalez Prieto et al., J. Nucl. Mater 450, 299 (2014).
- [3] R. Dressler et al., Ann Rep. LRC, 16 (2017).

REVIEW OF EXPERIMENTS ON IODINE EVAPORATION FROM LIQUID LEAD-BISMUTH EUTECTICUM, PART II: PRELIMINARY RESULTS

I.I. Danilov (Univ. Bern & PSI), A. Vögele, D. Hermann (PSI), R. Eichler (Univ. Bern & PSI), A. Türler (Univ. Bern), J. Neuhausen (PSI)

In the present report we will summarize the preliminary results of the experiments performed. Earlier studies showed that the gas phase composition [1] as well as impurities in the LBE matrix [2] may significantly influence the evaporation behaviour for polonium. In particular, it was found that oxygen impurities in the LBE and moisture in the gas phase can enhance polonium evaporation, probably caused by the formation of hydroxide and oxyhydroxide species of different oxidation states. Since for iodine many volatile species that can form in presence of water and oxygen are known, we tried to suppress the amount of these impurities to be able to study the behaviour of iodine in contact with LBE under dry and non-oxidizing conditions as a base line for later studies of humid and/or oxidising systems. As a consequence, all operations were performed in an inert gas box at O₂ and H₂O gas phase concentrations < 1ppm. Furthermore, for most of the studies the LBE was treated by contact with hot tantalum foil to reduce its oxygen content. Additionally, different qualities of LBE (technical LBE as to be used in the MYRRHA reactor and LBE prepared from high purity Pb and Bi) have been used to find potential influences of impurities contained in the raw material. Also, the influence of different carrier gases on the evaporation has been studied. Finally, the influence of iodine concentration on evaporation was investigated.

The iodine behaviour was studied making use of radioactive iodine isotopes produced in the neutron irradiation facilities available at PSI. Iodine isotopes with suitable half-life and decay characteristics are ¹³¹I (t_{1/2} = 8.02 d) and ¹²⁶I (t_{1/2} = 13.11 d). The former can be produced in non-carrier-added form by neutron irradiation of natural Te, while ¹²⁶I can be produced by neutron irradiation of iodine or its compounds. Both methods have been used in the present study. For the production of LBE samples containing non carrier added amounts of ¹³¹I, mixtures of LBE with 0.5 – 2 mass% Te were prepared by mixing at 850°C under vacuum and quenching to room temperature [4]. These were typically irradiated for 2-3 h in a neutron flux of nominally 1x10¹³ n/cm²/s. LBE samples containing iodine marked with ¹²⁶I-tracer were prepared by irradiating ca. 10 mg of PbI₂ for one month at a neutron flux of nominally 4x10¹³ n/cm²/s and subsequently mixing the PbI₂ with ca. 15 g of LBE. For this purpose, the irradiated PbI₂ and the LBE were molten at 900°C for 1 d in an evacuated silica ampoule, where it was shaken occasionally to ensure dissolution of the PbI₂ in the LBE. The mixture was then cooled to 500°C to avoid having a large fraction

of the iodine in the gas phase, and then quenched to room temperature.

The obtained sample had a uniform iodine distribution, judged from several small pieces cut and analysed by γ -spectrometry. The mole fraction of iodine in this samples was $x_I = 5.81 \times 10^{-4}$. Another sample of about tenfold lower concentration was obtained by diluting a part of the original sample with additional LBE.

Samples were prepared from LBE-batches with different purity, with or without reduction by tantalum. Several series of transpiration experiments were performed to determine Henry-constant data as a function of temperature according to the procedures described in [3, 4]. Two additional series of experiments were performed at constant temperature under variation of the flow rate to find out under which conditions saturation of the carrier gas with iodine is achieved. An overview of these series is given in Table 1.

Tab. 1: Summary of series of experiments.

Ser. No.	LBE	reduced	gas	Flow (ml/min)	x_I	Fast cooled
1	Tech.	yes	He	100	$\cong 10^{-10}$	no
2	Tech.	yes	He	25-1000	$\cong 10^{-10}$	some
3	Tech.	yes	He	280	$\cong 10^{-10}$	yes
3a	Tech.	yes	H ₂	200	$\cong 10^{-10}$	yes
3b	Tech.	yes	N ₂	200	$\cong 10^{-10}$	yes
4	6N Pb 5N Bi	yes	He	25-1000	$\cong 10^{-10}$	yes
5	6N Pb 5N Bi	yes	He	280	$\cong 10^{-10}$	yes
6	6N Pb 5N Bi	yes	He	100	$\cong 10^{-10}$	yes
7	Tech.	no	He	100	$\cong 10^{-10}$	yes
8	6N Pb 6N Bi	yes	He	100	$\cong 10^{-10}$	yes
9	6N Pb 6N Bi	no	He	100	6×10^{-4}	yes

Results and discussion

Saturation studies

The results of flow rate dependent iodine evaporation studies performed on technical and high purity LBE, respectively, are shown in Figures 1 and 2. For the technical LBE, a saturation plateau is visible ranging from approximately 100 to 400 ml/min. The identification of a saturation regime for the high purity LBE is less obvious. However, there is a range of flow rates between 50 and 150 ml/min where the values of apparent K_H do not change within the relatively large uncertainty margin. Based on these results, we chose a flow rate of 100ml/min for the measurements of the temperature function of the Henry constant of iodine for the high purity LBE. Experiments with the

technical LBE where performed using flow rates in the range between 100 and 280 ml/min. It is apparent from these two series of experiments, both performed at 385°C, that there is a large influence of the purity of LBE on the evaporation behaviour of iodine.

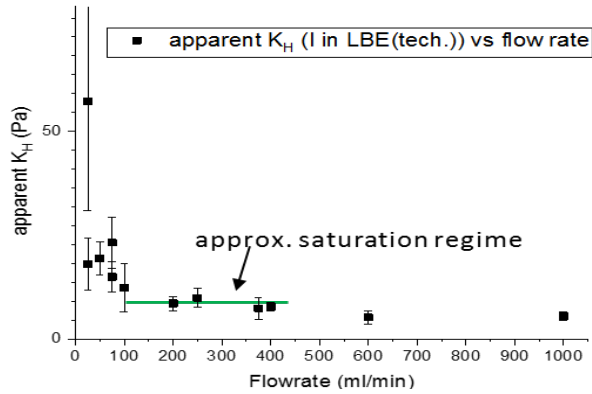


Fig. 1: Plot of apparent Henry constants vs. flow rate determined using technical LBE at 385°C. The approximate saturation regime is indicated by a green line.

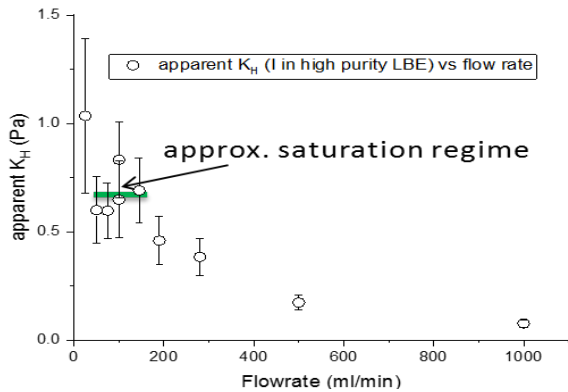


Fig. 2: Plot of apparent Henry constants vs. flow rate determined using high purity LBE at 385°C. The approximate saturation regime is indicated by a green line.

Studies of apparent K_H vs temperature

Data from most of the studies compiled in Table 1 are depicted in plots of the apparent Henry constant on a logarithmical scale vs the inverse temperature in Figs. 3 and 4. Fig. 3 shows a comparison of data obtained from technical LBE in He (reduced and not reduced), H_2 and N_2 gas. All data were obtained from samples containing non-carrier added ^{131}I produced from a 2% Te admixture, with an iodine mole fraction of $x_I \cong 10^{-13}$. The data show approximately linear behaviour over a large temperature range from 150 to 800 °C. No large influence of carrier gas and Ta-reduction is observed. The absolute values of K_H fall into a range that can be expected for solutions of Bi- or Pb-iodides that do not deviate too much from ideal behaviour of the dilute. In Fig. 4 we compare results of series 3 and 7 obtained from technical LBE with results obtained from 3 series performed with two different batches of nominally high purity LBE, series 6 and 8 containing ^{131}I at $x_I \cong 10^{-13}$ and a series of experiments with iodine at $x_I \cong 5.8 \times 10^{-4}$ marked with ^{126}I tracer. The fact that

series 9 yields higher values of apparent K_H can be explained by different species evaporating at higher concentrations. At $x_I \cong 10^{-13}$ BiI is the most likely species, while at $x_I \cong 5.8 \times 10^{-4}$ PbI_2 or BiI_3 may form. This assumption may be confirmed by systematic studies of the concentration dependence as well as thermodynamic modelling.

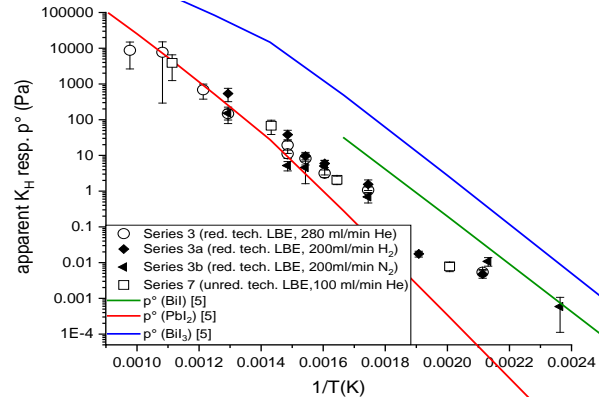


Fig. 3: Comparison of apparent K_H determined from reduced technical LBE doped with non-carrier-added amounts of ^{131}I produced from a 2 mass-% Te admixture in different gas atmospheres (He , H_2 , N_2).

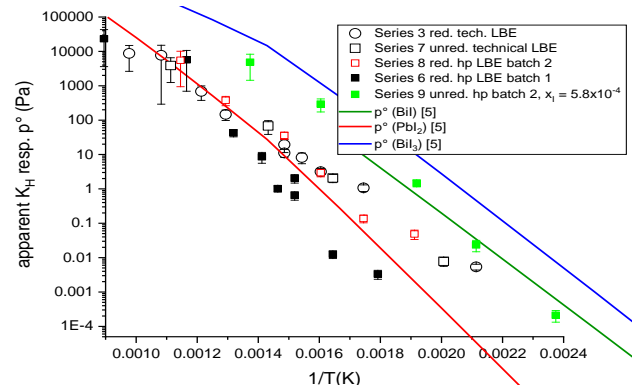


Fig. 4: Comparison of K_H determined from reduced technical LBE doped with non-carrier-added amounts of ^{131}I with data obtained from nominally highly pure LBE containing I at largely different concentrations.

The fact that the results of the two series containing non-carrier added ^{131}I in different batches of high purity LBE don't agree indicates the presence of an impurity that influences the evaporation behaviour of iodine. Careful elemental analyses of all used LBE batches as well as Pb and Bi raw materials are planned to find this contamination.

This work was funded by the project MYRTE under EURATOM HORIZON2020 Grant Agreement No. 662186.

- [1] E. A. Maugeri et al., J. Nucl. Mater 450, 292 (2014).
- [2] B. Gonzalez Prieto et al., J. Radioanal. Nucl. Chem. 309, 597 (2016).
- [3] I.I. Danilov et al., Ann. Rep. LRC, 20 (2017).
- [4] I.I. Danilov et al., Ann. Rep. LRC, 18 (2017).
- [5] I. Barin, Thermochemical data of pure substances, 3-th ed., VCH, Weinheim, 1995.

POLONIUM DEPOSITION BEHAVIOUR IN THE EVENT OF A BEAM GUIDE WINDOW PUNCTURE IN AN ACCELERATOR DRIVEN SYSTEM

E. Karlsson (Univ. Bern & PSI), A. Vögele (PSI), R. Eichler (Univ. Bern & PSI), A. Aerts (SCK-CEN), D. Hermann (PSI), A. Türler (Univ. Bern & PSI), J. Neuhausen (PSI)

Currently, all operating nuclear reactors are run as critical systems, meaning the neutron economy inside the reactor is self-sustaining. The reactor remains critical without outside influence and thus needs an outside influence to become non-critical. This in turn can lead to slow scram times with potentially disastrous excursions as consequences. The advantage of an accelerator driven system (ADS) is that the neutrons required to keep the reactor in a critical state are induced from a source outside of the reactor and can thus be removed by interrupting this source. These extra neutrons are produced by accelerating and impacting charged particles on a spallation target. This spallation target is preferentially a high-Z element to yield a sufficient neutrons per μA value [1]. The system concerned in this text utilizes high-energy protons impacting lead-bismuth eutectic (LBE) used as target to provide spallation neutrons and simultaneously as reactor coolant.

In an ADS there are two distinct possible ways to implement a beam guide. It can either be an open windowless channel with direct access to the coolant or it can utilize a window to achieve a vacuum inside the beam guide [2]. This provides an additional barrier against potential release of radionuclides from the coolant. This work was performed to determine the behavior of polonium released into the beam-guide of an accelerator driven lead-bismuth fast reactor during operation in the event of a window puncture. The beam guide is operated in near vacuum with a metallic window separating it from the coolant.

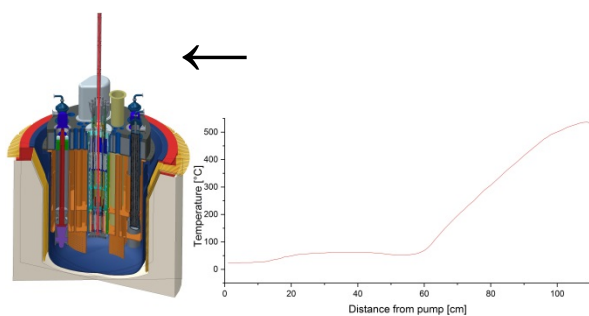


Fig. 1: Left: Technical sketch of an ADS system with the beam guide highlighted in red [3]. Right: Temperature gradient produced from a thermal gradient furnace combined with heating wire to produce a gradient which replicates the conditions of an ADS beam guide. The high point is approximately 540°C and the flat zone between 20 and 60 centimeters holds an even temperature of $50\text{-}60^{\circ}\text{C}$.

To replicate the conditions and geometry of the beam guide, a 4 mm diameter, 1100 mm long 316L stainless steel column was sealed at one end with a 4 mm long 316L plug which was inserted at one end of the column and welded in place. At the other end of the column a vacuum pump (Pfeiffer HiCube 80 Eco) was continuously active during the experiment. This pump produced a vacuum with a residual pressure of approximately 10^{-6} mbar (measured at the pump). The column itself was inserted into a thermal gradient furnace with a maximum temperature of approximately 540°C . In the cold zone a heating wire was wrapped around the column to assure accurately replicated conditions throughout the setup. This resulted in a final gradient with properties as described in figure 1.

Samples were prepared by irradiating 250 milligrams of lead-bismuth eutectic (LBE, 55% bismuth, 45% lead) in the SINQ neutron source ($\sim 10^{13}$ n/(s * cm^2)) for 2.5 hours to produce ^{210}Po from the neutron capture reaction of ^{209}Bi . From previous irradiations of the same material an activity of approximately 75 Bq/mg of ^{210}Po was assumed for the finished samples. This sample was cut into two smaller pieces weighing 65 and 85 milligrams. Before each experiment, the sample was dropped from the open end of the stainless steel column and allowed to settle at the far end. In order to prevent release of polonium into the lab during experiments a strip of silver was added at the open end of the column. This adsorbs residual polonium that did not deposit inside the column. To start the experiments the pump was ran to ensure stable conditions before starting the furnace to commence the evaporation. The experimental time chosen was 72 hours. This was mainly to ensure sufficient evaporation of polonium as available data for non-vacuum conditions suggested it would be very low [4]. During the experiment the pressure was monitored to ensure stable conditions. Additionally the dew point was measured using a dew point meter (Michell Easidew EA2-TX-100-HD). After the experiment the columns were cut into 1 cm pieces which were put in 1 ml of 7 M HNO_3 and allowed to leach out. The leached solution was measured using liquid scintillation counting (LSC).

From the results acquired from the LSC-measurement in combination with known experimental parameters such as temperature gradient, experimental time as well as a guess for the adsorption enthalpy, a Monte Carlo simulation was performed. This tracks the movement of one atom at a time inside the column for numerous adsorption/desorption events until one of three conditions are met: the experiment time expires, the atom leaves the column or the atom decays [5].

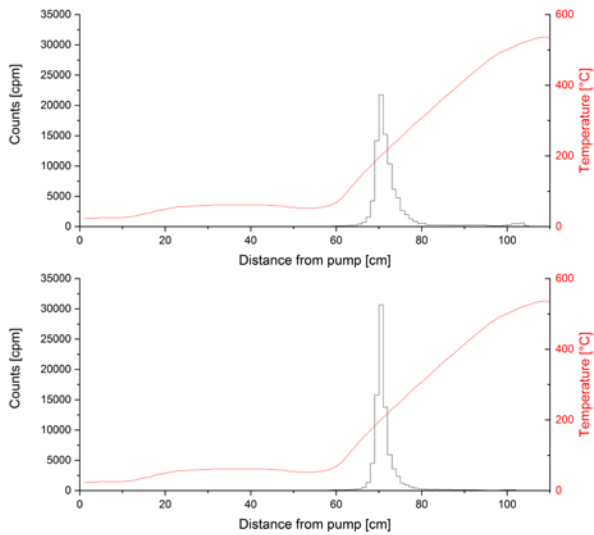


Fig. 2: The two evaluated chromatography experiments. The black step-curve indicates the position of the activity in the column after the experiment while the continuous red line shows the temperature throughout the column.

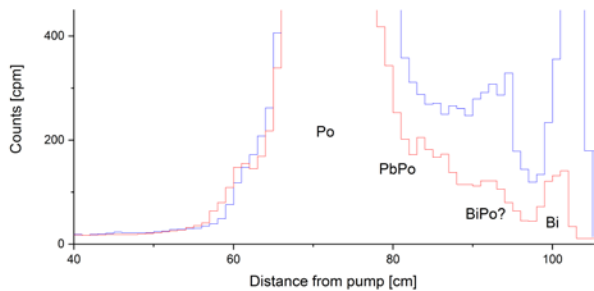


Fig. 3: Magnified overlay of deposition in experiment #1 (blue) and experiment #2 (red).

The Monte Carlo simulations for the two experiments determined an adsorption enthalpy of -150 ± 5 kJ/mol for the main deposition peak and -165 ± 5 kJ/mol for the high-temperature shoulder.

Quantum chemical calculations show that for a lead-bismuth eutectic system with trace polonium, the expected dominant species at ambient pressure is PbPo [6]. The key difference in the system considered in this work is the pressure. Low pressure will make molecules more prone to decomposition according to Le Chatelier's principle. In atmospheric pressure the monoatomic polonium mole fraction in the gas phase at the highest temperature in the gradient ($\sim 540^\circ\text{C}$) is approximately 0.1 [6]. By decreasing the pressure by 9 orders of magnitude the equilibrium should shift in favor of the decomposition products, making monoatomic polonium the dominant species. A remaining fraction of lead polonide would also explain the presence of a high-temperature shoulder on the deposition in Fig 3. Further data supporting this theory is the agreement of the adsorption enthalpy value found in this work with that for monoatomic polonium on steel in previously published work, as well as a fair agreement with the one for lead polonide [7-8]. Other potential contributions in the yet higher temperature region are bismuth polonide and metallic bismuth. The

peak around 100 cm is likely produced by bismuth as the number of counts changes significantly between experiments as ^{210}Bi decays into ^{210}Po over time. This peak is present due to the gradual decay of ^{210}Bi as the neutron activation does not directly produce ^{210}Po and the experiments were performed shortly after irradiation.

Throughout the column from the main deposition peak down to the pump a tailing was observed. This was concerning, had it been the result of the presence of a volatile polonium species. However, Monte Carlo simulations showed that this behavior has to be expected regardless of the input adsorption enthalpy. Further simulations utilizing other parameters such as the sticking factor (the probability of each surface interaction resulting in an adsorbed state) showed that this behavior is a consequence of the large amount of particles present as well as the geometry of the column. Given enough particles, in a vacuum some will always find a free path through the column to the low temperature zone without interacting with the column surface. In the simulations the amount of particles simulated was based on the detection limit of the LSC (approximately 3 cpm over background) combined with the number of polonium atoms present. There were $\sim 10^{11}$ ^{210}Po atoms in each sample and the detection limit is roughly 10^5 atoms meaning one million atoms would be sufficient to simulate the behavior.

From these experiments and simulations we can conclude that polonium evaporated from LBE in a vacuum does not behave in a particularly volatile way. However, due to the geometry of the system as well as the sheer number of atoms involved there will always be some transport to lower temperatures. This behavior persisted upon lengthening the simulated setup, however undetectable levels in the near-pump region were achieved with a simulated column of 130 cm.

- [1] M. Steinberg, in IIASA Workshop Proceedings, 1983.
- [2] F. Heidet et al., Rev. Accel. Sci. Technol., vol. 08, 99–114, 2015.
- [3] SCK-CEN, Available: <https://sckcen.be/en/MediaLibrary/Pictures/MYRRHA>. [Accessed: 17-Jan-2019].
- [4] B. Gonzalez Prieto et al., Radiochim. Acta, vol. 102, 1083–1091, 2014.
- [5] I. Zvara, Radiochim. Acta, vol. 38, 95–101, 1985.
- [6] M. Mertens et al., Submitted for publication.
- [7] E. A. Maugeri et al., Radiochim. Acta, vol. 104, 125–134, 2016.
- [8] B. Gonzalez Prieto et al., Ann Rep. Lab. of Radio- & Environ. Chem., Univ. Bern & PSI, (2016).

Cu-64 CHLORIDE AND Cu-64 LABELLED Cd-80/Cd-86-TARGETING FUSION PROTEINS FOR PET-IMAGING OF INFLAMMATION

M. Taddio, C. Castro (ETHZ), Z. Talip, R. Hasler, A. Blanc (PSI/CRS), R. Schibli (ETHZ/PSI), M. Behe (PSI/CRS), S. Krämer (ETHZ), N.P. van der Meulen (PSI/LRC)

^{64}Cu ($T_{1/2} = 12.7$ h) is used as part of a radiotracer for positron emission tomography (PET) and is a promising radiotherapy agent for the treatment of cancer. ^{64}Cu was produced at PSI by irradiation of ^{64}Ni using the $^{64}\text{Ni}(p,n)^{64}\text{Cu}$ nuclear reaction. The ^{64}Cu was separated from its target material and impurities using cation exchange chromatography, where the product was eluted using dilute HCl in acetone and, subsequently, evaporated to dryness before picking it up in dilute HCl (Fig. 1).



Fig. 1: The ^{64}Cu chemical separation system.

The ^{64}Cu final product was used in two related projects aiming at the non-invasive imaging of inflammatory processes by positron-emission tomography (PET).

In the first project, we continued evaluating the co-stimulatory molecule CD80 as a target for PET imaging. CD80 expression is upregulated in activated antigen-presenting cells (macrophages, dendritic cells, neutrophils), leads to T cell activation and is involved in various inflammatory pathologies.[1,2] We conjugated the commercially available CD80/CD86-targeting fusion protein belatacept with NODAGA and radiolabeled it with ^{64}Cu . The tracer was injected intravenously in immune-deficient SCID mice with human Raji xenografts expressing high levels of CD80. Similar to ^{111}In -DOTA-belatacept in Raji-xenograft-bearing CD1 nude mice [3], we observed accumulation in the xenograft (moderate) and abdomen (Fig. 2).

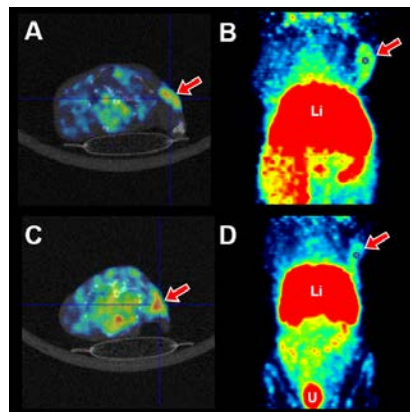


Fig. 2: PET/CT images of two SCID mice with human CD80-positive Raji xenografts on the right shoulder (red arrows), injected with [^{64}Cu]-NODAGA-belatacept 48h before imaging. Accumulation observed in xenograft, liver & intestines (Li) and urinary bladder (U). (A,C) Transverse view; (B,D) maximal intensity projections.

These experiments were conducted to confirm the availability of CD80 in this model for imaging. The model is used for the development of low-molecular weight hCD80-targeting tracers and CD80-targeting truncated proteins. Furthermore, we investigated whether ^{64}Cu -NODAGA-abatacept, which binds with improved affinity to human CD80, is able to image local inflammation in immune-competent BL/6 mice. The local inflammation was induced by lipopolysaccharide (LPS) deposited in matrigel. The tracer accumulated moderately on the site of inflammation 3 days after LPS inoculation. No accumulation was observed in BL/6 control mice inoculated with PBS/matrigel for control (data not shown).

In the second project, we investigated the uptake of $^{64}\text{CuCl}_2$ in brown fat in mice. Recent research identified brown fat as a tissue with immune-relevant functions [4] and our preliminary research indicated increased ^{64}Cu uptake in brown fat. We compared the uptake of ^{64}Cu in brown fat of mice, bearing a local LPS-induced (see above) inflammation (Fig. 3), with control mice without inflammation. We found a significantly higher accumulation of ^{64}Cu in the brown fat of LPS-induced mice, six days after LPS inoculation, than in the brown fat of the control mice (post mortem biodistribution). This would be in agreement with our hypothesis that ^{64}Cu may serve as a tracer for immunological processes. Other than the increased tracer uptake upon LPS challenge, we found an increase in the expression of proteins involved in Cu(II/III) cell uptake in the brown fat of LPS-treated mice (data not shown).

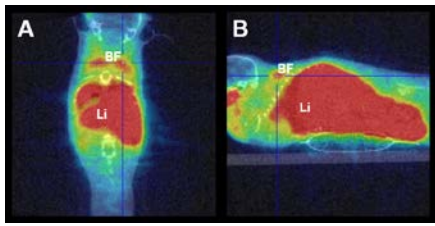


Fig. 3: Male BL/6 mouse injected with $^{64}\text{CuCl}_2$ and PET/CT scans at 3h after tracer injection. Accumulation in brown fat (BF) and liver & intestines (Li). (A) Coronal view; (B) sagittal view.

Outlook

We will investigate whether the xenograft uptake of [^{64}Cu]-NODAGA-belatacept is specific by PET scans under blocking conditions. To further investigate ^{64}Cu as a marker for inflammation and/or for activated brown fat, we will perform scans under inflammatory conditions and after pharmacodynamical activation of the brown fat. The expression of Cu(II/III) uptake related proteins will be analysed in parallel.

We acknowledge funding from the Swiss National Science Foundation (SNSF) [153352] and the KFSP Molecular Imaging Network Zurich (MINZ).

- [1] L. Chen, D. B. Flies. *Nature Reviews Immunology* **13**, 227 (2013).
- [2] A. B. Adams, M. L. Ford, C. P. Larsen. *J Immunol* **197**, 2045 (2016).
- [3] R. Meletta, A. Müller Herde, P. Dennler, E. Fischer, R. Schibli, S.D. Krämer, *EJNMMI Research* **6**,1 (2016).
- [4] S. M. van den Berg, A. D. van Dam, P. C. Rensen, M. P. de Winther, E. Lutgens. *Endocr Rev* **38**, 46 (2017).

USING THE (P,2N) NUCLEAR REACTION TO PRODUCE ^{43}Sc FROM ^{44}Ca

R. Hasler (PSI/CRS), N.P. van der Meulen (PSI/LRC)

Introduction

The favourable decay properties of ^{43}Sc and ^{44}Sc for cancer diagnosis using Positron Emission Tomography make them promising candidates for future application in nuclear medicine. An advantage ^{43}Sc ($T_{1/2} = 3.89$ h, $E_{\beta+\text{av}} = 476$ keV) exhibits over ^{44}Sc , however, is the absence of co-emitted high-energy γ -rays. While the production and application of ^{44}Sc has been comprehensively investigated [1-3], research with regard to ^{43}Sc is still in its infancy. This study aimed at developing a further option to produce ^{43}Sc , over and above what we published recently [4], by using ^{44}Ca target material and the $^{44}\text{Ca}(p,2n)^{43}\text{Sc}$ nuclear reaction (Fig. 1).

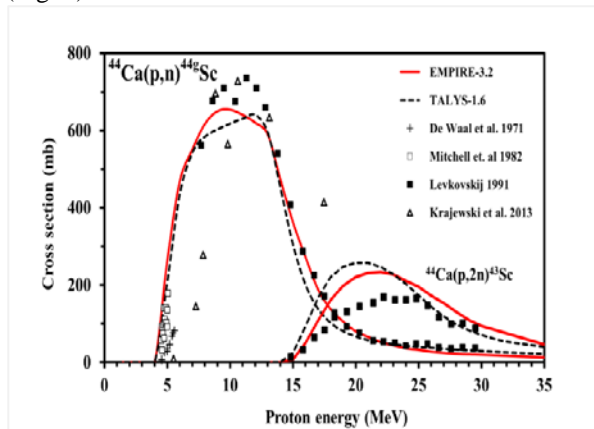


Fig. 1: Cross section measurements of ^{44}Sc and ^{43}Sc using ^{44}Ca as target material.

Experimental

Enriched ^{44}Ca was prepared in oxide form (31 mg), pressed into a pellet, encapsulated and irradiated using the 72 MeV proton beam provided by Injector 2 at Paul Scherrer Institute, degraded to various energies using Nb discs. The irradiated targets were processed chemically, based on the method described previously [2].

Results

The targets proved to be robust in the proton beam for a period of 90 minutes at 40-50 μA at various proton energies (Table 1, Fig. 2). The targets were chemically processed as before [2] and were determined to contain only ^{43}Sc and ^{44}Sc , at various ratios, respectively. The optimum conditions to obtain maximum ^{43}Sc yield was ~26-28 MeV, where 77% of desired product was obtained. The yields of the combined radionuclides were >4 GBq. DOTANOC was labelled with ^{43}Sc at ~20 MBq/nmol at >99% radiochemical purity.

Tab. 1: Irradiation energies calculated using TENDL when using Nb as degrader in the IP2 irradiation station at PSI.

Nb Degrader (mm)	Proton Energy (MeV)
3.4	10.3
2.8	18.6
2.4	22.8
2.2	24.7
2.0	26.4
1.8	28.1
1.0	34.1

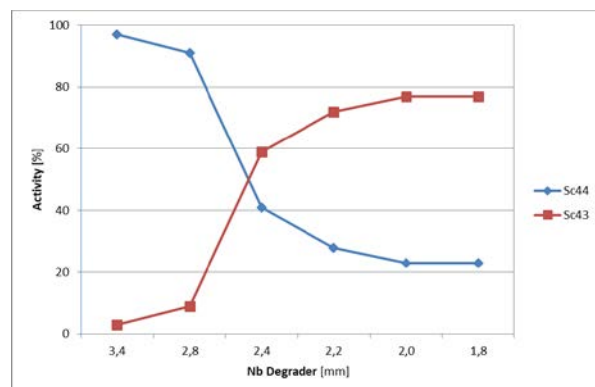


Fig. 2: Yields of $^{43}\text{Sc}/^{44}\text{Sc}$ obtained at various proton energies, using Nb degraders, after chemical separation.

Conclusions

^{43}Sc (>75%) was produced at high yields irradiating ^{44}Ca targets at >25 MeV. It is a favourable result over the $^{43}\text{Ca}(p,n)$ route. The high chemical purity was confirmed by ability to use it for high-specific radiolabeling of biomolecules.

- [1] C. Müller, M. Bunka, J. Reber, C. Fischer, K. Zernosekov, A. Turler et al., Promises of cyclotron-produced ^{44}Sc as a diagnostic match for trivalent β^- -emitters: in vitro and in vivo study of a ^{44}Sc -DOTA-folate conjugate. *J Nucl Med* 2013;54.
- [2] N.P. van der Meulen, M. Bunka, K. Domnanich, C. Müller, S. Haller, C. Vermeulen et al., Cyclotron production of ^{44}Sc : From bench to bedside. *Nuclear Medicine and Biology* 2015;42:745-51.

- [3] K. Domnanich, C. Müller, R. Farkas, RM. Schmid, B. Ponsard, R. Schibli et al., ^{44}Sc for labeling of DOTA- and NODAGA- functionalized peptides: preclinical in vitro and in vivo investigations. *EJNMMI Radiopharmacy and Chemistry* 2016;8:19.
- [4] K. Domnanich, R. Eichler, C. Müller, S. Jordi, V. Yakusheva, S. Braccini et al., Production and separation of ^{43}Sc for radiopharmaceutical purposes. *EJNMMI Radiopharmacy and Chemistry* 2017;2:14.

TARGETRY DEVELOPMENTS TOWARDS ^{44}Sc PRODUCTION USING ENRICHED CaO

R. Hasler (PSI/CRS), T.S. Carzaniga, S. Braccini (Univ. Bern), N.P. van der Meulen (PSI)

INTRODUCTION

The favourable decay properties of ^{44}Sc for cancer diagnosis using Positron Emission Tomography (PET) makes it a promising candidate for future application in nuclear medicine. While the production and application of ^{44}Sc has been comprehensively investigated [1-3], targetry optimization for this process has been lacking.

Optimized targets are a crucial issue for obtaining the required quantity and quality for clinical applications. The use of CaCO_3 has led to releases of radioactivity in gas form, with consequent radiation protection and product stability issues. As a result, the use of CaO as a more robust and effective target material was investigated.

EXPERIMENTAL

Enriched ^{44}Ca was prepared in oxide form, pressed into a pellet, encapsulated (Fig. 1) and irradiated using the 72 MeV proton beam provided by Injector 2 at Paul Scherrer Institute (PSI), degraded to various energies using Nb discs. The irradiated targets were processed chemically, based on the method described previously [2].

Enriched CaO pellets were subsequently prepared, encapsulated in a specially-designed holder and irradiated at the IBA Cyclone 18/9 solid target station at Inselspital Bern (UniBe). The irradiated targets were transported to PSI and chemically processed as before.

RESULTS AND DISCUSSION

The targets proved to be robust in the proton beam for a period of 90 minutes at 40-50 μA at various proton energies, as well as for a 5.45 h irradiation period at 18 μA at the UniBe medical cyclotron [4]. They were found to be a vast improvement over the previous rendition of CaCO_3 (Fig. 1). CaCO_3 pellets were tested at the UniBe medical cyclotron and the large radioactive gas releases strongly limited the beam current (below $\sim 2 \mu\text{A}$) and, consequently, the yield. These effects are negligible with CaO pellets and currents up to 20 μA were used.



Fig. 1: $^{44}\text{CaCO}_3$ pressed on to graphite (left). Enriched ^{44}CaO pressed into a 6 mm pellet (right).

CaCO_3 was heated to 900 $^\circ\text{C}$ to produce CaO . Samples of the product were analyzed using X-Ray Diffraction, indicating complete conversion to oxide form. It was subsequently determined that the targets had to be stored carefully to prevent contact with moisture, thereby, converting the target back to carbonate form.

Irradiation conditions for PSI and UniBe are described briefly in Tables 1 and 2, respectively. Irradiation of Target 2 at UniBe yielded vast activity, where over 3.2 GBq ^{44}Sc was obtained at end of separation (EOS) – 9 hours after end of bombardment (EOB). Target 1, on the other hand, was used for an initial low current function of the method.

Tab. 1: Irradiation of ^{44}CaO targets (diameter = 6 mm, mass = 30 mg) using degraded 72 MeV proton beam (Nb degrader, 3.4 mm) to ~ 11 MeV at PSI.

Target #	Irradiation Time (h)	Beam Current (μA)	EOS Yield (GBq)	Specific Activity (MBq/nmol)
1	1.0	50	2.691	5 (84%)
2	1.67	45	3.811	25 (99%)

Tab. 2: Irradiation of ^{44}CaO targets (diameter = 6 mm, mass = 30 mg) using the IBA Cyclone 18/9 at UniBe.

Target #	Irradiation Time (h)	Beam Current (μA)	EOS Yield (GBq)	Specific Activity (MBq/nmol)
1	4.0	2.5	0.209	-
2	5.75	18.2	3.21	10 (99%)

The targets were chemically processed (Fig. 2) using a slightly modified separation system than before, where it was ensured that the system is closed and the product collected in a vented, yet sealed, vial. This would ensure no environmental contamination of the final product would occur.

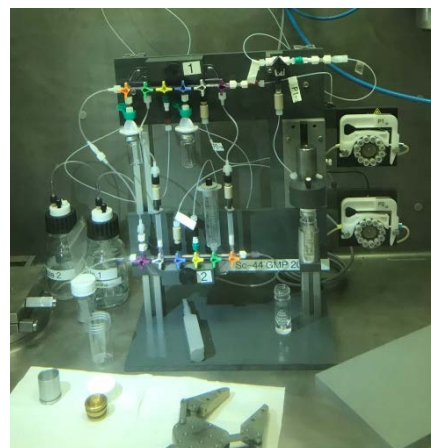


Fig. 2: ^{44}Sc chemical separation system using more modular parts.

The product was determined to contain only ^{44}Sc , with product yields >3 GBq at EOS. DOTANOC was labelled with ^{44}Sc at ~ 10 MBq/nmol at $>99\%$ radiochemical purity (irradiated at UniBe), while 25 MBq/nmol was achieved with targets irradiated at PSI.

This concept illustrates that enriched ^{44}Ca targets can be irradiated successfully using a medical cyclotron equipped with an external solid irradiation station, with high yields and radiochemical purity.

Further investigations are ongoing to optimize and standardize the full process in view of future clinical applications.

-
- [1] C. Müller, M. Bunka, J. Reber, C. Fischer, K. Zhernosekov, A. Türler et al., Promises of cyclotron-produced ^{44}Sc as a diagnostic match for trivalent β^- -emitters: in vitro and in vivo study of a ^{44}Sc -DOTA-folate conjugate. *J Nucl Med* 2013;54.
- [2] N.P. van der Meulen, M. Bunka, K. Domnanich, C. Müller, S. Haller, C. Vermeulen et al., Cyclotron production of ^{44}Sc : From bench to bedside. *Nuclear Medicine and Biology* 2015;42:745-51.
- [3] K. Domnanich, C. Müller, R. Farkas, RM. Schmid, B. Ponsard, R. Schibli et al., ^{44}Sc for labeling of DOTA- and NODAGA- functionalized peptides: preclinical in vitro and in vivo investigations. *EJNMMI Radiopharmacy and Chemistry* 2016;8:19.
- [4] S. Braccini, The new Bern PET cyclotron, its research beam line, and the development of an innovative beam monitor detector, *AIP Conference Proceedings* 1525 (2013) 144–150.

Sc-44 FOR KINETIC MEASUREMENTS OF GASTRIN DERIVATIVES

S. Krämer (ETHZ), A. Blanc, C. Keller, Z. Talip, R. Hasler (PSI/CRS), R. Schibli (ETHZ/PSI), N.P. van der Meulen (PSI/LRC), M. Behe (PSI/CRS)

We have developed a radiolabeled ligand to target the cholecystokinin receptor 2 (CCK2R), which is overexpressed in medullary thyroid cancer (MTC) and small lung cancer (SCLC). Patients with both tumors have no valuable therapeutic options in the metastatic stage. 50 % of MTC patients have a survival of up to 15-20 years, but they suffer from poor quality of life caused by an unregulated hormone secretion which results in uncontrollable and unpredictable flush, diarrhea or uncomfortable whole-body feeling/pain. SCLC, which is mainly caused by smoking or inhalation of poison vapor, have 5-year survival rate below 5%. They initially show good response to chemo-/radiotherapy, but relapse occurs within a short time afterwards. As a result, there is an urgent need for a new valuable therapeutic option for both cancers.

A clinical study is being performed (in collaboration with PSI) at the University Hospital Basel with the ^{177}Lu -labeled PPF11N. PPF11N is an optimized ligand with respect to kidney uptake and metabolic stability, which binds to the CCK2R. The clinical study with MTC patients showed very promising results. In an initial diagnostic study with six patients, we could detect all known and some additional tumor lesions. A dose escalating study for defining the optimal therapeutic activity to treat the patients is currently underway, however, these initial studies showed that the compound exhibits a very fast blood clearance and a slower kinetic would be preferable for optimal tumor uptake. Therefore, we initiated a project towards a compound with slower blood clearance. ^{44}Sc , as a PET nuclide with a suitable half-life of 4 h, is the ideal radionuclide to evaluate the *in vivo* compound kinetics. As part of the project, it was decided to establish a method for the *in vivo* kinetic in tumor-bearing nude rats.

We have established the labeling of ^{44}Sc -PPF11N at PSI, after which it was transported to ETH for injection and kinetic evaluation in the tumor-bearing nude rats. The rats were injected subcutaneously with MZCRC cells, a MTC cell line of human origin. The tumors grew for 7-10 days. On the day of the planned experiment, ^{44}Sc was produced and purified, as previously described [1], in the morning. The radiolabeling and quality control of PPF11N with ^{44}Sc was performed by CRS/PSI after internal transport from the hot cell facility to the radiopharmacy laboratory. Once the quality control produced the desired result, the surgery of the animals was initiated at CRS/ETH, while the compound was transported to ETH. An important parameter in the kinetic is the activity in the blood, therefore, the rats received

surgery for a blood stunt. The blood was led out of an artery into an activity measurement probe and, subsequently, back into the mouse. This ensured a high quality kinetic measurement and modelling. The results from the measures were analyzed in a simulation of a two-tissue compartment modelling.

The establishment of these logistically highly demanding experiments allowed one to evaluate further CCK2R ligands optimized for kinetic and for high tumor uptake.

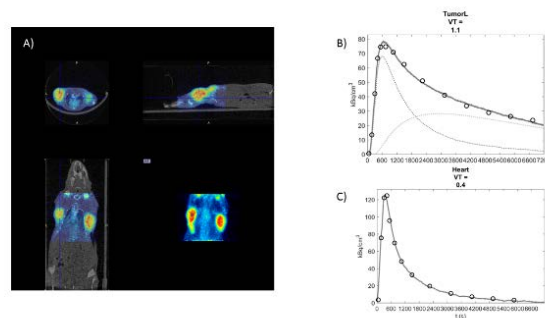


Fig. 1: Results from the kinetic study. A) PET/CT image of the tumor bearing rat. Kinetic modelling of B) tumor uptake and C) heart.

- [1] N.P. van der Meulen, M. Bunka, K. Domnanich, C. Müller, S. Haller, C. Vermeulen et al., Cyclotron production of ^{44}Sc : From bench to bedside. *Nuclear Medicine and Biology* 2015;42:745-51.

PRODUCTION AND PURIFICATION PROCESS OF THE MEDICALLY INTERESTING RADIOLANTHANIDE TERBIUM-161

N. Gracheva (ETHZ & PSI), J.R. Zeevaart (Necsa), U. Köster (ILL), Z. Talip (PSI), R. Schibli (ETHZ & PSI), N.P. van der Meulen (PSI)

INTRODUCTION

^{161}Tb is an interesting radionuclide for cancer treatment, as it decays by β^- -particle emission ($E_{\beta\text{-av}} = 154 \text{ keV}$ (100 %), $T_{1/2} = 6.9 \text{ d}$) [1]. It shows similar decay characteristics and chemical behavior to the clinically applied ^{177}Lu , but the therapeutic effect may be enhanced due to the co-emission of Auger and conversion electrons ($\sim 12.12 \text{ e}^-$, $\sim 36.1 \text{ keV}$ per decay) [2]. Theoretical calculations showed that due to the contribution of these electrons ^{161}Tb could deliver 1.8 and 3.6 times higher dose to the 100 μm and 10 μm diameter tumors, respectively, as compared to ^{177}Lu [3]. In vivo studies showed that ^{161}Tb may outperform ^{177}Lu in the preclinical settings [4, 5]. Therefore, ^{161}Tb was proposed as a better alternative to ^{177}Lu for the application in the targeted radionuclide therapy.

Herein we report on the ^{161}Tb production, on the development of the ^{161}Tb purification process, as well as on the characterization of the obtained final product ($^{161}\text{TbCl}_3$). The ^{161}Tb purity is compared with the “gold standard” for radionuclide therapy, ^{177}Lu .

EXPERIMENTAL

No-carrier-added ^{161}Tb was produced by neutron irradiation of enriched ^{160}Gd targets (98.2% enrichment) [6] at the SAFARI and ILL nuclear reactors and the spallation-induced neutron source SINQ. ^{161}Tb separation from the target material was performed using a cation exchange resin, while concentration and elution of the final product ($^{161}\text{TbCl}_3$) was done on an extraction resin. The pH, radionuclidic and radiochemical purity of $^{161}\text{TbCl}_3$ was determined. The radiolabeling capacity of ^{161}Tb was monitored over a two-week period post processing.

RESULTS AND DISCUSSION

Irradiations of enriched $^{160}\text{Gd}_2\text{O}_3/^{160}\text{Gd}(\text{NO}_3)_3$ targets resulted in productions of 6-20 GBq ^{161}Tb . The developed purification method allowed efficient separation of radionuclide of interest from the target material and co-produced radioactive impurities (Fig. 1). The final product ($^{161}\text{TbCl}_3$) was eluted at an activity concentration of 11-21 MBq/ μL (pH ~ 1.5) and radionuclidic and radiochemical purity being $>99\%$. The radiolabeling yield of ^{161}Tb -DOTANOC (180 MBq/nmol specific activity) was $\geq 99.0\%$ (Fig. 2). The radiolabeling capability of ^{161}Tb was comparable to ^{177}Lu over a two-week period.

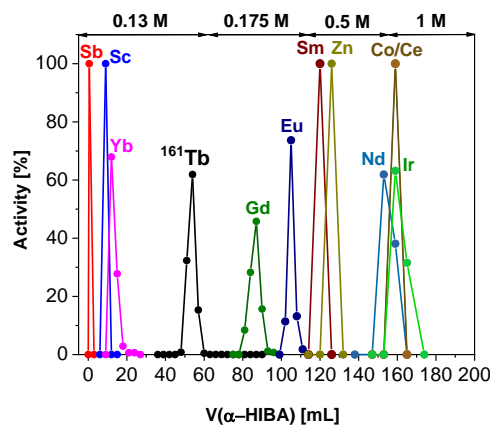


Fig. 1: Elution profile of ^{161}Tb separation from the irradiated target material and side products.

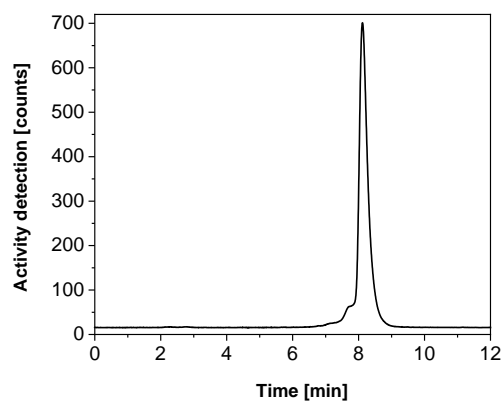


Fig. 2: HPLC chromatogram of ^{161}Tb -DOTANOC (2 min retention time would indicate “free” non-labeled ^{161}Tb and 8.2 min indicates ^{161}Tb -DOTANOC).

The final product ($^{161}\text{TbCl}_3$) was obtained in purity comparable to that of the commercially available no-carrier-added $^{177}\text{LuCl}_3$. The characteristics of the product were suitable to perform preclinical studies and, therefore, the product can be applied for Good Manufacturing Practice (GMP) processing with a focus on clinical application.

- [1] NuDat 2.7 <https://www.nndc.bnl.gov/nudat2/>
- [2] C. Müller et al., *Eur J Nucl Med Mol Imaging*, **41**, 476 (2014).
- [3] E. Hindie et al., *J Nucl Med*, **57**, 759 (2016).
- [4] C. Müller et al., *Eur J Nucl Med Mol Imaging*, **45** (Suppl 1), 53 (2018).
- [5] J. Grünberg et al., *Eur J Nucl Med Mol Imaging*, **41**, 1907 (2014).
- [6] S. Lehenberger et al., *Nucl Med Biol*, **38**, 917 (2011).

PRODUCTION AND PURIFICATION OF THE PURE AUGER ELECTON EMITTER ERBIUM-165

N. Gracheva, R. Schibli (ETHZ & PSI), N.P. van der Meulen (PSI)

INTRODUCTION

In the last decade, great interest has been shown with regard to the application of Auger electron emitters for targeted radionuclide therapy (TRNT). Auger electron emitters possess 4–26 keV/ μm energy deposition per unit length allowing controlled travel paths in water of $\sim 0.5 \mu\text{m}$ [1, 2]. The short penetration ranges make Auger electron emitters highly toxic when located in the cell nucleus, resulting in the DNA breakage [3]. An interesting pure Auger electron emitter is ^{165}Er with a half-life of 10.4 h. It decays by electron capture, resulting in the emission of Auger electrons and low energetic X-rays [4]. ^{165}Er can be produced by charged particle induced reactions, e.g. $^{165}\text{Ho}(p,n)^{165}\text{Er}$ direct route or $^{166}\text{Er}(p,2n)^{165}\text{Tm} \rightarrow ^{165}\text{Er}$ indirect route [5]. The highest theoretical production yield has been reported for the indirect route, being 315 MBq/ μAh at 16-23 MeV proton beam energies [5].

Herein we report on the production of ^{165}Er from the enriched $^{166}\text{Er}_2\text{O}_3$ target material (98.1% enrichment) via $^{166}\text{Er}(p,2n)^{165}\text{Tm} \rightarrow ^{165}\text{Er}$ nuclear reaction and on the development of the ^{165}Er purification method.

EXPERIMENTAL

Irradiation: Due to the high cost of the enriched $^{166}\text{Er}_2\text{O}_3$, $^{nat}\text{Er}_2\text{O}_3$ was used for the development work. ^{nat}Er targets were prepared by placing 60 mg $^{nat}\text{Er}_2\text{O}_3$ into a target pellet of 0.4 mm thickness and 6 mm in diameter. In order to find optimal production conditions, target irradiations were performed for 1-8 hours with various proton energies (22.8, 34.1 and 72.0 MeV) and different beam current (5-20 μA) at PSI cyclotron. **Purification:** By performing bench tests, ^{165}Er purification method was developed, resulted in the module construction. The module was introduced to the hot cell, making it possible to accomplish purification process with high activities of ^{165}Er , produced via $^{166}\text{Er}(p,2n)^{165}\text{Tm} \rightarrow ^{165}\text{Er}$ nuclear reaction. ^{165}Tm separation from the target material was performed by means of cation exchange chromatography with the use of α -hydroxy-isobutyric acid (HIBA) as an eluent. After elution of ^{165}Tm from the cation-exchange resin, the radionuclide was left to decay for 24 hours to ^{165}Er to ensure the maximum activity ingrowth of the latter. $^{165}\text{Tm}/^{165}\text{Er}$ separation was performed by means of cation exchange chromatography, followed by the concentration of ^{165}Er on LN3 extraction resin and final elution in 500 μL 0.1M HCl. **Radiolabelling:** The isolated from the target material ^{165}Er was radiolabeled with DOTANOC.

RESULTS AND DISCUSSION

The highest production yield of ^{165}Tm at the end of bombardment (EOB) was achieved by irradiation of the $^{nat}\text{Er}_2\text{O}_3$ target at 22.8 MeV proton beam and 20 μA beam current (Table 1). The cross-sections for $^{nat}\text{Er}(p,2n)^{165}\text{Tm} \rightarrow ^{165}\text{Er}$ production route were previously discussed in literature and the values are 2-3 times lower (456 mb at 22.9 MeV [1] and 586 mb at 22 MeV [6]), as compared to the $^{166}\text{Er}(p,2n)^{165}\text{Tm} \rightarrow ^{165}\text{Er}$ production route (1.234 b at 21 MeV [1]). This means the change of the target material from $^{nat}\text{Er}_2\text{O}_3$ to the enriched $^{166}\text{Er}_2\text{O}_3$ may result in 2-3 times higher production yield of ^{165}Tm under the same conditions.

Tab. 1: Irradiation data of $^{166}\text{Er}(p,2n)^{165}\text{Tm} \rightarrow ^{165}\text{Er}$ production route (1 h irradiation time, 60 mg $^{166}\text{Er}_2\text{O}_3$).

Proton beam energy, MeV	Beam current, μA	^{165}Tm activity at EOB, MBq
22.8	5	23.4
22.8	15	63.3
22.8	20	114.0
34.1	5	40.0
34.1	15	73.9
34.1	20	65.5
72.0	15	69.0
72.0	20	70.6

The investigated irradiation conditions (22.8 MeV, 20 μA) were afterwards applied for the 8 h bombardment of 60 mg $^{166}\text{Er}_2\text{O}_3$ and resulted in the elution of 319 MBq ^{165}Er after the purification. The final product ($^{165}\text{ErCl}_3$) contained 8% of the parent ^{165}Tm , indicating the necessity to improve the purification method. However, the presence of ^{165}Tm did not affect the radiolabeling of DOTANOC with the obtained ^{165}Er at 50 MBq/nmol specific activity (>99% radiolabeling yield).

-
- [1] F. Rösch et al., *Radiochim Acta*, **95**, 303 (2007).
 [2] Al. Kassis et al., *Semin Nucl Med*, **38**, 358 (2008).
 [3] Al. Kassis et al., *Radiat Prot Dosimetry*, **143**, 241 (2011).
 [4] NuDat 2.7 <https://www.nndc.bnl.gov/nudat2/>.
 [5] N. Zandi et al., *J Radioanal Nucl Chem*, **295**, 923 (2012).
 [6] SV Gudkov et al., *Int J Mol Sci* **17** (2015).

DEVELOPMENT OF NOVEL RUTHENIUM-BASED RADIOPHARMACEUTICALS

B. Happel^{1,2,3}, M. Brandt^{1,2}, T. Balber^{1,2}, P. Heffeter⁴, Z. Talip⁵, A. Vögele⁵, R. Hasler⁵, M. Jakupec³, R. Schibli⁵, M. Mitterhauser^{1,2}, B. Keppler³, W. Kandioller³, N.P. van der Meulen⁵, T.L. Mindt^{1,2,3}

- 1) Ludwig Boltzmann Institute Applied Diagnostics, 2) Department of Biomedical Imaging and Image Guided Therapy, Medical Univ. of Vienna, 3) Univ. of Vienna, Faculty of Chemistry, 4) Institute of Cancer Research and Comprehensive Cancer Center, Medical Univ. of Vienna, 5) Paul Scherrer Institute

There are only few publications describe the use of Ru radionuclides in nuclear medicine field, even though a large number of medically interesting Ru-compounds are known [1-3] (Fig 1).

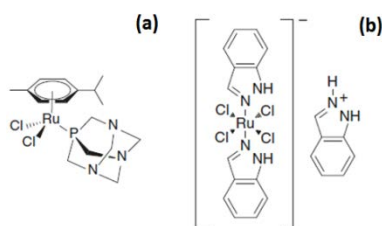


Fig. 1: Examples of medically interesting Ru compounds RAPTA C (1,3,5-triaza-7-phosphaadamantane) (a), KP-1019 ((indazolium trans-[tetrachlorobis(1H-indazole)- ruthenate(III)]) (b).

The aim of this study is to replace ^{nat}Ru with ^{97/103}Ru in anti-cancer compounds and to perform *in vitro* and *in vivo* experiments to study their mode of action. Ampoules containing 40-50 mg RuCl₃ × H₂O each (Fig 2), were irradiated (for three weeks) at PSI SINQ facility. They were crushed and dissolved in 3 mL conc. HCl. Dissolution in warm HCl dramatically increased the final activity of the ¹⁰³Ru sample (up to 185 MBq ¹⁰³Ru). ⁹⁷Ru (T_{1/2} = 2.9 d) and ¹⁹²Ir (T_{1/2} = 73.83 d) were also detected in the samples other than the desired ¹⁰³Ru (T_{1/2} = 39.26 d) (Fig. 3).



Fig. 2: Photo of the ampoules containing RuCl₃ × H₂O.

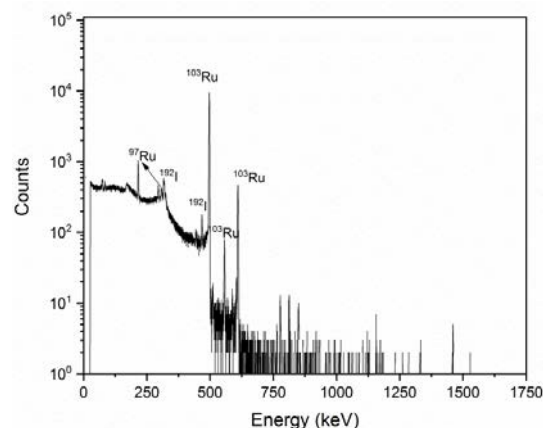


Fig. 3: An example of γ - spectrum of the ¹⁰³Ru sample.

The carrier-added ¹⁰³RuCl₃ is used at the Ludwig Boltzmann Institute Applied Diagnostics (LBIAD) in Vienna for the 3-step synthesis of a ruthenium complex with known anticancer activities. Goal of the described investigations is a direct comparison of the radiolabelled Ru-103 complex with the non-radioactive ^{nat}Ru reference compound *in vitro* and *in vivo*. This will assure that the radioactive compound will exhibit exactly the same properties as the non-radioactive drug and thus provide the basis for future clinical trials.

After optimization of the individual reaction steps, the desired ¹⁰³Ru-complex was obtained in good radiochemical yield and purity and with sufficient specific activity. The ¹⁰³Ru-complex was characterized by UV-spectroscopy and gamma-HPLC; mass spectrometric analysis will follow after radioactive decay. A comparison of the radioactive complex with the reference compound by cell viability assays (MTT test) and biodistribution experiments with allografted mice is currently ongoing. First results indicate that the compounds have, as expected, very similar biological characteristics. Completion of the studies and publication of the results is expected in summer 2019.

- [1] Weiss et al., Chem. Sci. 5 (2014) 4742.
 [2] Jakupec et al., Dalton Trans., 2008, 183.
 [3] C. Scolaro et al., J. Med. Chem., 48, (2005) 4161.

LIST OF PUBLICATIONS

A. Adamczak, A. Antognini, N. Berger, T.E. Cocolios, R. Dressler, A. Eggenberger, R. Eichler, R. Indelicato, K. Jungmann, K. Kirch, A. Knecht, A. Papa, R. Pohl, M. Pospelov, E. Rapisarda, P. Reiter, N. Ritjoho, S. Roccia, N. Severijns, A. Skawran, F. Wauters, L. Willmann
Nuclear structure with radioactive muonic atoms
 EPJ Web of Conferences 193, 04014 (2018), DOI: 10.1051/epjconf/201819304014

T. Al-Abdullah, D. Bemmerer, Z. Elekes, D. Schumann
The Feasibility of Studying $^{44}\text{Ti}(\alpha,p)^{44}\text{V}$ Reaction at Astrophysical Energies
 Journal of physics: conference series 940, 012028 (2018), DOI: 10.1088/1742-6596/940/1/012028

O. Aviv, R. Sasson, H.B. Spitz, S. Halfon, E.A. Maugeri, Z. Yungrais, E. Daniely, J. Koch
In vitro solubility of ^7Be particles released from a damaged source
 Journal of radioanalytical and nuclear chemistry 318, 753 (2018), DOI: 10.1007/s10967-018-6109-5

M. Barbagallo, J. Andrzejewski, M. Mastromarco, J. Perkowski, L.A. Damone, A. Gawlik, L. Cosentino, P. Finocchiaro, E.A. Maugeri, A. Mazzone, R. Dressler, S. Heinitz, N. Kivel, D. Schumann, N. Colonna, O. Aberle, S. Amaducci, L. Audouin, M. Bacak, J. Balibrea, F. Becvár, G. Bellia, R. Berthoumieux, J. Billowes, D. Bosnar, A. Brown, M. Caamaño, F. Calviño, M. Calviani, D. Cano-Ott, R. Cardella, A. Casanovas, F. Cerutti, Y.H. Chen, E. Chiaveri, G. Cortés, M.A. Cortés-Giraldo, S. Cristallo, M. Diakaki, M. Dietz, C. Domingo-Pardo, E. Dupont, I. Durán, B. Fernández-Domínguez, A. Ferrari, P. Ferreira, V. Furman, K. Göbel, A.R. García, S. Gilardoni, T. Glodariu, I.F. Gonçalves, E. González-Romero, E. Griesmayer, C. Guerrero, F. Gunsing, H. Harada, J. Heyse, D.G. Jenkins, E. Jericha, K. Johnston, F. Käppeler, Y. Kadi, A. Kalamara, P. Kavragin, A. Kimura, M. Kokkoris, M. Krticka, D. Kurtulgil, E. Leal-Cidoncha, C. Lederer, H. Leeb, J. Leredegui-Marco, S. Lo Meo, S.J. Lonsdale, D. Macina, A. Manna, J. Marganec, T. Martínez, J.G. Martins-Correia et al.
Experimental setup and procedure for the measurement of the $^7\text{Be}(n,p)^7\text{Li}$ reaction at n_TOF
 Nuclear Instruments and Methods in Physics Research Section A: Accelerators, Spectrometers, Dectectors and Associated Equipment 887, 27 (2018), DOI: 10.1016/j.nima.2017.12.025

L. Damone, M. Barbagallo, M. Mastromarco, A. Mengoni, L. Cosentino, E.A. Maugeri, S. Heinitz, D. Schumann, R. Dressler, F. Käppeler, N. Colonna, P. Finocchiaro, J. Andrzejewski, J. Perkowski, A. Gawlik, O. Aberle, S. Altstadt, M. Ayrarov, L. Audouin, M. Bacak, J. Balibrea-Correa, J. Ballof, V. Becares, F. Becvar, C. Beinrucker, G. Bellia, A.P. Bernardes, E. Berthoumieux, J. Billowes, M.J.G. Borge, D. Bosnar, A. Brown, M. Brugger, M. Busso, M. Caamano, F. Calvino, M. Calviani, D. Cano-Ott, R. Cardella, A. Casanovas, D.M. Castelluccio, R. Catherall, F. Cerutti, Y.H. Chen, E. Chiaveri, J.G.M. Correia, G. Cortes, M.A. Cortes-Giraldo, S. Cristallo, M. Diakaki et al.
 $^7\text{Be}(n,p)^7\text{Li}$ Reaction and the Cosmological Lithium Problem: Measurement of the Cross Section in a Wide Energy Range at n_TOF at CERN
 Physical review letters 121, 042701 (2018), DOI: 10.1103/PhysRevLett.121.042701

A. Di Pietro, J.P. Fernandez-Garcia, F. Ferrera, P. Figuera, M. Fisichella, M. Lattuada, S. Marletta, C. Marchetta, D. Torresi, M. Alcorta, M.J.G. Borge, T. Davinson, S. Heinitz, A.M. Laird, A.C. Shotton, D. Schumann, N. Soic, O. Tengblad, M. Zadro
Experimental investigation of exotic clustering in ^{13}B and ^{14}C using the resonance scattering method
 Journal of physics: conference series 966, 012040 (2018), DOI: 10.1088/1742-6596/966/1/012040

L.F. Gerchow, S. Braccini, T.S. Carzaniga, D. Cooke, M. Döbeli, K. Kirch, U. Köster, A. Müller, N.P. van der Meulen, A. Rubbia, C. Vermeulen, P. Crivelli
High efficiency cyclotron trap assisted positron moderator
 Instruments 2,10 (2018), DOI: 10.3390/instruments2030010

J. Halleröd, C. Ekberg, I. Kajan, E. Aneheim
Solubility Thermodynamics of CyMe4-BTBP in Various Diluents Mixed with TBP
 Journal of solution chemistry 47, 1021 (2018), DOI: 10.1007/s10953-018-0774-4

S. Heinitz, N. Kivel, D. Schumann, U. Köster, M. Balata, M. Biasotti, V. Ceriale, M. De Gerone, M. Faverzani, E. Ferri, G. Gallucci, F. Gatti, A. Giachero, S. Nisi, A. Nucciotti, A. Orlando, G. Pessina, A. Puiu, S. Ragazzi
Production and separation of ^{163}Ho for nuclear physics experiments
 Plos one 13, e0200910 (2018), DOI: 10.1371/journal.pone.0200910

- I. Kajan, S. Heinitz, R. Dressler, P. Reichel, N. Kivel, D. Schumann
Emission probability of the 66.7 keV gamma transition in the decay of ^{171}Tm
 Physical Review C 98, 055802 (2018), DOI: 10.1103/PhysRevC.98.055802
- J. Leredegui-Marco, C. Guerrero, E. Mendoza, J.M. Quesada, K. Eberhardt, A.R. Junghans, M. Krlicka, O. Aberle, J. Andrzejewski, L. Audouin, V. Becares, M. Bacak, J. Balibrea, M. Barbagallo, S. Barros, F. Becvar, C. Beinrucker, E. Berthoumieux, J. Billowes, D. Bosnar, M. Brugger, M. Caamano, F. Calvino, M. Calviani, D. Cano-Ott, R. Cardella, A. Casanovas, D.M. Castelluccio, F. Cerutti, Y.H. Chen, E. Chiaveri, N. Colonna, G. Cortes, M.A. Cortes-Giraldo, L. Cosentino, L.A. Damone, M. Diakaki, M. Dietz, C. Domingo-Pardo, R. Dressler, E. Dupont, I. Duran, B. Fernandez-Dominguez, A. Ferrari, P. Ferreira, P. Finocchiaro, V. Furman, K. Goebel, A.R. Garcia, A. Gawlik, T. Glodariu, I. F. Gonçalves, E. González-Romero, A. Goverdovski, E. Griesmayer, F. Gunsing, H. Harada, T. Heftrich, S. Heinitz, J. Heyse, D.G. Jenkins, E. Jericha, F. Käppeler, Y. Kadi, T. Katabuchi, P. Kavargin, V. Ketlerov, V. Khryachkov, A. Kimura, N. Kivel, M. Kokkoris, E. Leal-Cidoncha, C. Lederer, H. Leeb, S. Lo Meo, S.J. Lonsdale, R. Losito, D. Macina, J. Marganec, T. Martínez, C. Massimi, P. Mastinu, M. Mastromarco, F. Matteucci, E.A. Maugeri, A. Mengoni, et al.
Radiative neutron capture on ^{242}Pu in the resonance region at the CERN n_TOF-EAR1 facility
 Physical Review C 97, 024605 (2018), DOI: 10.1103/PhysRevC.97.024605
- E.A. Maugeri, J. Neuhausen, B.G. Prieto, A. Aerts, T.M. Mendonca, T. Stora, R. Eichler
Adsorption of volatile polonium species on metals in various gas atmospheres: Part III - Adsorption of volatile polonium on stainless steel 316L
 Radiochimica Acta 106, 125 (2018), DOI: 10.1515/ract-2017-2807
- E.A. Maugeri, S. Heinitz, R. Dressler, M. Barbagallo, J. Ulrich, D. Schumann, N. Colonna, U. Köster, M. Ayranov, P. Vontobel, M. Mastromarco, J. Schell, J. Correia Martins, T. Stora
Preparation and characterization of three ^7Be targets for the measurement of the $^7\text{Be}(n, p)^7\text{Li}$ and $^7\text{Be}(n, \alpha)^4\text{He}$ reaction cross sections
 Nuclear Instruments and Methods in Physics Research Section A: Accelerators, Spectrometers, Detectors and Associated Equipment 889, 138 (2018), DOI: 10.1016/j.nima.2018.01.078
- E. Mendoza, D. Cano-Ott, S. Altstadt, S. Andriamonje, J. Andrzejewski, L. Audouin, J. Balibrea, V. Bécaries, M. Barbagallo, F. Becvár, F. Belloni, B. Berthier, E. Berthoumieux, J. Billowes, D. Bosnar, M. Brugger, F. Calviño, M. Calviani, C. Carrapiço, F. Cerutti, E. Chiaveri, M. Chin, N. Colonna, G. Cortés, M.A. Cortés-Giraldo, M. Diakaki, I. Dillmann, C. Domingo-Pardo, I. Durán, N. Dzysiuk, C. Eleftheriadis, A. Ferrari, K. Fraval, V. Furman, M.B. Gómez-Hornillos, S. Ganesan, A.R. García, G. Giubrone, I.F. Gonçalves, E. González, A. Goverdovski, F. Gramegna, E. Griesmayer, C. Guerrero, F. Gunsing, P. Gurusamy, T. Heftrich, S. Heinitz, Hernández-Prieto A, Heyse J, D.G. Jenkins, E. Jericha, F. Käppeler, Y. Kadi, D. Karadimos, T. Katabuchi, V. Ketlerov, V. Khryachkov, P. Koehler, M. Kokkoris, J. Kroll, M. Krlicka, C. Lampoudis, C. Langer, E. Leal-Cidoncha, C. Lederer, H. Lee, L.S. Leong, J. Leredegui-Marco, M. Licata, D. López, R. Losito, A. Manousos, J. Marganec, T. Martínez, C. Massimi, P. Mastinu, M. Mastromarco, A. Mengoni, P.M. Milazzo et al.
Measurement and analysis of the ^{241}Am neutron capture cross section at the n_TOF facility at CERN
 Physical Review C 97, 054616 (2018), DOI: 10.1103/PhysRevC.97.054616
- C. Müller, K.A. Domnanich, C.A. Umbricht, N.P. van der Meulen
Scandium and Terbium Radionuclides for Radiotheranostics: Current State of Development Towards Clinical Application
 The British Journal of Radiology 91, 20180074 (2018)
- J. Praena, M. Sabaté-Gilarte, I. Porras, J.M. Quesada, S. Altstadt, J. Andrzejewski, L. Audouin, V. Bécaries, M. Barbagallo, F. Becvár, F. Belloni, E. Berthoumieux, J. Billowes, V. Boccone, D. Bosnar, M. Brugger, F. Calviño, M. Calviani, D. Cano-Ott, C. Carrapiço, F. Cerutti, E. Chiaveri, M. Chin, N. Colonna, G. Cortés, M.A. Cortés-Giraldo, M. Diakaki, M. Dietz, C. Domingo-Pardo, R. Dressler, I. Durán, C. Eleftheriadis, A. Ferrari, K. Fraval, V. Furman, K. Göbel, M.B. Gómez-Hornillos, S. Ganesan, A.R. García, G. Giubrone, I.F. Gonçalves, E. González-Romero, A. Goverdovski, E. Griesmayer, C. Guerrero, F. Gunsing, T. Heftrich, A. Hernández-Prieto, J. Heyse, D.G. Jenkins, E. Jericha, F. Käppeler, Y. Kadi, D. Karadimos, T. Katabuchi, V. Ketlerov, V. Khryachkov, N. Kivel, P. Koehler, M. Kokkoris, J. Kroll, M. Krlicka, C. Lampoudis, C. Langer, E. Leal-Cidoncha, C. Lederer-Woods, H. Leeb, L.S. Leong, J. Leredegui-Marco, R. Losito, A. Mallick, A. Manousos, J. Marganec, T. Martínez, C. Massimi, P. Mastinu, M. Mastromarco, E. Mendoza, A. Mengoni, P.M. Milazzo et al.
Measurement and resonance analysis of the $^{33}\text{S}(n, \alpha)^{30}\text{Si}$ cross section at the CERN n_TOF facility in the energy region from 10 to 300 keV
 Physical Review C 97, 064603 (2018), DOI: 10.1103/PhysRevC.97.064603

J. Praena, F.J. Ferrer, W. Vollenberg, M. Sabaté-Gilarte, B. Fernández, J. García-López, I. Porras, J.M. Quesada, S. Altstadt, J. Andrzejewski, L. Audouin, V. Bécaries, M. Barbagallo, F. Becvár, F. Belloni, E. Berthoumieux, J. Billowes, V. Boccone, D. Bosnar, M. Brugger, F. Calviño, M. Calviani, D. Cano-Ott, C. Carrapiço, F. Cerutti, E. Chiaveri, M. Chin, N. Colonna, G. Cortés, M.A. Cortés-Giraldo, M. Diakaki, M. Dietz, C. Domingo-Pardo, R. Dressler, I. Durán, C. Eleftheriadis, A. Ferrari, K. Fraval, V. Furman, K. Göbel, M.B. Gómez-Hornillos, S. Ganesan, A.R. García, G. Giubrone, I.F. Gonçalves, E. González-Romero, A. Goverdovski, E. Griesmayer, C. Guerrero, F. Gunsing, T. Heftrich, A. Hernández-Prieto, J. Heyse, D.G. Jenkins, E. Jericha, F. Käppeler, Y. Kadi, D. Karadimos, T. Katabuchi, V. Ketlerov, V. Khryachkov, N. Kivel, P. Koehler, M. Kokkoris, J. Kroll, M. Krticka, C. Lampoudis, C. Langer, E. Leal-Cidoncha, C. Lederer, H. Leeb, L.S. Leong, J. Lerendegui-Marco, R. Losito, A. Mallick, A. Manousos, J. Marganiec, T. Martínez, C. Massimi, P. Mastinu et al.

Preparation and characterization of ^{33}S samples for $^{33}\text{S}(n,\alpha)^{30}\text{Si}$ cross-section measurements at the n_TOF facility at CERN
Nuclear Instruments and Methods in Physics Research Section A: Accelerators, Spectrometers, Detectors and Associated Equipment 890, 142 (2018), DOI: 10.1016/j.nima.2018.02.055

D. Schumann, G. Sibbens, A. Stolarz, K. Eberhardt, B. Lommel, C. Stodel
ANITA (Advanced Network for Isotope and TArget Laboratories) - the Urgent Need for a European Target Preparation Network

Proceedings of the 28th world conference of the international nuclear target development society (intds2016)
1962, UNSP 020001 (2018), DOI: 10.1063/1.5035514

J. Schniering, F. Borgna, K. Siwowska, M. Benesova, S. Cohrs, R. Hasler, N.P. van der Meulen, B. Maurer, R. Schibli, C. Müller

In-Vivo-Labeling of Plasma Proteins for Imaging of Enhanced Vascular Permeability in the Lungs
Molecular Pharmaceutics, 15,4995 (2018), DOI: 10.1259/bjr.20180074

C.A. Umbricht, M. Benesova, R. Hasler, R. Schibli, N.P. van der Meulen, C. Müller
Design and Preclinical Evaluation of an Albumin-Binding PSMA Ligand for ^{64}Cu -Based PET Imaging
Molecular Pharmaceutics (2018), DOI: 10.1021/acs.molpharmaceut.8b00712

INTERNAL REPORTS

N. Gracheva

Production possibilities and purification process of therapeutic radiolanthanides ^{161}Tb and ^{165}Er
ETHZ Doktorandentag, 12 September, 2018

Z. Talip

Importance of Nuclear Data in Different Fields
CRS Seminar Day, 9 November, 2018

N.P. van der Meulen

The Potential of ^{161}Tb for Targeted Radionuclide Therapy: Combining β^- - Particles and Auger Electrons for More Efficient Cancer Therapy,
ASI Seminar (presented with C. Müller), 20 November, 2018

Y. Wang, Y. Wittwer, J. Zhang, J. Yang, H. Haba, Y. Komori, T. Yokokita, S. Cao, F. Fan, R. Eichler, A. Türler, Z. Qin
Mass spectrometric speciation of mononuclear Re carbonyls in the gas phase
RIKEN Accelerator Progress Report, 2018

CONTRIBUTIONS TO CONFERENCES, WORKSHOPS AND SEMINARS

I.I. Danilov

Summary on iodine and Cs-doped LBE transpiration experiments

MYRTE WP4-Meeting, Paul Scherrer Institut, Villigen, Switzerland, 26 April, 2018

I.I. Danilov

Volatilisation of ^{134}Cs , ^{131}I and ^{210}Po from lead bismuth liquid metal solutions studied by the transpiration method

18th Radiochemical Conference (RADCHEM-2018), Marianske Lazne, Czech Republic 13-18 May, 2018

I.I. Danilov

Volatilisation of ^{134}Cs , ^{131}I and ^{210}Po from lead bismuth liquid metal solutions studied by the transpiration method

NES-PhD-Day, Paul Scherrer Institut, Villigen, Switzerland, 24 May, 2018.

I.I. Danilov

Volatilisation of ^{134}Cs , ^{131}I and ^{210}Po from lead bismuth liquid metal solutions studied by the transpiration method

HLMC-2018, JSC "SSC RF – IPPE A.I. Leypunsky", Obninsk, Kaluga region, Russia, 8 October, 2018

I.I. Danilov

Volatilisation of ^{134}Cs , ^{131}I and ^{210}Po from lead bismuth liquid metal solutions studied by the transpiration method

PhD Seminar of the Laboratory of Radiochemistry, Paul Scherrer Institut, Villigen, Switzerland, 5 November, 2018

I.I. Danilov

Volatilisation of ^{134}Cs , ^{131}I and ^{210}Po from LBE: Troubles, Solutions and Think Tank

Seminar of the Laboratory of Radiochemistry, Paul Scherrer Institut, Villigen, Switzerland, 19 November, 2018

R. Dressler, D. Schumann

^{53}Mn the Aims, the Needs and the Problems

Soreq Applied Research Accelerator Facility, Yavne, Israel, 18 January, 2018

R. Dressler, R. Dölling, L. Calabretta

Contact free measurement of carbon stripper foil thickness variation for IsoDAR experiments

International Nuclear Target Development Society Conference 2018, East Lansing, USA, 8-12 October, 2018

R. Eichler

Status and Prospects of Gas Phase Chemistry with Transactinides

Russian Academy of Science Symposium on Heaviest Elements, Dubna, Russia, 26 October, 2018

N. Gracheva

Medically interesting radiolanthanide Terbium-161 – from production towards clinical application

Terachem 18, Bressanone, Italy, 28 September, 2018

P. Ionescu

Superheavy Element Chalcogenides – Gas Chromatographic Design & Experiments for Groups 12, 14

JINR Seminar, Dubna, Russia, 25 April, 2018

P. Ionescu

Superheavy Element Chalcogenides – Gas Chromatographic Design & Experiments for Groups 12, 14

1st year Graduate Symposium, Bern, Switzerland, 10 September, 2018

P. Ionescu

Superheavy Element Chalcogenides – Gas Chromatographic Design & Experiments for Groups 12, 14

Seminar of the Laboratory of Radiochemistry, Paul Scherrer Institut, Villigen, Switzerland, 5 October, 2018

I. Kajan, C. Ekberg

Is ruthenium really noble or does it interact with plebs?

Accident Phenomena of Risk Importance seminar (APRI-9), Stockholm, Sweden, 8 March, 2018

I. Kajan, D. Schumann

On nuclides mining from used nuclear fuel

XI Methods and Applications of Radioanalytical Chemistry (MARC), Kailua-Kona, USA, 8-13 April, 2018

I. Kajan, M. Florianova, D. Schumann

Investigations of diluent effect on europium extraction behavior with TODGA

18th Radiochemical Conference (RADCHEM-2018), Marianske Lazne, Czech Republic 13-18 May, 2018

E. Karlsson

Studies on radionuclides evaporated from LBE based on thermochromatographic data

MYRTE WP4-Meeting, Paul Scherrer Institut, Villigen, Switzerland, 26 April, 2018

E. Karlsson

Studies on radionuclides evaporated from LBE based on thermochromatographic data

PhD Seminar of the Laboratory of Radiochemistry, Paul Scherrer Institut, Villigen, Switzerland, 27 April, 2018

E. Karlsson

Studies on volatility and speciation of iodine evaporated from the coolant in the MYRRHA heavy liquid metal reactor

NES-PhD-Day, Paul Scherrer Institut, Villigen, Switzerland, 24 May, 2018.

E. Karlsson

Investigating the deposition behavior of volatile radionuclides present in the MYRRHA-reactor

NES ETH Evaluation, Paul Scherrer Institut, Villigen, Switzerland, 10.-13. September, 2018

E. Karlsson

Determination of adsorption properties of fission products released from lead-bismuth eutectic

Seminar of the Laboratory of Radiochemistry, Paul Scherrer Institut, Villigen, Switzerland, 5 October, 2018

E. Karlsson

Evaporation and adsorption behaviour of iodine released from irradiated tellurium-doped LBE

HLMC-2018, JSC "SSC RF – IPPE A.I. Leypunsky", Obninsk, Kaluga region, Russia, 8 October, 2018

B. Kraus

Diamond-based detectors for future chemistry experiments with superheavy elements (Poster)

Cross-Divisional Poster Event, Paul Scherrer Institut, Villigen, Switzerland, 26 April, 2018

B. Kraus

Diamond-based detectors for future chemistry experiments with superheavy elements

18th Radiochemical Conference (RADCHEM-2018), Marianske Lazne, Czech Republic 13-18 May, 2018

B. Kraus

Diamond-based detectors for future chemistry experiments with superheavy elements (Poster)

NES-PhD-Day, Paul Scherrer Institut, Villigen, Switzerland, 24 May, 2018

B. Kraus

Challenges of Vacuum Chromatography and High-Temperature α -Spectroscopy

Seminar of the Laboratory of Radiochemistry, Paul Scherrer Institut, Villigen, Switzerland, 5 November, 2018

B. Kraus

High-Temperature α -Spectroscopy with Diamond-based Detectors

7th ADAMAS Workshop, Vienna, Austria, 13-14 December, 2018

M. Lin

Selective Removal of Cs From Highly acidic solutions

NES-PhD-Day, Paul Scherrer Institut, Villigen, Switzerland, 24 May, 2018

M. Lin

Selective Removal of Cs From Highly acidic solutions

PhD Seminar of the Laboratory of Radiochemistry, Paul Scherrer Institut, Villigen, Switzerland, 25 May, 2018

M. Lin

Selective Removal of Cs From Highly acidic solutions

Seminar of the Laboratory of Radiochemistry, Paul Scherrer Institut, Villigen, Switzerland, 5 October, 2018

E.A. Maugeri

Production and characterization of ^7Be targets used for the measurement of the $^7\text{Be}(n, p)^7\text{Li}$ reaction cross sections
 XI Methods and Applications of Radioanalytical Chemistry (MARC), Kailua-Kona, USA, 8-13 April, 2018

E.A. Maugeri

Targetry of rare isotopes at PSI

International Nuclear Target Development Society Conference 2018, East Lansing, USA, 8-12 October, 2018

E.A. Maugeri

Exotic Radioisotopes Targetry at PSI and Preparation of ^{10}Be Target

York University, York, UK, 27 September, 2018

E.A. Maugeri

Characterization of the ^7Be target used for the measurement of the $^7\text{Be}(n, p)^7\text{Li}$ reaction cross sections

n_TOF Collaboration meeting, University of Granada, Granada, Spain, 27-28 November, 2018

I. Mihalcea, M. Veicht

Implementing new isotopes for environmental research: Redetermination of the ^{32}Si half-life

Kickoff Meeting (SINCHRON Project), Laboratory of Ion Beam Physics, Swiss Federal Institute of Technology, Zurich, Switzerland, 8 November, 2018

J. Neuhausen

Chemistry of volatile radionuclides: Status and prospects of MYRTE-WP4

MYRTE WP4-Meeting, Paul Scherrer Institut, Villigen, Switzerland, 26 April, 2018

J. Neuhausen

Chemistry of volatile radionuclides

MYRTE TEC-Meeting, SCK·CEN Headquarters, Brussels, Belgium, 29 May, 2018

J. Neuhausen

Chemistry of volatile radionuclides

MYRTE TEC-Meeting, SCK·CEN Headquarters, Brussels, Belgium, 7 November, 2018

J. Neuhausen

Chemistry of volatile radionuclides

MYRTE Governing Board-Meeting, SCK·CEN Headquarters, Brussels, Belgium, 7 November, 2018

T.K. Sato, M. Asai, K. Tsukada, Y. Kaneya, T. Tomitsuka, A. Toyoshima, A. Mitsukai, A. Osa, H. Makii, K. Hirose, K. Nishio, Y. Nagame, H. Kamada, M. Shibata, M. Sakama, K. Ooe, K. Shirai, D. Sato, S. Goto, Y. Shigekawa, Y. Kasamatsu, R. Naguwa, K. Shingu, S. Miyashita, P. Steinegger, R. Eichler, J. Grund, Ch.E. Düllmann, V. Pershina, A. Yakushev, K. Eberhardt, J.V. Kratz, J. Runke, P. Thörle-Pospiech, N. Trautmann, T. Stora, M. Schädel
Chemical Properties of Lawrencium (Lr, Z=103): Adsorption Behaviour on a Tantalum Surface
 18th Radiochemical Conference (RADCHEM-2018), Mariánské Lázně, Czech Republic 13-18 May, 2018

D. Schumann

Exotic Radionuclides: What are they good for?

Colloquium Weizmann Institute, Rehovot, Israel, 15 January, 2018

D. Schumann

Development of mass separation and implantation technique

SANDA core group meeting, Madrid, Spain, 26 January, 2018

D. Schumann

Isotope and Target Production at PSI

CHANDA-WP3 meeting, Geel, Belgium, 6 March, 2018

D. Schumann

PSI contribution to WP11

PSI contribution to WP2/3

CHANDA final meeting, Madrid, Spain, 17 April, 2018

D. Schumann

Harvesting Exotic Radionuclides at PSI

Nuclear Science Seminar, MSU, East Lansing, USA, 10 October, 2018

D. Schumann

Welcome to SINCHRON!

Kickoff meeting SINCHRON, Laboratory of Ion Beam Physics, Swiss Federal Institute of Technology, Zurich, Switzerland, 8 November, 2018

P. Steingger, N.V. Aksenov, Y.V. Albin, G.A. Bozhikov, V.I. Chepigin, I. Chuprakov, N.S. Gustova, A.Sh. Madumarov, O.N. Malyshev, Y.A. Popov, A.V. Sabelnikov, A.I. Svirikhin, M.G. Voronyuk, A.V. Yerebin, R. Eichler, D. Herrmann, P. Ionescu, B. Kraus, D. Piguat, B. Gall, Z. Asfari, S. N. Dmitriev

The chemical investigation of Nihonium

IX International Symposium on EXOtic Nuclei (EXON-2018), Petrozavodsk, Russia, 10-15 September, 2018

J. Ulrich, R. Dressler, D. Schumann, A. Türler

Measurement of astrophysical relevant properties of ^{53}Mn

NES-PhD-Day, Paul Scherrer Institut, Villigen, Switzerland, 24 May, 2018

J. Ulrich, R. Dressler, D. Schumann

Measurement of astrophysical relevant properties of ^{53}Mn

NES ETH Evaluation, Paul Scherrer Institut, Villigen, Switzerland, 10.-13. September, 2018

J. Ulrich

Measurement of astrophysical relevant properties of Mn-53

Seminar of the Laboratory of Radiochemistry, Paul Scherrer Institut, Villigen, Switzerland, 5 November, 2018

J. Ulrich, R. Dressler, D. Schumann

Measurement of (n,g)-cross-section of ^{53}Mn

n_TOF Collaboration Meeting, Univ. Granada, Granada, Spain, 27 November, 2018

N.P. van der Meulen

The use of ^{149}Tb and ^{152}Tb in preclinical and clinical investigations: its mass separation and subsequent application for imaging and therapy

255th ACS Meeting, New Orleans, USA, 18 March, 2018

N.P. van der Meulen

The Targetry Development of ^{44}Sc Using Enriched CaO

17th International Workshop on Targetry and Target Chemistry, Coimbra, Portugal, 29 August, 2018

N.P. van der Meulen, C. Müller

Preclinical development and application using exotic radionuclides

Institut de Recherche en Cancérologie de Montpellier, Montpellier, France, 6 September, 2018

N.P. van der Meulen

The Possibility of Producing ^{43}Sc From ^{44}Ca via the (p,2n) Nuclear Reaction

Terachem 18, Bressanone, Italy, 28 September, 2018

N.P. van der Meulen

Radionuclide Development Towards Theragnostics

CIAE Information Exchange Meeting, Paul Scherrer Institut, Villigen, Switzerland, 8 October, 2018

N.P. van der Meulen, C. Müller

An update on the chemical separation of ^{149}Tb and its subsequent application for preclinical therapy studies

60th Meeting of the INTC, CERN, Geneva, Switzerland, 7 November, 2018

N.P. van der Meulen

An update on the chemical separation of ^{149}Tb and its subsequent application for preclinical therapy studies

ISOLDE Workshop and Users Meeting 2018, Geneva, Switzerland, 5 December, 2018

N.P. van der Meulen

The use of ^{149}Tb and ^{152}Tb in preclinical and clinical investigations: its mass separation and subsequent application for imaging and therapy

IAEA Technical Meeting on Novel Multidisciplinary Applications with Unstable Ion Beams and Complementary Techniques, Vienna, Austria, 11 December, 2018

M. Veicht

Implementing new isotopes for environmental research: Redetermination of the ^{32}Si half-life

Seminar of the Laboratory of Radiochemistry, Paul Scherrer Institut, Villigen, Switzerland, 22 October, 2018

Y. Wittwer

On the formation and stability of metal carbonyl complexes from superheavy elements and their homologues (Poster)

Cross-Divisional Poster Event, Paul Scherrer Institut, Villigen, Switzerland, 26 April, 2018

Y. Wittwer

On the formation and stability of metal carbonyl complexes from superheavy elements and their homologues (Poster)

18th Radiochemical Conference (RADCHEM-2018), Mariánské Lázně, Czech Republic 13-18 May, 2018

Y. Wittwer

Optimizing the in-situ production yield of transition metal carbonyls

Seminar of the Laboratory of Radiochemistry, Paul Scherrer Institut, Villigen, Switzerland, 5 November, 2018

Y. Wittwer

Optimizing the in-situ production yield of transition metal carbonyls

TASCA 18, Darmstadt, Germany, 25 September, 2018

MEMBERS OF SCIENTIFIC COMMITTEES EXTERNAL ACTIVITIES

Dr. Robert Eichler

- Associate Editor of the International Journal of Modern Physics E (IJMPE)World Scientific Publishing
- Curatorial Board of the Laboratory for Ion beam Physics ETH Zurich, member

Dr. Dorothea Schumann

- Nuklearforum Schweiz, member
- Schweizerische Gesellschaft der Kernfachleute, member

Dr. Nicholas van der Meulen

- United States Department of Energy (DOE Isotope R&D FOA), Panel Reviewer
- Accelerator for Research in Radiochemistry and Oncology at Nantes Atlantique (ARRONAX)
- International Scientific Committee, member
- PSI internal research commission (FoKo), member

PUBLIC RELATIONS AND OUTREACH ACTIVITIES

Die Botschaft

Wertvolles Wissen weitergeben

29 December 2018

BACHELOR THESIS

Carl Laurens Pascal Saint-Germain

Design study for a rotating heavy ion irradiation target

Dr. Robert Eichler / PSI

Dr. Rugard Dressler / PSI

Prof. Thierry Viollet / Université de Technologie de Belfort Montbeliard

Juli 2018

AWARDS

Mu Lin

Selective removal of radioactive Cs from spent nuclear fuel solutions

Best presentation award (2nd year PhD)

NES-PhD-Day, Villigen, Switzerland

May 2018

Yves Wittwer

On the formation and stability of metal carbonyl complexes from superheavy elements and their homologues

1st place students poster presentation

18th Radiochemical Conference, Mariánské Lázně, Czech Republic

17 May 2018

Ivan Danilov

Volatilisation of ^{134}Cs , ^{131}I and ^{210}Po from lead bismuth liquid metal solutions studied by the transpiration method

3rd place students poster presentation

18th Radiochemical Conference, Mariánské Lázně, Czech Republic

17 May 2018

**Christoph A. Umbricht, Martina Benešová, Raffaella Schmid, Andreas Türler, Roger Schibli,
Nicholas P. van der Meulen, Cristina Müller**

*⁴⁴Sc-PSMA-617 for RadioTheragnostics in Tandem with ¹⁷⁷Lu-PSMA-617 – Preclinical
Investigations in Comparison with ⁶⁸Ga-Based PSMA Ligands*

Springer Prize for Best Paper 2018 (EJNMMI Research)

**Katharina A. Domnanich, Cristina Müller, Martina Benešová, Rugard Dressler, Stephanie Haller,
Ulli Köster, Bernard Ponsard, Roger Schibli, Andreas Türler, Nicholas P. van der Meulen**

⁴⁷Sc as useful β -emitter for the radiotheragnostic paradigm: a comparative study of feasible production routes

Springer Prize for Best Paper 2018 (EJNMMI Radiopharmacy and Chemistry)

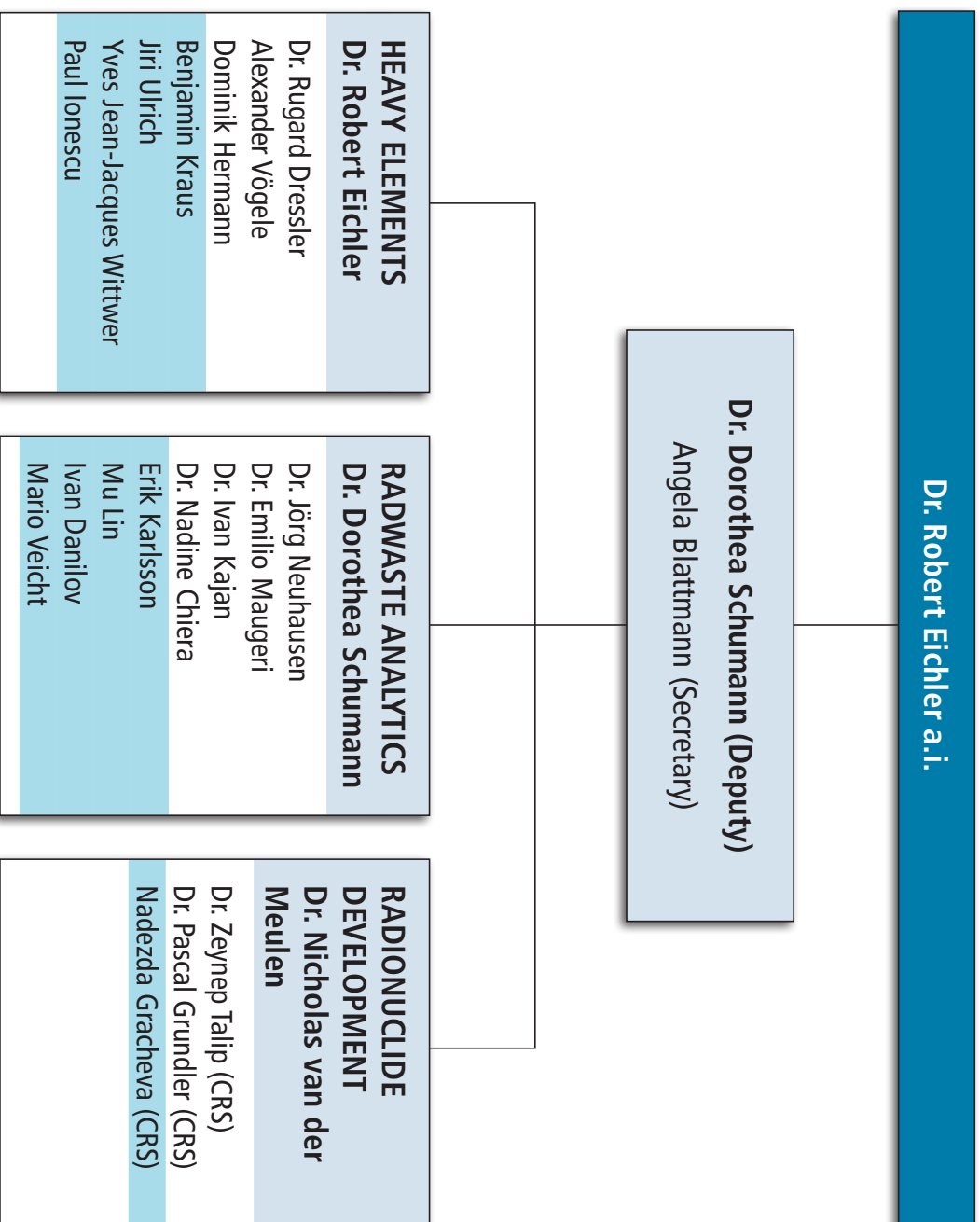
**Cristina Müller, Christoph A. Umbricht, Nadezda Gracheva, Viviane J. Tschan, Giovanni Pellegrini,
Peter Bernhardt, Jan Rijn Zeewaart, Ulli Köster, Roger Schibli, Nicholas P. van der Meulen**

Terbium-161 for PSMA-targeted radionuclide therapy of prostate cancer

Marie Curie Award 2018

for outstanding scientific work presented at the 31st Annual Congress of EANM

LABOR FÜR RADIOCHEMIE DES PAUL SCHERRER INSTITUTS
31.12.2018



AUTHOR INDEX

- Aerts, A., 48
 Aksenov, N.V., 3
 Albin, Y.V., 3
 Ayrarov, M., 35,36
 Balber, T., 59
 Ballof, J., 35,36
 Barbagallo, M., 36
 Behe, M., 50,56
 Blanc, A., 50,56
 Blau, B., 33
 Borge, M.J.G., 36
 Bozhikov, G.A., 3
 Braccini, S., 21,42,54
 Brandt, M., 59
 Camarda, M., 9
 Cao, S., 13
 Carzaniga, T.S., 21,42,54
 Castro, C., 50
 Catherall, R., 35
 Chepigin, V.I., 3
 Chiera, N.M., 3
 Chrysalidis, K., 35
 Chuprakov, I., 3
 Damone, L., 36
 Danilov, I.I., 44,46
 David, J.C., 25
 Dmitriev, S.N., 3
 Dressler, R., 3,9,15,17,19,21,25,30,36,42,44
 Düllmann, Ch.E., 27
 Eberhardt, K., 27
 Eichler, R., 3,5,7,9,11,13,44,46,48
 Fan, F., 13
 Fedorov, D., 35
 Fedosseev, V., 35
 Fiebiger, S., 27
 Gäggeler, H., 3
 Glorius, J., 27
 Göbel, K., 27
 Goodacre, T.D., 35,36
 Gracheva, N., 57,58
 Griesmayer, E., 9
 Guerrero, C., 27
 Haas, R., 27
 Haba, H., 13
 Hapfl, B., 59
 Hasler, R., 50,52,54,56,59
 Heffeter, P., 59
 Heftrich, T., 27
 Heinitz, S., 27,30,32,33,35,36,42
 Heinke, R., 42
 Herrmann, D., 3,7,9,11,19,44,46,48
 Ionecu, P., 3
 Jakupcek, M., 59
 Johnston, K., 35,36
 Käppeler, F., 27
 Kaiser, J.D., 27
 Kajan, I., 28,30
 Kandioller, W., 59
 Karlsson, E., 48
 Keller, C., 56
 Keppler, B., 59
 Kiselev, D., 33
 Kivel, N., 33,36
 Köster, U., 27,35,36,42,57
 Komori, Y., 13
 Krämer, S., 50,56
 Kraus, B., 3,5,7,9
 Langer, C., 27
 Lerendegui-Marco, J., 27
 Lin, M., 28
 Lohse, S., 27
 Ludwig, F., 27
 Madumarov, A.S., 3
 Malyshev, O.N., 3

- Marsh, B., 35,36
- Martins Correia, J.G., 36
- Maugeri, E.A., 35,36
- Mihalcea, I., 38,40
- Mindt, T.L., 59
- Mitterhauser, M., 59
- Naubereit, P., 42
- Neuhausen, J., 44,46,48
- Pautz, A., 38,40
- Popov, Y.A., 3
- Qin, Z., 13
- Raeder, S., 42
- Reifarth, R., 27
- Renisch, D., 27
- Rothe, S., 35,36
- Rüthi, M., 33
- Sabelnikov, A.V., 3
- Sato, T.S., 3,7
- Schell, J., 35,36
- Scheutwinkel, K., 27
- Schibli, R., 50,56,57,58,59
- Schumann, D., 15,23,25,27, 28,32,33,35,38,40
- Seiffert, C., 35,36
- Steinegger, P., 3,7,9
- Stora, T., 36
- Studer, D., 42
- Svirikhin, A.I., 3
- Taddio, M., 50
- Talip, Z., 23,25,50,56,57,59
- Tomandl, I., 35
- Türler, A., 3,5,7,9,11,13,28, 44,46,48
- Ulrich, J., 15,17,19,21,42
- Vacik, J., 35
- van der Meulen, N.P., 21,50, 52,54,56,57,58,59
- Veicht, M., 38,40
- Viererbl, L., 35
- Vockenhuber, C., 25
- Vögele, A., 3,44,46,48,59
- Vostokin, G.K., 3
- Wang, Y., 13
- Weigand, M., 27
- Weiss, C., 9
- Wendt, K., 42
- Wiehl, N., 27
- Wittwer, Y., 3,11,13
- Wolf, C., 27
- Yang, J., 13
- Yeremin, A.V., 3
- Yokokita, T., 13
- Zeevaart, J.R., 57
- Zhang, J., 13

AFFILIATION INDEX

AEC-LHEP	Albert Einstein Center for Fundamental Physics - Laboratory for High Energy Physics, University of Bern, Sidlerstrasse 5, 3012 Bern, Switzerland
ASRC-JAEA	Advanced Science Research Center, Japan Atomic Energy Agency, Tokai, Ibaraki, 319-1195, Japan
CERN-ISOLDE	European Organization for Nuclear Research, CERN, 1211, Genève 23, Switzerland
CIVIDEC	Instrumentation GmbH, Schottengasse 3A/1/41, AT-1010 Wien, Austria
CRS	Center for Radiopharmaceutical Sciences, Paul Scherrer Institut, 5232 Villigen, Switzerland
EPFL	École polytechnique fédérale de Lausanne, EPFL, CH-1015, Lausanne, Switzerland
ETHZ	Eidgen. Technische Hochschule Zürich, 8092 Zürich, Switzerland
EU	European Union
European Commission, DG-Energy	European Commission, DG-Energy, 10 rue Rober Stumper, 2557 Luxembourg City, Luxembourg
FLNR	Flerov Laboratory of Nuclear Reactions, Joliot-Curie, 6, Dubna, Moscow region 141980, Russia
GFA	Division Large Research Facilities (GFA), Paul Scherrer Institut, 5232 Villigen, Switzerland
Goethe Uni.	Goethe University Frankfurt, Theodor-W.-Adorno-Platz 1, 60323 Frankfurt am Main, Germany
GSI	Zentrum für Schwerionenforschung GmbH, 64291 Darmstadt, Germany
HIM	Helmholtz-Institut Mainz, 55099 Mainz, Germany
ILL	Institut Laue-Langevin, 71 avenue des Martyrs 38000 Grenoble, France
IMP	Institute of Modern Physics (IMP), No. 509 Nanchang Road, Lanzhou 730000, Gansu, China
INFN	Laboratori Nazionali del Sud, Via S. Sofia, 62, 95125 Catania, Italy
Irfu CEA	Irfu, CEA Paris-Saclay, Bât 141, 91191 Gif sur Yvette Cedex, France
JAEA	Japan Atomic Energy Agency, Tokai, Ibaraki 319-1195, Japan
JGU	Johannes Gutenberg-Universität Mainz, Saarstr. 21, 55122 Mainz, Germany
JINR	International Intergovernmental Organization, Joint Institute for Nuclear Research Joliot-Curie, 6, Dubna, Moscow region 141980, Russia
KIT	Karlsruher Institut für Technologie, Kaiserstraße 12, 76131 Karlsruhe, Germany
LMN	Laboratory for Micro- and Nanotechnology, Paul Scherrer Institut, 5232 Villigen, Switzerland
LOG	Fachbereich Logistik (LOG), Paul Scherrer Institut, 5232 Villigen, Switzerland
LRC	Laboratory of Radiochemistry (LRC), Paul Scherrer Institut, 5232 Villigen, Switzerland
NESCA	Radiochemistry, South African Nuclear Energy Corporation (Necsa), Pelindaba, 0240, South Africa
NPI Petersburg	Petersburg Nuclear Physics Institute, NRC Kurchatov Institute, 188300 Gatchina, Russia
NPI Řež	Nuclear Physics Institute, Academy of Sciences of the Czech Republic, CZ-25068~Řež, Czech Republic
n_TOF	n_TOF Collaboration, European Organization for Nuclear Research (CERN), Genève 23, Switzerland
NUM	Forschung mit Neutronen und Myonen, Paul Scherrer Institut, 5232 Villigen, Switzerland
PSI	Paul Scherrer Institut, 5232 Villigen, Switzerland
RC Rež	Research Centre Rež, CZ-25068~Řež, Czech Republic

RIKEN	Institute of Physical and Chemical Research, 2-1 Hirosawa, Wako, Saitama 351-0198, Japan
SCK CEN	SCK-CEN: Belgian Nuclear Research Centre, Boeretang 200, B-2400 Mol, Belgium
SINQ-NIS	PSI SINQ Neutron Irradiation Station
Univ. Bern	Departement für Chemie und Biochemie, Universität Bern, Freiestr. 3, 3012 Bern, Switzerland
Univ. Duisburg-Essen	University of Duisburg-Essen, 45141 Essen, Germany
Univ. Mainz	Johannes Gutenberg-Universität Mainz, Saarstr. 21, 55122 Mainz, Germany
Univ. Manchester	School of Physics and Astronomy, The University of Manchester, Manchester, United Kingdom
Univ. Paris-Saclay	Universite Paris Saclay: Espace Technologique, Bat. Discovery - RD 128 - 2e ét., 91190 Saint-Aubin, France
Univ Sevilla	University of Seville, 4 San Fernando Str. Sevilla 41004, Spain
ZRW	Zentrum Für Radiopharmazeutische Wissenschaften, Paul Scherrer Institut, 5232 Villigen, Switzerland

